Graduate School ETD Form 9
(Revised 12/07)

PURDUE UNIVERSITY
GRADUATE SCHOOL
Thesis/Dissertation Acceptance

This is to certify that the thesis/dissertation prepared

By Christopher A. Williamson

Entitled
Power Management for Multi-Actuator Mobile Machines with Displacement Controlled Hydraulic Actuators

For the degree of Doctor of Philosophy

Is approved by the final examining committee:

Prof. Monika Ivantysynova
Chair

Prof. John Lumkes

Prof. Bin Yao

Prof. Gregory Shaver

To the best of my knowledge and as understood by the student in the *Research Integrity and Copyright Disclaimer (Graduate School Form 20)*, this thesis/dissertation adheres to the provisions of Purdue University's "Policy on Integrity in Research" and the use of copyrighted material.

Approved by Major Professor(s): Prof. Monika Ivantysynova

Approved by: Prof. David C. Anderson 12/06/2010
Head of the Graduate Program Date

Graduate School Form 20
(Revised 9/10)

PURDUE UNIVERSITY
GRADUATE SCHOOL

Research Integrity and Copyright Disclaimer

Title of Thesis/Dissertation:

Power Management for Multi-Actuator Mobile Machines with Displacement Controlled Hydraulic Actuators

For the degree of Doctor of Philosophy

I certify that in the preparation of this thesis, I have observed the provisions of *Purdue University Executive Memorandum No. C-22,* September 6, 1991, *Policy on Integrity in Research.**

Further, I certify that this work is free of plagiarism and all materials appearing in this thesis/dissertation have been properly quoted and attributed.

I certify that all copyrighted material incorporated into this thesis/dissertation is in compliance with the United States' copyright law and that I have received written permission from the copyright owners for my use of their work, which is beyond the scope of the law. I agree to indemnify and save harmless Purdue University from any and all claims that may be asserted or that may arise from any copyright violation.

Christopher A. Williamson
_____
Printed Name and Signature of Candidate

12/06/2010
_____
Date (month/day/year)

*Located at http://www.purdue.edu/policies/pages/teach_res_outreach/c_22.html

POWER MANAGEMENT FOR MULTI-ACTUATOR MOBILE MACHINES WITH DISPLACEMENT CONTROLLED HYDRAULIC ACTUATORS

A Dissertation

Submitted to the Faculty

of

Purdue University

by

Christopher A. Williamson

In Partial Fulfillment of the

Requirements for the Degree

of

Doctor of Philosophy

December 2010

Purdue University

West Lafayette, Indiana

ProQuest LLC
789 East Eisenhower Parkway
P.O. Box 1346
Ann Arbor, MI 48106-1346

To Leah,

without whose constant support

this work would have never begun and

certainly would not have finished.

ACKNOWLEDGMENTS

Advancing the state of the art is rarely an individual effort, and this dissertation is no exception. I would like to thank first Prof. Monika Ivantysynova for her guidance and support over the last five years. Thanks to the researchers of the Maha Fluid Power Research Center, both past and present. I would like to specifically acknowledge Josh Zimmerman and Matteo Pelosi for their work on dynamic models of the DC excavator. Josh also designed much of the hydraulic and electrical circuits for the prototype. Edward Hughes was responsible for mechanical design and CAD modeling, which was no small job. Fabrication and assembly of the DC excavator was accomplished by Anthony Franklin with support from Edat Kaya. Thanks to all of you for making the DC excavator a working reality. Aside from the excavator itself, others contributed directly to this thesis. Thanks to Jess Rose for running CASPAR pump simulations and to Rohit Hippalgoankar for the DC circuit stability analysis. I am also grateful to the professors on my graduate committee and the industrial and academic members of the CCEFP whose comments and questions have improved this work.

This thesis was made possible by the generous support of the National Science Foundation through the Center for Compact and Efficient Fluid Power. Corporations from the fluid power industry also made valuable contributions, including Parker Hannifin, Bobcat, Caterpillar and Moog. Joe Kovach, Bruce Larkin, Scott Schuh, and Viral Mehta were particularly instrumental.

On a personal note, I am grateful to my wife Leah for supporting me during this lengthy endeavor. And thanks to the rest of you who I didn't acknowledge by name. I appreciate your help, too.

TABLE OF CONTENTS

Page

Page

LIST OF TABLES

Table Page

Appendix Table

LIST OF FIGURES

Figure Page

Figure Page

Figure Page

LIST OF SYMBOLS

Symbol	Definition	Unit
α	Cylinder area ratio	-
α_D	Orifice discharge coefficient	-
β	Pump swash plate angle	rad, %
β_d	Reference pump swash plate angle (pump displacement volume)	%
$\beta_d^{\dagger}$	Pump displacement reference, output from power optimization	%
β_d^{*}	Pump displacement reference, output from engine speed control	%
ϕ	Angle of shaft rotation	rad
φ	Vector of basis functions	various
θ	Joint angle	rad
θ_p	Vector of uncertain parameters	various
ρ	Fluid density	kg/m^3
ζ	Damping ratio	-
μ	Fluid dynamic viscosity	$N{\cdot}s/m^2$
ξ	Turbulent drag coefficient	-
ω_v	Control valve natural frequency	rad/s
ω_e	Engine rotational speed	rad/s
Δ	Unmodeled additive uncertainty	Pa
Δp	pressure difference	Pa
b_p	Pump gain	$\%/\mathrm{s}\cdot\sqrt{\mathrm{Pa}}$
c_p	Pump gain	1/s
d	Diameter	m

e	Control error	%
f_β	Pump displacement polynomial function	%
f_C	Coulomb friction coefficient	N
f_s	Static friction coefficient	N
f_T	Pump torque polynomial function	Nm
f_v	Viscous friction coefficient	N·s/m
g_{cp}	Charge pump torque polynomial function	Nm
k_L	Pressure-dependent internal leakage coefficient	m^3/Pa·s
k_{Le}	Pressure-dependent external leakage coefficient	m^3/Pa·s
k_{Lv}	Velocity-dependent leakage coefficient	m^2
$k_{p,e}$	Proportional gain, engine speed control	%·min/rev
k_x	Pump swash plate centering spring rate	N/m
r_p	Pump piston pitch radius	m
l	Length	
m	Mass	kg
m_e	Engine fuel mass	kg
m_{eq}	Equivalent linear inertia	kg
n_e	Engine crankshaft rotational speed	rev/min
$n_{e,d}$	Reference engine speed	rev/min
n_p	Pump rotational speed	rev/min
p	Fluid pressure	Pa
p_{cp}	Charge pump pressure	Pa
$p_{p,P}$	Pump control supply pressure	Pa
$p_{p,A}$, $p_{p,B}$	Pump control cylinder pressure	Pa
r_p	Pump swash plate radius	m
u	Valve control signal (normalized)	-
v	Velocity	m/s
x_{act}	Actuator piston position	m
x_p	Pump control cylinder position	m
y_v	Valve spool position (normalized)	-

A	Area	m^2
A_p	Area of pump swash plate control piston	m^2
C_a	Accumulator capacitance	m^3/Pa
C_q	Linear valve flow gain coefficient	m^3/s
C_v	Valve flow gain coefficient	$m^3/s \cdot \sqrt{Pa}$
C_H	Hydraulic capacitance	m^3/Pa
F	Force	N
F_f	Friction force	N
F_L	Load force	N
H	Switching feedback control signal	%
I	Mass moment of inertia	$kg \cdot m^2$
K_{oil}	Fluid bulk modulus of elasticity	Pa
M	Moment	Nm
M_x	Pump swash plate control moment	Nm
Q	Volumetric flow rate	m^3/s
Q_d	Reference pump flow rate	m^3/s
Q_s	Pump volumetric loss flow rate	m^3/s
T	Torque	$N \cdot m$
T_e	Engine crankshaft (brake) torque	Nm
T_f	Engine frictional torque	Nm
T_i	Engine fueling (indicated) torque	Nm
T_L	Engine load torque	Nm
T_p	Pump shaft torque	Nm
T_{cp}	Charge pump shaft torque	Nm
V	Fluid volume	m^3
V_i	Pump displacement volume	m^3/rev
CAN	Controller Area Network	
DC	Displacement Controlled	
EHA	Electro-Hydrostatic Actuator	

FF	Feedforward
IMV	Independent Metering Valve
PD	Proportional-Derivative
PI	Proportional-Integral
SMC	Sliding Mode Control

ABSTRACT

Williamson, Christopher A. Ph.D., Purdue University, December 2010. Power Management for Multi-Actuator Mobile Machines with Displacement Controlled Hydraulic Actuators. Major Professor: Monika Ivantysynova.

Economic and environmental factors provide the motivation for a continuing trend toward more energy efficient fluid power systems in construction and agricultural machinery. One of the energy-efficient alternatives to today's valve-controlled hydraulic systems is displacement controlled (DC) actuation, in which hydraulic cylinders and motors are controlled directly by variable displacement pumps.

The primary contribution of this thesis is a novel method for optimizing the operation of mobile machines with multiple DC actuators. The proposed power management method improves fuel economy by adjusting the operating points of the hydraulic pumps and diesel engine. The instantaneous rate of fuel consumption is minimized based on operator commands and detailed maps of pump and engine efficiency, including hydraulic energy recovery. Tradeoffs between dynamic response and steady-state efficiency are also considered. In order to facilitate real-time operation, the multi-actuator optimization problem is reduced to a one-dimensional minimization problem without compromising the solution.

In support of the new power management method, nonlinear models are derived for variable displacement pumps and DC linear and rotary actuators. A sliding mode control law is proposed for robustly controlling pump displacement in spite of uncertain control pressure and swash plate moment. DC actuators operate in

two modes, depending on the direction of the load. While actuating inertial loads, DC actuators can experience a limit cycle behavior with repeated switching between modes. Stability characteristics are analyzed. Stability can be assured by design (increasing damping or static load) or by feedback control. Robust control of pumps and actuators is demonstrated by simulation and experiment.

A prototype 5-ton compact excavator was developed as part of the research. The DC excavator was fully instrumented for measuring energy efficiency and fuel consumption. The proposed power management algorithm reduced measured fuel consumption for a load-positioning duty cycle by 56% compared to the same system without optimization. Fuel measurements for a truck loading cycle yielded a 69% improvement in fuel efficiency (soil loaded per fuel consumed) compared to a conventional mini excavator.

CHAPTER 1 INTRODUCTION

1.1. Motivation

In general, hydraulic actuators offer smaller size and faster dynamic response than electro-mechanical actuators of comparable power. Consequently, mobile equipment in construction, agriculture, defense, and aviation depend almost exclusively on fluid power technology. However, hydraulic systems also have disadvantages, including noise, leakage and low energy efficiency. The latter topic provides the motivation for the proposed research. In the current generation of mobile hydraulic systems, fluid pressure and flow rate to each actuator (motor or cylinder) is controlled with valves. These valve-controlled systems have favorable properties in terms of cost and performance, but their energy efficiency is often poor. Analysis of multi-actuator hydraulic systems shows that the power transmission efficiency for a typical duty cycle may be less than 15% (Williamson, Zimmerman and Ivantysynova, 2008). Low efficiency is partly due to energy losses from individual components (e.g. pumps, connectors, valves, actuators), but the largest source of losses is the system configuration, the topology of the hydraulic circuit itself.

The essential problem in designing an energy-efficient hydraulic circuit is one of supply and demand. The power supply (pump pressure and flow rate) must be nearly the same as the power demand (actuator pressure and flow rate). When demand exceeds supply, machine productivity suffers. When supply exceeds demand, energy efficiency is reduced. When multiple actuators operate simultaneously at different pressures and flow rates, it is difficult to supply the required power efficiently with a single pump. Simple hydraulic circuits that

operate at constant pressure or constant flow are obviously over-supplied, resulting in a poor utilization of hydraulic energy. Such systems are now only common in low-cost, low-power equipment. Modern mobile machines rely on circuit configurations where both supply pressure and flow rate are variable. In these circuits, pump pressure is set by the actuator loads and the pump displacement is adjusted with hydraulic feedback of pressure (e.g. load sensing) or flow rate (e.g. negative flow control). However, the supply and demand problem still exists. The pump must operate at a pressure higher than the highest actuator pressure, which then must be throttled down to the operating pressure of the other actuators. This disparity between pump pressure and actuator pressure is a major source of power losses for multi-actuator systems.

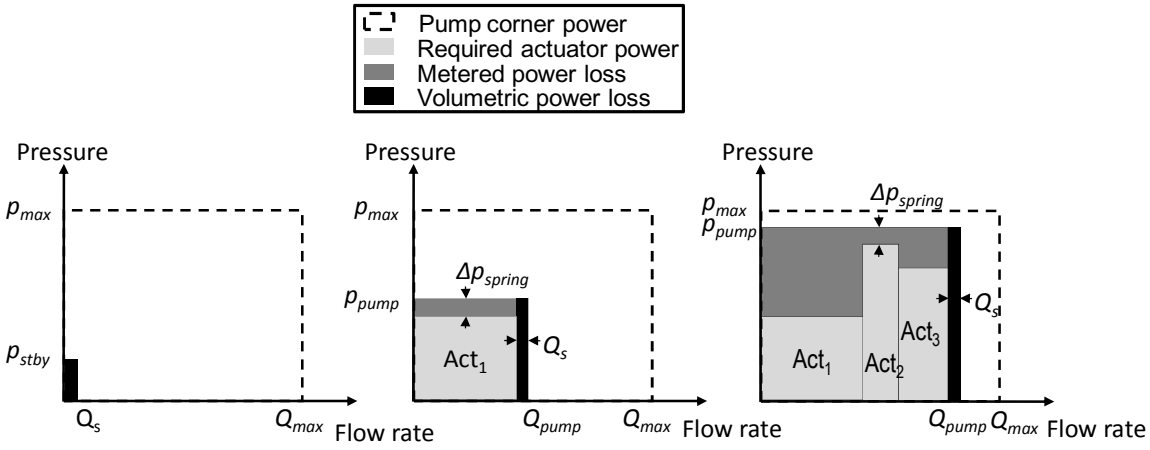

Figure 1.1 Power losses in a load-sensing valve controlled hydraulic system at idle (left) and with one (center) and multiple working actuators (right)

Power utilization in a load-sensing system is illustrated in Figure 1.1. In an idle state (left), the pump outputs a standby power level which is entirely wasted. With a single actuator (center), most of the pump power is transferred to the actuator. The pump maintains a constant pressure margin Δp_{spring} above the load pressure and its effective flow rate is reduced by volumetric losses Q_s. Yet the power efficiency is still quite good. When multiple actuators work simultaneously (right), load pressures are often poorly matched. The mismatch

of pressure supply and demand results in a large percentage of wasted power, as much as 40% of the total (Williamson, Zimmerman and Ivantysynova, 2008).

Moreover, traditional valve controlled systems do not allow energy recovery. Potential and kinetic energy that could be recovered and reused is wasted by the control valves because the circuit topology only permits unidirectional power flow to the actuators.

Poor energy efficiency in hydraulic systems is not a minor issue. The fluid power industry is estimated to use roughly 6% of all energy and generate 7.5% of all CO_2 emissions in the United States (Love, 2009). Although how much of these totals can be assigned to mobile machinery is not precisely known (a study is currently being conducted by the National Fluid Power Association), it is clear that improving the energy efficiency of these machines would have a significant environmental and economic impact. As the cost of petroleum generally continues to rise and governmental restrictions on engine exhaust emissions are increasingly stringent, many research projects are underway in industry and academia to improve the energy efficiency of fluid power components and systems.

1.2. Objective

The research described in this thesis is funded by the United States National Science Foundation through the Center for Compact and Efficient Fluid Power (CCEFP), Project 1A.2: Optimal power management with displacement controlled actuators. The goal of this project is to reduce the fuel consumption of mobile, multi-actuator machines by developing advanced electro-hydraulic control systems. New methods will be experimentally evaluated on a five-ton mini excavator which serves as a testbed for multiple research projects within the Center.

1.3. Organization

The relevant technical literature is surveyed in Chapter 2, providing an overview of the state of the art. New research in optimal power management is presented in Chapter 3, with supporting topics in subsequent chapters. Modeling and simulation is the subject of Chapter 4. Chapter 5 covers the design and analysis of control systems for variable displacement pumps and displacement controlled linear actuators. An experimental evaluation of the proposed methods is presented in Chapter 6, followed by a summary and conclusion in Chapter 7.

CHAPTER 2 STATE OF THE ART

2.1. Mobile Machinery

Mobile machinery is essential to construction and agriculture throughout the world. Machines such as those pictured below are equipped with multiple hydraulic actuators (cylinders and motors) for digging, loading, and other material handling tasks. Specialized attachments increase their functional capabilities.

Figure 2.1 Mobile, multi-actuator machines (top left: backhoe loader; top right: telehandler; bottom: excavator)

With few exceptions, the hydraulic actuators on these machines are controlled by spool-type flow control valves. There is an ongoing trend toward electro-hydraulic control valves in place of pilot-operated valves. Digital communication (e.g. CAN) and electro-hydraulic valves are now standard on new larger machines and are becoming more common in compact equipment. However,

many equipment operators prefer the “feel” of pilot-operated systems, which is difficult to duplicate with electronic controls. Position sensing is available on some machines as an option. Closed-loop position control of hydraulic manipulators has been the subject of many successful research projects, and servo actuators are common in industrial applications. However, due to cost and complexity, this technology has not yet become widely available in mobile machines.

There is an ongoing trend toward more sophisticated control in construction equipment, which may eventually result in fully autonomous machines. Research in automated excavation has been pursued for more than 15 years (Singh, 1997; Singh, 2002; Karhu, et al., 2007; Jang, et al., 2009). Significant advances have been made in teleoperation and haptic human-machine interfaces (Lawrence, et al., 1995; Kontz, 2007; Uusisalo, Huhtala and Vilenius, 2009). However, the vast majority of excavators are still operated by hand without closed-loop actuator controls.

As an alternative to traditional spool-type control valves, poppet-type cartridge valves allow the meter-in and meter-out orifices to be controlled independently, which improves controllability (Yao and Liu, 2002) and reduces power losses (Shenouda and Book, 2008). The most common independent metering valve (IMV) configuration consists of four valves (Kramer and Fletcher, 1984; Jansson and Palmberg, 1990), although alternative circuits with five (Yao and Liu, 2002), or six valves (Andruch and Lumkes, 2009) have been developed. The latter work proposes configuring actuators in a network topology with common high and low pressure lines for energy recovery. IMV circuits with energy recovery capability have also been investigated by Heybroek, Larsson, and Palmberg (2009). Another independent metering concept consists of on/off valves of various flow capacities arranged in parallel for digital flow control (Linjama, Laamanen, and Vilenius, 2003).

As part of the effort toward greater energy efficiency, electric hybrid excavators have been developed in recent years (Kagoshima et al., 2007; Xiao, Wang and Zhang, 2008; Ahn and Truong, 2009; Lin and Wang, 2010).

2.2. Power Management

As applied to passenger vehicles and mobile machinery, the term "power management" refers to a control system that governs energy conversion and transmission in order to achieve the desired system operation. Power management accomplishes two main tasks:

1. Managing limits. Components and subsystems have operational limits, such as maximum engine power and minimum battery voltage. The power management algorithm must respect these boundaries to avoid undesired behavior or damage. To the extent possible, performance objectives should still be met when limits are encountered. For example, power distribution may be prioritized when competing functions require more power than is available.
2. Optimizing operation. Modern vehicle powertrains are complex dynamic systems with many inputs, outputs and states. Power management controls the system at a high level so that desired objectives such as performance, energy efficiency and reliability are maximized.

The first task is essentially practical in nature, while the second has more theoretical implications. It is not surprising then that engineers in the industry are often more concerned with power management in the first sense, and academic study focuses on the second.

Over the last 15 years, the development of optimal power management strategies has closely followed advances in continuously variable mechanical transmissions and hybrid electric powertrains for passenger vehicles. In spite of

its relatively short history, power management has been the subject of many publications. In reviews of the literature, power management approaches are classified in three categories: rule-based control, static optimization, and dynamic optimization (Cook et al., 2006; Crolla et al., 2008). Rule-based control is the simplest and most common method. Rules are developed heuristically from experience and engineering intuition and are implemented in the form of if-then-else statements and look-up tables (Pfiffner, Guzzella and Onder, 2003). Fuzzy logic and neural networks fall into this category as formalizations of rule-based control. Instantaneous or static optimization refers to minimizing the rate of fuel consumption at each moment in time. For example, Ossyra and Ivantysynova (2004) designed and tested a static optimization algorithm for controlling a hydrostatic transmission. Williams (2008) improved their method and applied it to a hydraulic power-split transmission. Dynamic optimization solves the optimization problem by dynamic programming, finding the optimal trajectory by working backward from the final state to the initial state. Therefore, the duty cycle must be known a priori. A stochastic version of the dynamic programming algorithm has been formulated that is causal and guarantees the global optimum on average (Crolla, et al., 2008). A simpler alternative is to implement a rule-based control that approximates the operation recommended by dynamic optimization (Filipi et al., 2004).

Each optimization approach offers advantages and disadvantages. Rule-based methods are simple to design and implement, and their computational requirements are low. However, optimal performance is not guaranteed. Static optimization guarantees pointwise optimality by minimizing the objective criterion at each point in time. This is certainly an improvement over a suboptimal heuristic approach. The computational burden associated with instantaneous optimization is not negligible, but real-time operation is possible with the processors available today. The disadvantage of static optimization is that system dynamics are neglected. If the system is at steady-state, then the pointwise optimum is equivalent to the global optimum. Likewise, quasi-steady-

state can be assumed if the input signal frequency is lower than that of the system's eigenvalues. However, if the system dynamics cannot be neglected, then static optimization does not guarantee global optimality. This drawback is particularly significant in the case of hybrid vehicles, where managing time-varying states related to energy storage is essential to minimizing fuel consumption over an entire duty cycle.

The primary advantage of dynamic optimization is global optimality, with system dynamics considered. Dynamic programming provides a benchmark for the best possible performance. However, the necessity of the having the entire time history a priori makes it impossible to implement on a mobile machine where future inputs are unknown. As mentioned previously, this obstacle can be avoided by stochastic dynamic programming in which the system inputs are represented as a Markov process with known probabilities. Another disadvantage of dynamic optimization is the so-called "curse of dimensionality": the computation time required for optimization increases exponentially with the number of system states (Cook et al., 2006). Solving the dynamic optimization problem and implementing a real-time control law for an on-road vehicle with a few states (say, five or less) is a challenging but tractable problem. For a multi-actuator system with 15 or more states, the computational burden of dynamic programming is very high indeed. High performance computing resources would be required to solve the optimization problem in a reasonable amount of time. Real-time implementation would be prohibitively expensive, since the computing hardware that is currently available for mobile machinery is inadequate.

For mobile fluid power machinery, power management in the first sense (handling power limitations) has been well-developed for many years. Hydraulic power controls of different kinds have been developed for various components and systems. For example, variable displacement hydraulic pumps on mobile machines are commonly equipped with pilot-operated displacement controls for limiting hydraulic power demand to match available engine power. Mechanical

"inch" pedals allow separate control of engine speed for driving and hydraulic working functions on wheel loaders and fork lift trucks. Electronic control systems can perform the same functions and offer the advantages of programmable logic (Ivantysynova, Rahmfeld and Weber, 2008).

Multi-actuator power management in the second sense (optimization) has received much less attention. Rule-based strategies have been implemented for adjusting engine speed on excavators according to defined working modes (Kakuzen, Hayashi and Fujioka, 1988; Chun and Seo, 1993). Recent electric hybrid excavators utilize rule-based power management with incremental changes in component operating points based on working conditions (Nanjo, et al., 2007; Kagoshima, et al., 2007; Xiao, Wang and Zhang, 2008; Ahn and Truong, 2009; Lin and Wang, 2010). Power optimization for an excavator swing drive by means of model predictive control was attempted by Thuring (2008). Montgomery and Alleyne (2006) designed a multi-actuator powertrain control based on static optimization, which was demonstrated on a hardware-in-the-loop test stand emulating a wheel loader. Pedersen simulated a similar static optimization algorithm for a backhoe loader (2007). Dynamic optimization has not been attempted for a multi-actuator mobile machine.

2.3. Displacement Controlled Actuation

The power losses inherent to valve control are a major source of power losses in today's hydraulic systems. Pump control is an energy-efficient alternative. In pump controlled circuits, each cylinder is directly connected to a pump, without control valves in between to meter the flow. The position and velocity of the actuator is controlled by varying the pump flow rate. Pump-controlled actuation owes much of its development to aviation. Electro-hydrostatic actuators (EHA) consisting of electric motors driving hydraulic pumps were designed to eliminate the weight associated with long hydraulic hoses connected to a central supply.

The reduced energy requirement of efficient pump-controlled actuators was also attractive (Ivantysynova, Kunze and Berg, 1995). There are two types of EHA systems: a fixed displacement pump and a variable speed electric motor, or a variable displacement pump and a constant speed motor. Fixed displacement EHA requires a less expensive pump, but variable displacement EHA has the advantage of faster dynamic response due to the small inertia of the pump swash plate.

In terms of the hydraulic circuit, pump controlled actuation for motors and double-rod cylinders is straightforward. Controlling a single-rod cylinder requires compensation for the asymmetric actuator volume. Possible solutions include a servo valve (Berbuer, 1988; Ziegler, 1990), a pilot-operated three-way valve connected to a low pressure source (Hewett, 1994; Lawrence, et al., 1995), two pilot-operated check valves (Rahmfeld and Ivantysynova, 1998) or one pilot-operated check valve with restricted operating conditions (Wendel, 2000).

In the circuit designed by Rahmfeld and Ivantysynova, single-rod cylinders are connected to variable displacement pumps driven by a diesel engine. This displacement controlled (DC) actuator circuit was successfully demonstrated on a wheel loader (Rahmfeld, 2002) and a skid-steer loader (Williamson, 2007). Displacement controlled rotary actuators were also investigated (Grabbel, 2004).

DC pumps must be sized much larger than open circuit pumps in a comparable valve-controlled system due to the unequal fluid volumes of the single-rod cylinder. Heybroek, Larsson and Palmberg proposed an alternative DC concept with an open hydraulic circuit and four valves for directing fluid flow (2006). This solution has the advantage of smaller sized units, but requires a more complicated control law. Open-circuit DC actuators were demonstrated on a wheel loader (Heybroek, 2008). Variable speed EHA circuits have also been tested on mobile construction equipment (Ruhlike, 1997; Habibi and Singh, 2000; Kagoshima et al., 2007; Ahn and Truong, 2009).

In recent years, alternative concepts such as secondary control, hydraulic transformers, and on/off valve control have been proposed for controlling hydraulic cylinders without metering valves.

Secondary motor control refers to a circuit in which the rotary actuator is an overcenter variable displacement unit which is capable of four quadrant operation (bidirectional torque and flow rate) and is supplied by a constant pressure line. Advantages of this approach include high bandwidth, low losses and energy recovery capability (Berg, 1999). Linjama, et al. (2009) applied the secondary control concept to a linear actuator with multiple, discretely variable piston areas. The secondary controlled cylinder is limited to a few special applications involving high inertial loads and high velocities.

Hydraulic transformers are intended to convert hydraulic power between pressure and flow rate like an electrical transformer converts voltage and current. Cylinder control with a two-unit transformer was investigated by Lodewyks (1994). A transformer based on a single hydrostatic unit with three ports was designed by Achten (1997). Another design consisting of a linear actuator with a discretely variable piston area has been proposed (Bishop, 2009). Transformers are an intriguing concept, but significant barriers related to efficiency, high pressure capability, noise and control bandwidth stand in the way of a commercially viable design.

Controlling a cylinder with fast switching valves is another idea borrowed from power electronics. In a hydraulic version of pulse width modulation (PWM), on/off valves produce an effectively variable flow rate and pressure supply to the actuator by rapidly switching between the pump and tank lines (Scheidl, Garstenauer and Manhartsgruber, 2000). If the valves could open and close instantly, this would be a meterless control concept. Of course, real valves have a nonzero response time which results in reduced orifice areas and metering during the transition time as the switching frequency increases. On/off control

with slow switching (e.g. bang-bang control) offers higher efficiency at the cost of reduced controllability (Long and Lumkes, 2010).

2.4. Pump Displacement Control

Electrohydraulic control systems for variable displacement pumps were introduced as early as the 1960s (Keyworth, 1969). Development continued through the 1970s and 1980s, primarily for industrial applications (Hahmann, 1973; Kreth, 1979; Sprockhoff, 1979; Roth, 1983). Later researchers developed more comprehensive analytical models, including swash plate kinematics and flow saturation through the control valve (Berbuer, 1988; Ziegler, 1990). The dynamic effect of parameter variations was also considered (Manring and Johnson, 1996).

In industrial practice, servo pump displacement controls often consist of simple proportional or PI type control laws, perhaps with gain scheduling. Academic research has mainly focused on linear methods. Berg (1999) designed an LQG/LTR optimal control for secondary-controlled hydraulic motors. Rahmfeld (2002) adapted the same method to servo pumps for DC actuators. Grabbel (2004) used robust pole/zero cancellation to reduce the effect of underdamped servo valve poles and increase the feedback gain. Dean and Fales (2007) designed a robust PD control law with H_∞ techniques.

Considering the nonlinear dynamics of servo pumps (including quadratic pressure/flow relationship, valve dead band, valve and swash plate position saturations, static friction and control moment disturbance), there have been remarkably few applications of nonlinear control theory to variable displacement pumps. Du (2002) designed a feedback linearizing control law for controlling pump swash plate position and pump outlet pressure. Lee, Park and Kim (2009) used a robust sliding mode technique to control the pressure in the swash plate

control cylinder. Other nonlinear tools such as fuzzy logic and neural networks have also been investigated (Bonivento et al., 1997; Ming-Hui et al., 2003).

2.5. Research Objectives

Considering the state of the art, there is much opportunity for research in optimal power management for mobile machinery. Existing methods are typically based on engineering intuition rather than optimal control theory. Where an optimal control strategy has been developed, steady-state conditions or slow actuator dynamics are assumed. Moreover, combining power management with energy-efficient hydraulic circuits based on displacement controlled hydraulic actuators is an entirely new topic of study. Favorable characteristics of DC actuation such as energy recovery and decoupled actuator pressures and flow rates promise additional opportunity for optimizing power transmission.

The goal of this research is to propose and analyze an optimal power management methodology for mobile machines with multiple DC actuators. The feasibility of this problem will be evaluated, and an appropriate solution will be selected and tested. The effectiveness of the new method will be studied in simulation and verified experimentally in a fully operational excavator with DC actuators. In addition, the suitability of existing pump and actuator controls for multi-actuator machines will be examined, and advancements will be made where necessary to ensure stability and robustness. Effects related to pump parameter uncertainty and pump/motor mode transitions are particularly relevant and will be studied.

2.6. Chapter Summary

- Mobile multi-actuator machines are trending toward more sophisticated sensing, actuation and control. There is also a continuing demand for higher energy efficiency.
- Several innovative hydraulic circuit designs have been proposed in recent years that allow more efficient energy utilization than traditional hydraulic system configurations. Among these is displacement controlled (DC) actuation, which eliminates valve metering power losses and recovers kinetic and potential energy from aiding loads.
- Power management is a general term for a supervisory control system that regulates energy conversion, storage and transmission. Optimal power management for on-road hybrid vehicles is an active area of research, but there has been little application of these theories to off-road, multi-actuator machines.
- The goal of the present work is to propose and evaluate an optimal power management methodology for mobile machines with multiple DC actuators. The proposed method will be proven on an excavator by simulation and experiment.

CHAPTER 3 OPTIMAL POWER MANAGEMENT

A new method for optimizing the operation of multi-actuator machines is proposed in this chapter. The chapter begins with an explanation of the functional requirements of mobile equipment and continues with an assessment of the capabilities and limitations of current technology. Displacement controlled actuation is introduced in more detail, and its advantages for power management are described. A procedure for static power optimization is presented which selects fuel-optimal operating points for the combustion engine and hydraulic pumps. Simulations of a mini excavator demonstrate the functionality of the proposed power management method.

3.1. Functional Requirements of Mobile Multi-Actuator Machines

The class of mobile multi-actuator machines encompasses various types of equipment. Specialized machines such as timber harvesters are designed for a single purpose. Other machines, like tractor backhoe loaders, are multi-functional. Mobile machines can be equipped with hundreds of different attachments for a variety of tasks. There is also a large range of sizes. Excavators span from 1.6 metric tons and 14 kW to 980 tons and 3400 kW—three orders of magnitude. Mobile machines operate outdoors in all seasons and all climates. Operators of large machines are typically highly skilled and certified, while rental machines are operated by contractors or property owners with little experience and no formal training. The point is that there is great diversity in the machines themselves as well as their uses and operating environments.

Despite the diversity of applications, nearly all mobile machines are powered by diesel engines, and their hydraulic systems are very similar. As discussed previously, equipment manufacturers are now developing new designs with greater energy efficiency. However, energy efficiency must be balanced with other design criteria. Few owners and operators will accept improvements in fuel economy at the expense of performance and controllability.

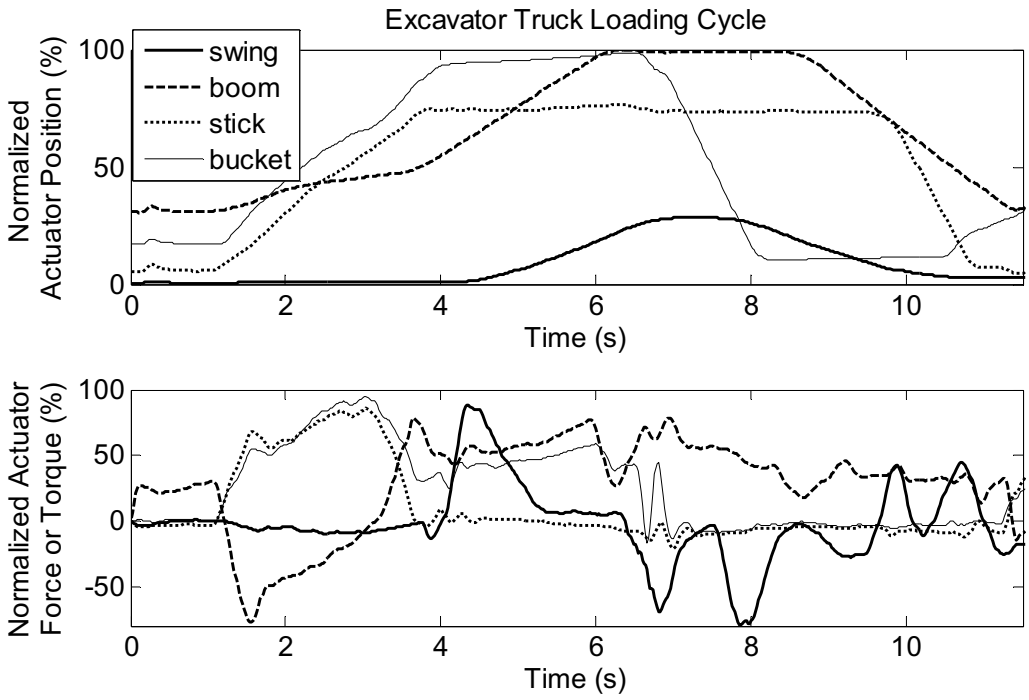

Figure 3.1 Selection from excavator truck loading duty cycle

Figure 3.1 illustrates a multi-actuator machine (an excavator) in operation as soil is removed from the ground and loaded into a truck. Four actuators are used: one motor (swing function) and three cylinders. As shown in the upper plot, multiple actuators work simultaneously. The lower plot shows that the actuators experience both opposing loads (positive force/torque) and aiding loads (negative force/torque), indicating that there is opportunity to recover some of the machine's kinetic and potential energy. It is clear that although the actuators operate simultaneously, their efforts (pressures) and velocities (flow rates) may

be very different. All of these characteristics are typical of multi-actuator machines.

Power requirements depend greatly on the application and the duty cycle. To demonstrate this point, selections from three standard engine test cycles for off-road vehicles are presented in Figure 3.2. In the excavator cycle, the engine alternates between extended periods near maximum power and idling at low speed. One can imagine digging a trench, waiting for utilities to be installed or repaired, then backfilling the excavation. The backhoe and wheel loader cycles have periods of low, high and intermediate power. Large transients can be observed in all three cycles. Of course, these duty cycles are only examples, and typical operations vary with the task and the operator.

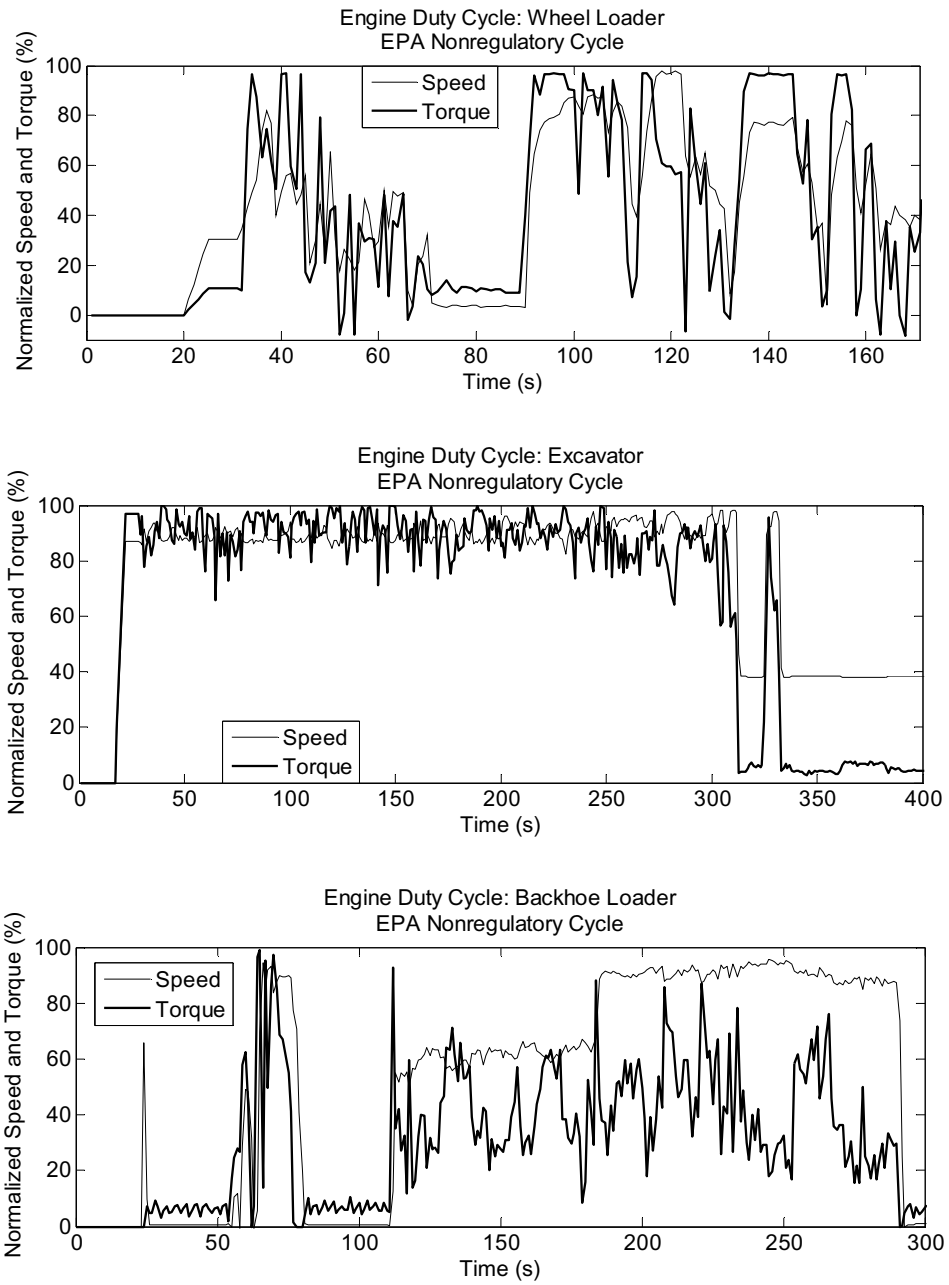

Figure 3.2 Selections from standard off-road engine duty cycles (EPA, 1999)

3.2. Limitations of Existing Technology

The hydraulic actuators in today's mobile systems are typically arranged in parallel. Control valves divert pressurized fluid from a central supply line to each actuator. Machines that travel frequently are often equipped with hydrostatic transmissions, i.e. the motors are pump-controlled. However, valve control is the norm, especially for linear actuators. As was explained in Chapter 1, one of the disadvantages of traditional circuit configurations is that the actuator pressures and flow rates are coupled. The pump pressure is determined by the highest actuator load, and the pump flow rate is at least the sum of the actuator flow rates. The mismatch between power supply and demand results in lost energy. That is, the excess energy is converted into heat. Cooling equipment is required to remove this heat from the hydraulic fluid, which requires additional energy provided by the engine.

Moreover, traditional valve-controlled circuit designs such as load-sensing and negative flow control have limited potential for optimal power management. Supplying multiple actuators from a single source means that the pump flow rate is frequently saturated. At the maximum flow condition, the pump displacement and engine speed cannot be adjusted without reducing the actuator velocities. Coupled actuator pressures tends to saturate the available power, since metering losses can cause the pump and engine power to be much higher than the total actuator power. Consequently, the pump and engine operating points can only be optimized when all actuators operate at low speed and low pressure.

Hydraulic power coupling is not the only obstacle. The lack of energy recovery and storage capability means that the engine must supply enough power to meet peak demands, even though the duration of these intervals may be short (see Figure 3.2). The required system dynamic response is also an issue. The bandwidth of linear actuators on mobile machines is typically in the range of 1 to 5 Hz, which is much faster than the rate at which diesel engines can change speed. Hence, it is not feasible to control the speed of linear actuators by

accelerating the engine, even though such an approach is common for motors used for propulsion.

Due to the aforementioned limitations, it is common practice for operators to choose a constant engine speed setpoint while working, often at the maximum idle speed. In this way, the maximum power and speed is always available for moving the actuators.

3.3. Displacement Controlled Multi-Actuator Systems

An alternative to traditional hydraulic circuit architectures is displacement controlled (DC) actuation, in which the actuators are controlled by variable displacement pumps (Rahmfeld, 2002). Each actuator is powered and controlled by a separate pump. A single charge pump and low pressure accumulator compensates for the difference between the rod-side and piston-side actuator volumes. Pilot-operated check valves connect the low pressure side of each circuit to the charge line. An example circuit is provided in Figure 3.3 for a two-actuator crane.

The main advantage of DC actuation is higher energy efficiency. Metering losses are eliminated, and power can be recovered and shared between actuators while lowering loads. The main disadvantage of DC actuation is the necessity of one pump per actuator, which requires more pumps and a larger total hydraulic pump capacity than comparable valve-controlled systems.

In DC multi-actuator systems, the actuator pressures and flow rates are decoupled. The pump outlet flow rate Q is determined by the shaft speed n_p and the displacement volume V_i, as in Eq. 3.1. Q_s represents volumetric losses due to internal and external leakage and fluid compressibility. For swash plate type pumps, the displacement volume can be written equivalently in terms of the swash plate angle β, since $V_i = k\beta$ for some constant k.

$$Q = n_p V_i - Q_s \qquad \text{Eq. 3.1}$$

All actuators can operate simultaneously at maximum speed (within the available power), which allows higher productivity (Zimmerman and Ivantysynova, 2009). Decoupling the actuators is also beneficial for power management. The minimum engine speed is constrained by the maximum actuator flow rate, and the required engine power is the sum of the power demanded by the actuators. These constraints are much more lenient than in traditional valve-controlled systems (see section 3.2). Since both speed and displacement are continuously variable, there is an extra degree of freedom in Eq. 3.1 which allows the engine speed and pump displacement to be optimized.

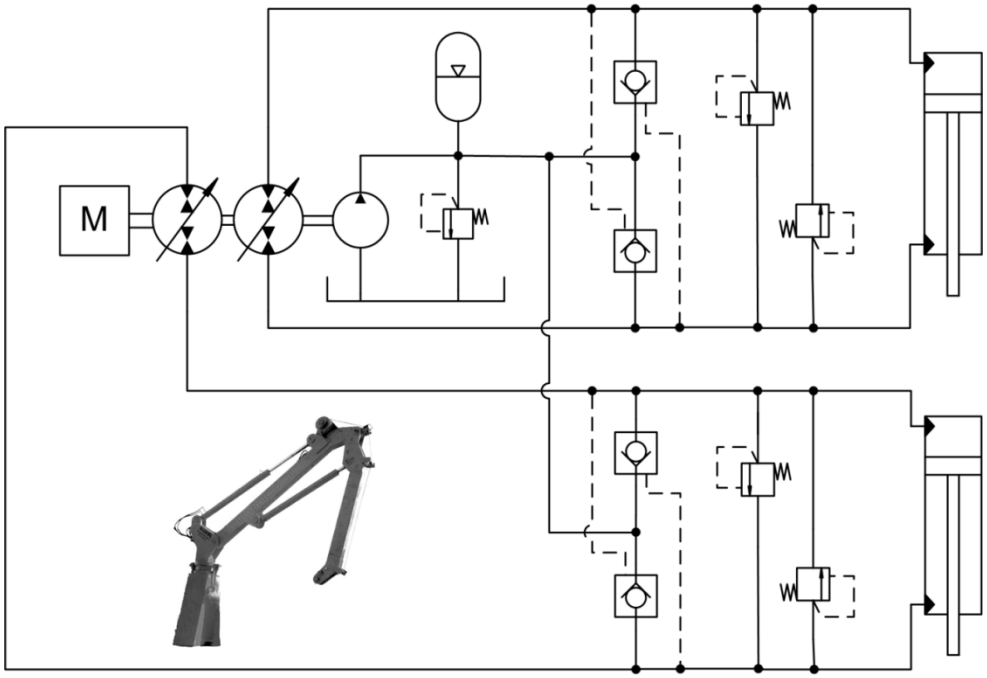

Figure 3.3 Displacement controlled multi-actuator circuit

3.4. Component Efficiency Characteristics

The purpose of the optimal power management method which will be proposed in the next section is to minimize the power required to accomplish a given machine motion. In order to minimize power, the energy efficiency characteristics of each component in the system must be known. Steady-state models of pump and engine efficiency are presented in this section.

3.4.1. Pump Power Map

Axial piston pump/motor units have many moving parts, including reciprocating pistons and a rotating cylinder block. At each mechanical interface (piston / cylinder, cylinder block / valve plate and slipper / swash plate), a thin film of oil lubricates the parts and seals the pressurized fluid chambers. Leakage and friction are determined by these lubricating gaps. Consequently, the pump's volumetric, mechanical and total efficiencies are determined by rather complicated tribological interactions which determine the gap height at each of those interfaces. There are also power losses associated with churning oil in the pump case and friction at shaft seals and bearings. Operating conditions such as fluid temperature and pressure strongly influence pump losses. Due to the complexity of the pump's physical processes, it is more accurate to model its loss characteristics with a purely empirical model based on measured data than an approximation of the governing equations (Ivantysyn and Ivantysynova, 2001). Such models may be created with least-squares polynomial regression, fitting a three-dimensional surface to volumetric or torque losses as a function of the pump pressure, speed and displacement, such as in Eq. 3.3 and Eq. 3.4 (Mikeska, 2002; Williamson, Zimmerman and Ivantysynova, 2008). The form of a third order polynomial of three variables is given in Eq. 3.2.

$$f(x_1,x_2,x_3)=a_{111}x_1^3+a_{112}x_1^2x_2+a_{113}x_1^2x_3+a_{11}x_1^2+a_{122}x_1x_2^2+a_{123}x_1x_2x_3 \\ +a_{12}x_1x_2+a_{133}x_1x_3^2+a_{13}x_1x_3+a_1x_1+a_{222}x_2^3+a_{223}x_2^2x_3+a_{22}x_2^2+a_{233}x_2x_3^2 \\ +a_{23}x_2x_3+a_2x_2+a_{333}x_3^3+a_{33}x_3^2+a_3x_3+a_0 \quad \text{Eq. 3.2}$$

$$Q_s=f_Q(n_p,\Delta p,\beta) \quad \text{Eq. 3.3}$$

$$T_s=f_s(n_p,\Delta p,\beta) \quad \text{Eq. 3.4}$$

Conventionally, shaft torque in pumping mode is written as in Eq. 3.5.

$$T_p=\frac{\Delta pV_i}{2\pi}+T_s \quad \text{Eq. 3.5}$$

In the present work, it is proposed to define a polynomial f_T that maps the pump pressure Δp, speed n_p and flow rate Q to the shaft torque T_p (Eq. 3.6). Likewise, a polynomial β maps outlet flow rate to displacement volume at a given speed and pressure (Eq. 4.2). Both equations have the form of Eq. 3.2. The polynomial coefficients may be found in Appendix B in the pump_model function. A similar polynomial function $g(x_1,x_2)$ can be created for a fixed displacement pump with one input fewer (Eq. 3.8). Polynomial surfaces are illustrated in Eq. 3.8.

$$T_p=f_T(n_p,\Delta p,Q) \quad \text{Eq. 3.6}$$

$$\beta=f_\beta(n_p,\Delta p,Q) \quad \text{Eq. 3.7}$$

$$T_{cp}=g_{cp}(n_p,p_{cp}) \quad \text{Eq. 3.8}$$

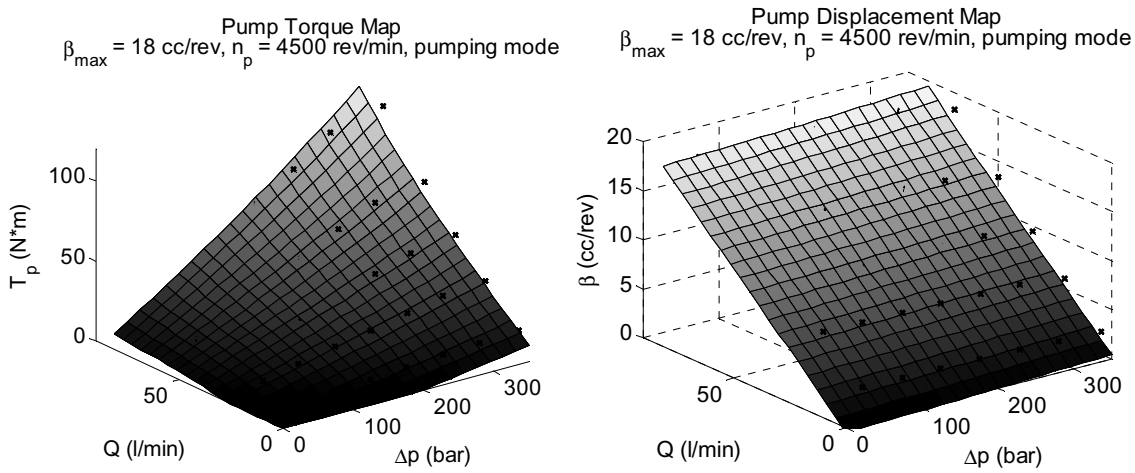

Figure 3.4 Pump power maps

3.4.2. Engine Fuel Map

The operation of compression-ignition combustion engines also involves many physical processes, so an empirical approach is appropriate for modeling fuel consumption characteristics. Let m_e represent the fuel mass combusted in the engine. The rate of fuel consumption $\dot{m}_e$ at steady-state conditions is a function of engine speed n_e and torque T_e and can be described by a two-dimensional polynomial (Eq. 3.9 and Eq. 3.10). Alternately, the rate of fuel consumption could be calculated by linear interpolation of tabulated data. An engine fuel map is depicted in Figure 3.5.

$$g(x_1, x_2) = b_{11}x_1^2 + b_{12}x_1x_2 + b_1x_1 + b_{22}x_2^2 + b_2x_2 + b_0 \qquad \text{Eq. 3.9}$$

$$\dot{m}_e = g_e(T_e, n_e) \qquad \text{Eq. 3.10}$$

The engine's dynamic behavior is approximated as a first-order system (Eq. 3.11), where T_i is the indicated torque produced by fuel combustion, $T_f = c_e\omega_e$ is viscous friction, and T_L is the external load on the crankshaft. The load torque is the sum of the torque from the hydraulic pumps (Eq. 3.12), where there are r

variable displacement pumps connected to the engine. Output torque (brake torque) T_e is the sum of the load torque T_L and the inertial torque required for acceleration (Eq. 3.13), or equivalently, $T_e = T_i - T_f$.

$$I_e\dot{\omega}_e = T_i - T_f - T_L \qquad \text{Eq. 3.11}$$

$$T_L = T_{cp} + \sum_{j=1}^{r} T_{p,j} \qquad \text{Eq. 3.12}$$

$$T_e = T_L + I_e\dot{\omega}_e \qquad \text{Eq. 3.13}$$

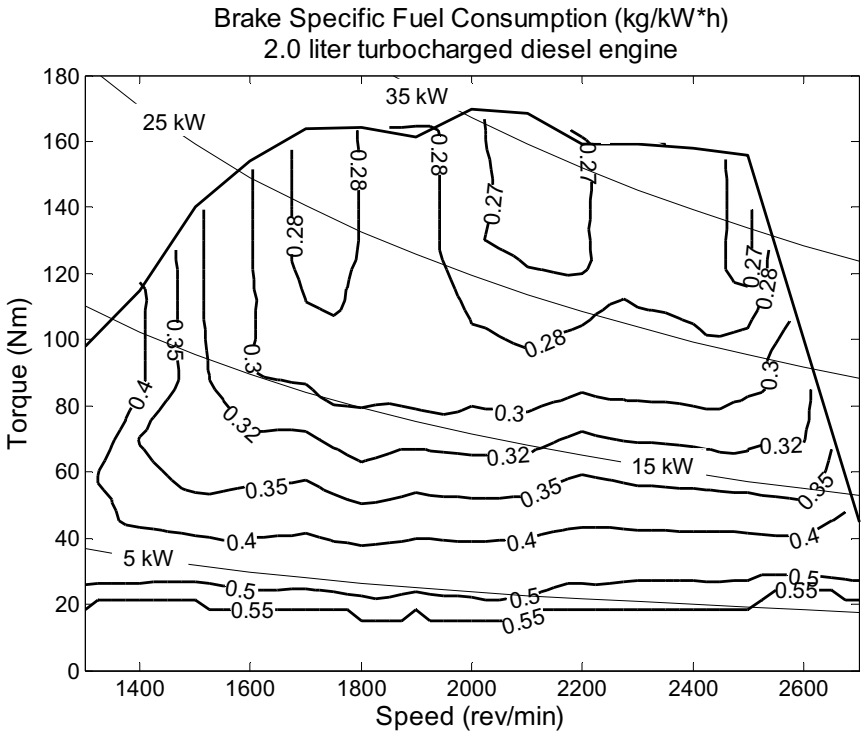

Figure 3.5 Engine fuel map

3.5. Proposed Optimization Method

3.5.1. Optimization with a Single DC Actuator

In order to communicate the idea clearly, the optimization problem is presented first for a single pump and actuator. Pump and engine speeds are assumed to be the same, and the system dynamics are not considered in this simplified example. In words, the problem is to satisfy the required actuator motion while using the least amount of fuel possible by adjusting the engine speed and pump displacement. Mathematically, the problem is posed as follows.

Minimize:

$$\dot{m}_e = g_e\left(T_e, n_e\right) = g_e\left(f_T\left(n_e, \Delta p, Q\right), n_e\right) \qquad \text{Eq. 3.14}$$

Subject to constraints:

$$\begin{aligned} & Q = n_e k \beta - Q_s \\ & n_{e,min} \le n_e \le n_{e,max} \\ & \beta_{min} \le \beta \le \beta_{max} \\ & T_e \le T_{e,max}\left(n_e\right) \end{aligned} \qquad \text{Eq. 3.15}$$

The control variables which can be adjusted are the engine speed n_e and the pump displacement β. The reference input from the operator is the pump flow rate Q. The first equation of constraint is the requirement that the pump must provide the desired flow rate and hence, the commanded actuator velocity. The other constraints are determined by the physical limits of the pump and engine. Pump pressure Δp is an independent parameter which cannot be controlled. The optimal values for n_e and β can be found by numerically evaluating the objective function Eq. 3.14 with the pump and engine efficiency maps described previously.

3.5.2. Optimization with Multiple DC Actuators

Now that the basic idea has been understood for a single DC actuator, the more complicated case of multiple actuators can be presented. Component dynamics are considered, so a notational distinction is made between the desired or reference parameter value (subscript *d*) and the actual value (no additional subscript). Figure 3.6 may also be helpful for understanding the notation. As there are *k* actuators in the system, vector quantities (in bold) have dimension *k*. In addition to the *k* variable displacement pumps, there is also a fixed displacement charge pump (subscript *cp*). The multi-actuator optimization problem definition is as follows.

Minimize:

$$J = \dot{m}_e = g_e\left(T_e, n_{e,d}\right) = g_e\left(\sum_{i=1}^{m} f_T\left(n_{e,d}, \Delta p_i, Q_{d,i}\right) + g_{cp}(n_{e,d}, p_{cp}), n_{e,d}\right) \quad \text{Eq. 3.16}$$

Subject to constraints:

$$Q_{d,i} = n_e k \beta_{d,i}^{\dagger} - Q_{s,i} \quad \text{Eq. 3.17}$$

$$n_{e,min} \le n_{e,d} \le n_{e,max} \quad \text{Eq. 3.18}$$
$$\beta_{min} \le \beta \le \beta_{max}$$
$$T_e \le T_{e,max}\left(n_e\right)$$

The control variables are the reference engine speed $n_{e,d}$ and pump displacements $\boldsymbol{\beta}_d^{\dagger}$. Independent parameters include the desired actuator flow rates $\mathbf{Q}_d$ and the pump pressures $\mathbf{\Delta p}$ and p_{cp}. As before, the solution is subject to constraints on speed, displacement and torque. The flow constraint Eq. 3.17 can be written equivalently as Eq. 3.19.

$$\beta_{d,i}^{\dagger} = f_{\beta}\left(n_{e,d}, \Delta p_i, Q_{d,i}\right) \quad \text{Eq. 3.19}$$

As posed above, the optimization problem is nonlinear, multivariable and constrained. Finding a solution to an unconstrained optimization problem is simpler than one with constraints, so it is advantageous to incorporate Eq. 3.17 and Eq. 3.18 into the objective function Eq. 3.16. Physical constraints can be enforced implicitly by adding a large penalty J_c to the objective function if the constraint is violated. As for the flow constraint, comparing Eq. 3.6 and Eq. 3.7 shows that there is a one-to-one mapping between pump torque and displacement for the same conditions. Therefore, Eq. 3.19 does not restrict the solution, but rather explicitly defines a relationship between β and the other parameters which already exists implicitly in the solution of $T_p = f_T\left(n_{e,d}, \Delta p, Q_d\right)$.

The optimization problem then reduces to minimizing Eq. 3.20, an unconstrained nonlinear function with a single control variable $n_{e,d}$.

$$J = g_e\left(\sum_{i=1}^{m} f_T\left(n_{e,d}, \Delta p_i, Q_{d,i}\right) + g_{cp}(n_{e,d}, p_{cp}), n_{e,d}\right) + J_c \qquad \text{Eq. 3.20}$$

It bears mention that energy recovery is implicit in Eq. 3.20. If one or more pumps operate in motoring mode, the total power required from the engine is reduced. The combination of pump speeds and displacements that minimizes fuel consumption will simultaneously make the best use of recoverable energy, without any additional mathematical consideration. This is true because the DC hydraulic system is designed to use recovered energy immediately rather than by storing and reusing it later. The presence of an energy storage device would necessitate a different approach.

3.5.3. Consideration of System Dynamics

The optimization method proposed in the previous subsection follows an instantaneous or static approach; the solution is only optimal when the inputs and states are constant. As explained in section 2.2, the practical considerations of

limited computational capacity make dynamic optimization prohibitively costly for a mobile multi-actuator application, so a static approach is more appropriate. However, steady-state conditions cannot be assumed for multi-actuator machines in general. While digging or handling material, large fluctuations in actuator pressure and velocity can be expected. The question is then how to deal with these transients in a way that preserves the efficiency obtained at steady-state without sacrificing performance in terms of actuator dynamic response. The key is managing the combustion engine well, since it has the slowest response in the system. Continually accelerating and decelerating the engine to track required actuator velocities may result in greater fuel consumption and particulate emissions in addition to slow actuator response.

In previous research, the issue of statically optimizing a dynamic, multi-DOF system has been solved by a compromise between efficiency and performance. Both Pedersen (2007) and Montgomery and Alleyne (2006) included an error term in the objective function to penalize deviations from the required performance in terms of pump flow rate (Pedersen) or engine power (Montgomery). The author of the present work also published a similar strategy (Williamson and Ivantysynova, 2010, 1). Such an approach seems reasonable as a tradeoff between competing objectives, especially if the system often operates at quasi-steady-state conditions. In general, however, it is unsatisfying. How can a power management algorithm be called optimal if it can cause both efficiency and performance to be worse than the original system?

An alternative is to filter the input signals and apply constraints so that the optimization routine only considers quasi-steady-state conditions. To accomplish this, choose a digital filter $h(z)$ that operates on a signal so as to reduce its frequency content. The filter may be linear or non-linear, of infinite or finite impulse response. Three possible choices for $h(z)$ include a linear low-pass filter (Eq. 3.21), a moving average of w samples (Eq. 3.22), and a moving maximum of w samples (Eq. 3.23).

$$h_{lp}(z) = \frac{a_0 + a_1 z^{-1}}{b_0 + b_1 z^{-1}} \quad \text{Eq. 3.21}$$

$$h_{avg}(z) = \frac{1}{w}\left(1 + z^{-1} + z^{-2} + \cdots + z^{-w+1}\right) \quad \text{Eq. 3.22}$$

$$h_{\max}(z) = \max\left(z^0, z^{-1}, \cdots, z^{-w+1}\right) \quad \text{Eq. 3.23}$$

Let *h(z)* filter the maximum absolute value of the operator input vector $\mathbf{Q}_d$ so as to produce a quasi-steady-state flow command $\bar{Q}_d$.

$$\bar{Q}_d = h\left(\max\left(\text{abs}\left(\mathbf{Q}_d\right)\right)\right) \quad \text{Eq. 3.24}$$

The minimum engine speed is then defined in terms of the steady-state flow command, as in Eq. 3.25.

$$n_{e,min} = \frac{\bar{Q}_d}{k\beta_{max}} \quad \text{Eq. 3.25}$$

In this way, the engine is constrained to run at a steady-state speed when other inputs or states are transient. This prevents the slow actuator response and higher fuel consumption that would result from rapid changes in engine speed. When the commanded flow rates are constant or slowly varying, the additional engine speed constraint has no effect and optimality is conserved.

3.5.4. Optimization Problem Solution

A real-time solution is preferred for practicality. For the system shown in Figure 3.6, the optimization problem has 2*k*+3 inputs, *k*+1 design variables and *k*+1 outputs. Calculating all possible solutions offline and implementing a lookup table or function that gives the solution for all input combinations would be much more computationally expensive than finding a minimum on a bounded 1D interval in real time. The golden section (Fibonacci) search algorithm is a

common method for solving bounded max/min problems in one dimension. It works by iteratively moving upper and lower solution bounds toward the function until the solution converges within a specified tolerance (Press, et al., 2007).

3.5.5. Control System Structure

The proposed control system for a DC multi-actuator hydraulic system is laid out in Figure 3.6. Operator joystick signals are interpreted as desired flow rates $\mathbf{Q}_d$ to the actuators. The operator also specifies a maximum engine speed $n_{e,max}$. The power management algorithm is a high-level system control layer that interprets the operator's inputs and determines the subsystem operating points that will best satisfy the desired motion. As explained in section 3.5.2, the power optimization routine calculates the combination of pump displacements $\boldsymbol{\beta}_d^{\dagger}$ and engine speed $n_{e,d}$ that will result in the lowest instantaneous rate of fuel consumption. The current actuator pressures $\boldsymbol{\Delta p}$ and other loads (such as a charge pump at pressure p_{cp}) are also considered. It should be noted that $\mathbf{Q}_d$, $\boldsymbol{\beta}_d^{\dagger}$ and $\boldsymbol{\Delta p}$ are $k\times1$ vectors, where k is the number of DC actuators. The power management also limits the engine torque in order to enforce the desired speed and prevent stalling. The $\boldsymbol{\beta}_d^{\dagger}$ vector is passed to the low-level hydraulic system control layer that regulates the pump displacements $\boldsymbol{\beta}$ and actuator positions $\mathbf{x}_{act}$. Pump and actuator control will be presented in Chapter 5.

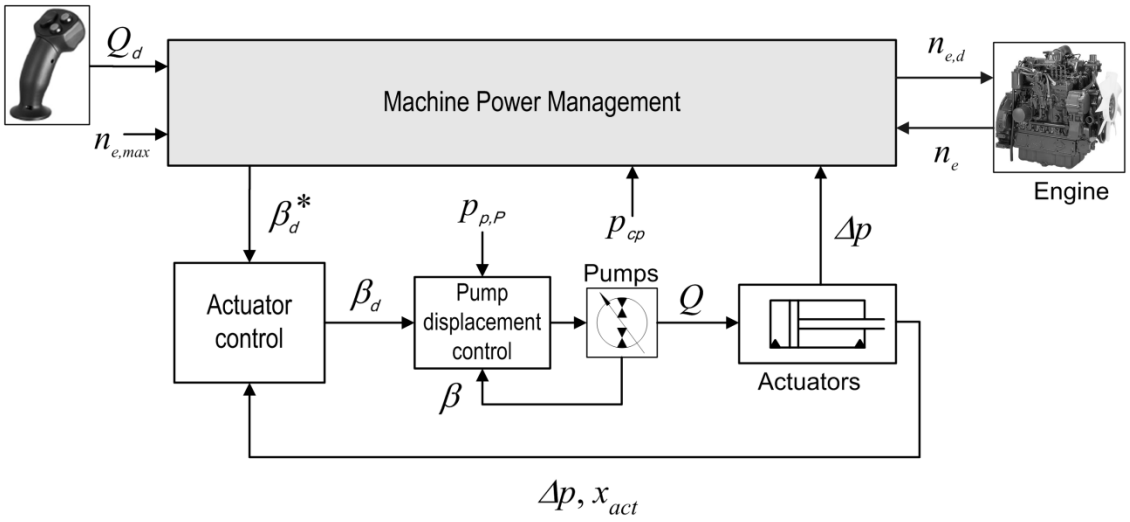

Figure 3.6 Block diagram of multi-actuator control system with power optimization

3.5.6. Engine Speed Control

The total maximum pump torque is much higher than the maximum available engine torque. Hence, a speed control law is necessary to avoid stalling the engine. For optimal operation, it is also desirable to maintain the engine speed near the setpoint established by the optimization algorithm. Engine speed can be controlled with a simple proportional control law in which the commanded pump displacements $\boldsymbol{\beta}_d^{\dagger}$ (and hence the pump torques) are reduced according to the engine speed error (Eq. 3.26).

$$\boldsymbol{\beta}_d^* = k_{p,e}\left(n_{e,d} - n_e\right)\boldsymbol{\beta}_d^{\dagger} \qquad \text{Eq. 3.26}$$

The entire power optimization algorithm is represented graphically in Figure 3.7.

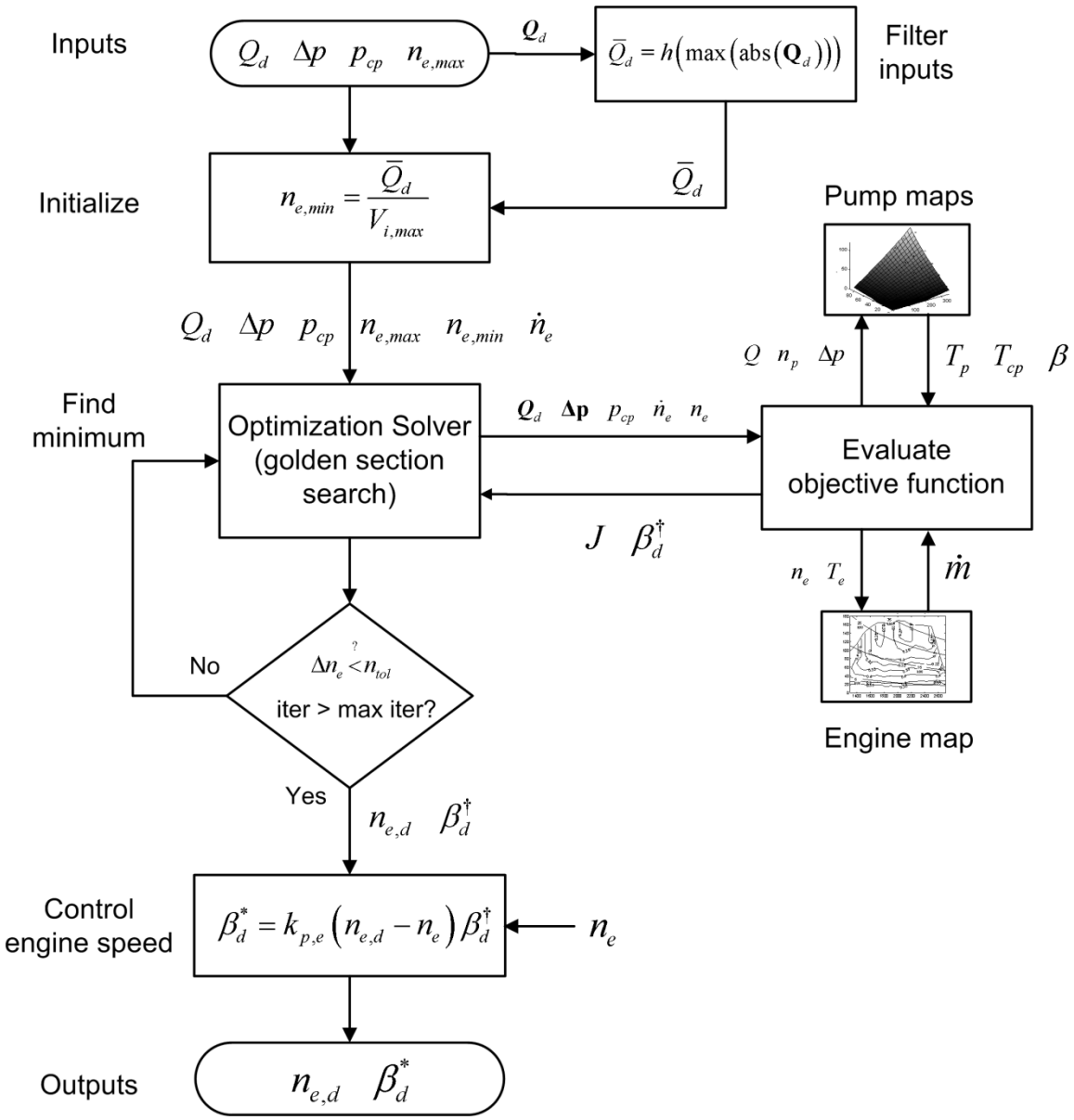

Figure 3.7 Power management flowchart

3.6. Simulation of Optimal Power Management

To demonstrate the proposed power management method, an excavator with DC actuators is simulated. More information about the simulation model will be given in Chapter 4. The purpose here is to provide an example of how the optimization method works and the possible energy and fuel savings.

The duty cycle consists of 2.7 minutes of digging in loose soil. Actuator loads and reference trajectories are based on measurements from the DC excavator. Results from two simulations are presented: with a constant engine speed setpoint and with power management. Figure 3.8 compares moving average and moving maximum methods of filtering operator joystick signals, both with a time window of 7.5 seconds. The moving maximum was used in simulation. Figure 3.9 shows how the engine operating point changes during the simulation.

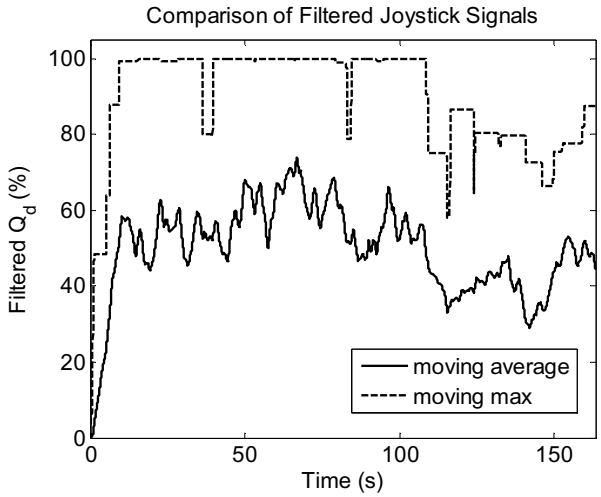

Figure 3.8 Filter comparison for determining minimum engine speed

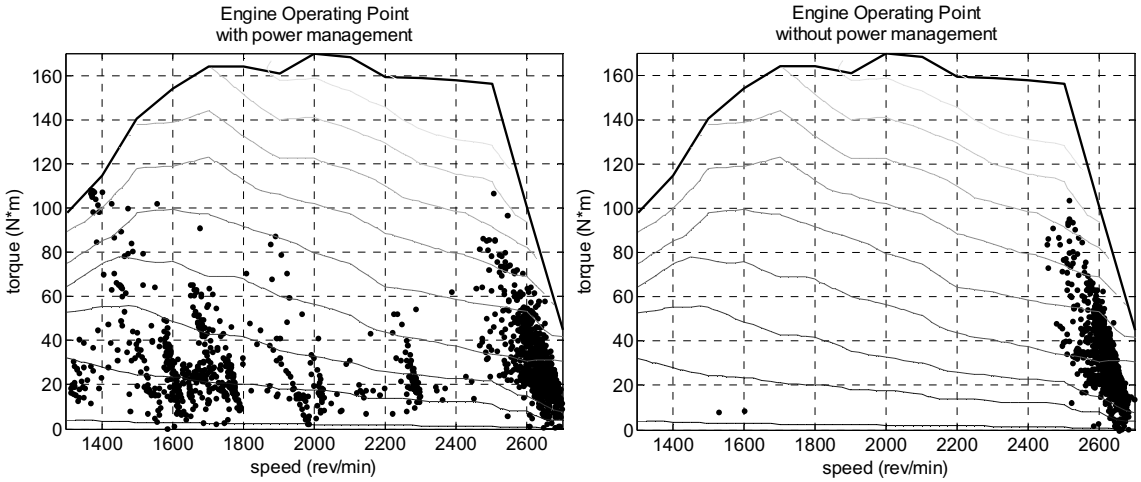

Figure 3.9 Simulated engine operating point with power optimization

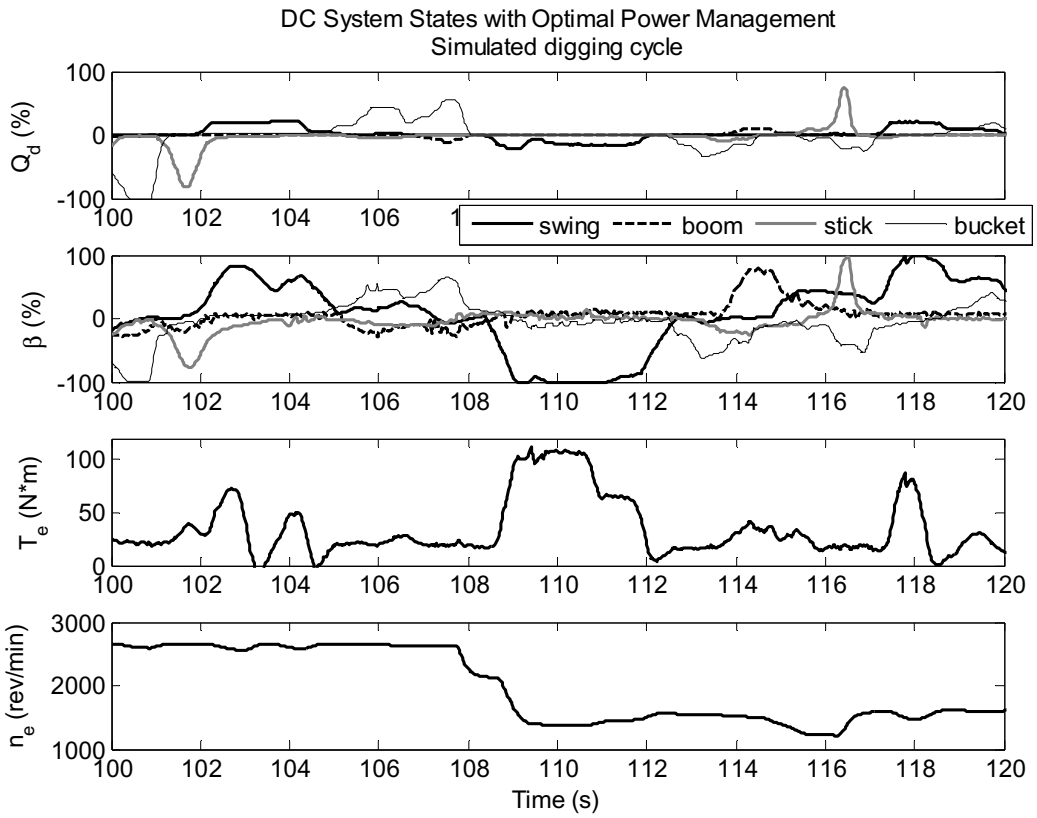

Figure 3.10 Engine and pump operation during simulated digging cycle

Figure 3.10 shows more detail from the simulation, with a 30 second excerpt from the 163 second digging cycle. The top line is the commanded flow rates from the operator for each actuator. The swash plate angles are plotted on the second line, and the engine torque and speed take up the remaining lines. It is evident that the engine speed and pump displacements are adjusted continuously according to the forces and velocities required by the actuators. It is also apparent that the engine speed changes more slowly than the pump displacements, due to the moving speed constraint described previously.

As shown in Table 1, the simulated power management reduces fuel consumption by 13.1%. Energy savings from the servo pumps and charge pump are due to operating at lower speeds where the units have lower power losses.

Table 1. Simulated energy and fuel results

	Actuator Work (kJ)	Pump Losses (kJ)	Charge & cooling (kJ)	Other Losses (kJ)	Total Energy (kJ)	Fuel (g)
No power mgt.	218	382	502	311	1413	176
With power mgt.	225	330	428	311	1294	153
Change (%)	3.2	-13.6	-14.7	0	-8.4	-13.1

3.7. Chapter Summary

- Mobile multi-actuator machines are a diverse class of vehicles spanning a wide range of sizes and applications. In spite of this diversity, their hydraulic systems have similar architectures.
- Traditional valve-controlled hydraulic systems allow little room for optimizing the operating points of the engine and hydraulic pump(s). Displacement controlled systems relax the constraints by decoupling the actuator pressures and flow rates.
- An optimal power management algorithm is proposed which adjusts the engine speed and hydraulic pump displacements in order to minimize fuel consumption. The optimization problem is reduced to one dimension and is solved online. Optimal power management for DC systems is considered for the first time in this work.
- The proposed method is applied to a compact excavator. Simulations of a digging cycle show how the power management method saves energy and fuel by optimizing the system operation.

CHAPTER 4 MULTI-ACTUATOR SYSTEM MODEL

Chapter 4 documents a mathematical model of a DC multi-actuator machine. The chapter begins with a dynamic model of the variable displacement pumps, followed by the actuators and the multi-body mechanics of the machine structure. A comparison of simulations and experimental results at the end of the chapter allows the accuracy of the model to be qualitatively assessed. The model presented in this chapter is not intended to be an original research contribution. Rather, it is included for completeness in support of the simulations presented in Chapter 3 and the control design that follows in Chapter 5.

4.1. Variable Displacement Pump

The heart of a DC hydraulic system is the variable displacement pumps. Axial piston swash plate type pumps are preferred because of their fast dynamic response and high efficiency compared to other pump designs. A cross sectional view of an axial piston type pump is shown in Figure 4.1. There are several common mechanisms for adjusting the swash plate angle β. In the example shown, β is controlled by means of two single-acting cylinders which act against opposite ends of the swash plate. Fluid pressure and flow rate to the cylinders are controlled by a spool-type proportional valve. The swash plate position can be measured directly with an angular position sensor or indirectly with a linear transducer connected to one of the adjustment cylinders.

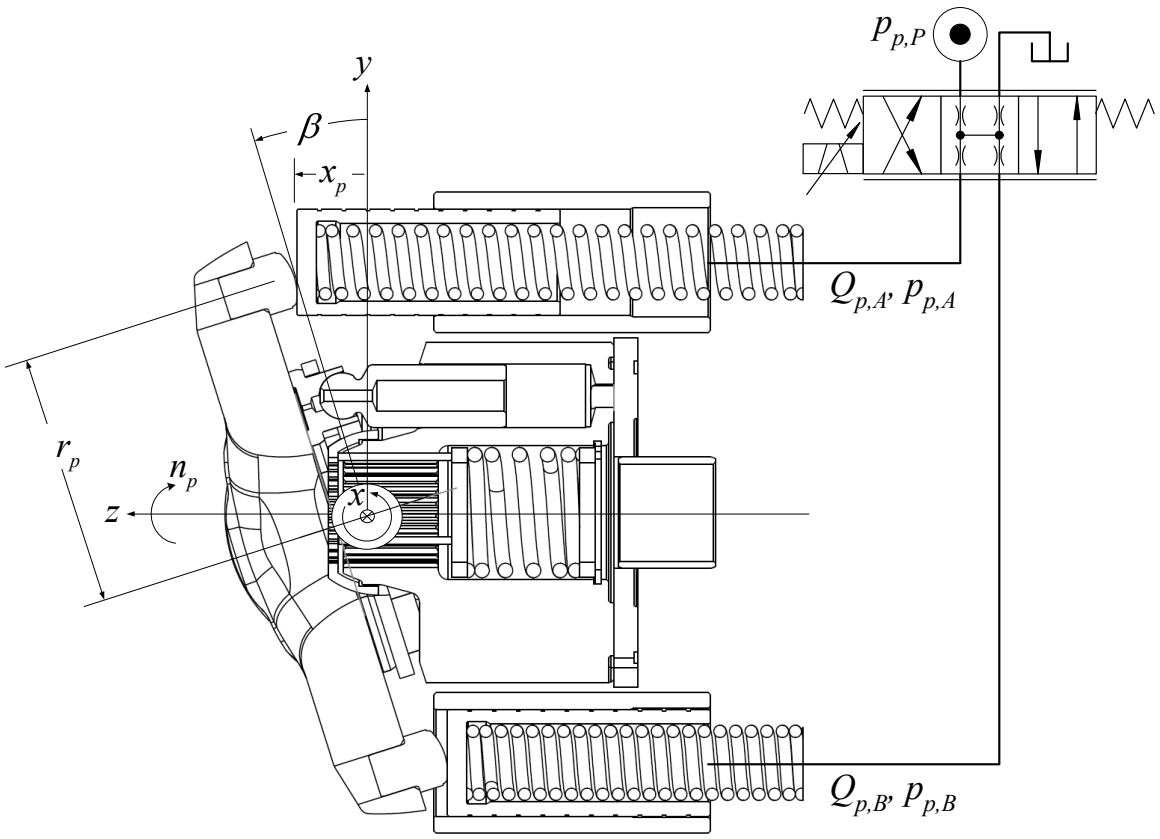

Figure 4.1 Cross section of variable displacement pump

To avoid ambiguity, the mechanical and hydraulic components that vary the pump displacement (control valve, control cylinder, swash plate linkage) are called the pump adjustment system. The swash plate position sensor, control computer and the algorithm for controlling the pump displacement are called the pump control system.

4.1.1. Pump Displacement Adjustment System

Fluid flow rate through the control valve is a function of valve spool position and the pressure difference across the valve, as described by the orifice equation.

$$Q = A\alpha_D \text{sign}(\Delta p)\sqrt{\frac{2}{\rho}|\Delta p|} \qquad \text{Eq. 4.1}$$

So long as the pump adjustment system is sized correctly, the supply pressure $p_{p,P}$ can be assumed to be higher than the pressures $p_{p,A}$ and $p_{p,B}$ in the control cylinders. The return (pump case) pressure is negligible. Constant terms are lumped together into a single flow gain coefficient C_v. The valve orifice area varies linearly with the normalized spool position y and is equal for metering flow in and out. With these simplifications, Eq. 4.1 can be applied to the control valve's four metering orifices in the following equations.

$$Q_{p,A} = y_v C_v \sqrt{p_{p,P} - p_{p,A}} \qquad y_v \geq 0 \qquad \text{Eq. 4.2}$$

$$Q_{p,B} = y_v C_v \sqrt{p_{p,B}} \qquad y_v \geq 0 \qquad \text{Eq. 4.3}$$

$$Q_{p,A} = y_v C_v \sqrt{p_{p,A}} \qquad y_v < 0 \qquad \text{Eq. 4.4}$$

$$Q_{p,B} = y_v C_v \sqrt{p_{p,P} - p_{p,B}} \qquad y_v < 0 \qquad \text{Eq. 4.5}$$

The control valve's dynamic response at a particular amplitude can be approximated by a linear, second order transfer function from the command signal u (a voltage) to the spool position y (Eq. 4.6). Frequency response measurements of a single-stage (direct drive) servo valve are plotted in Figure 4.2. It is clear from the figure that the valve's response depends strongly on the signal amplitude. This nonlinearity can be modeled by combining Eq. 4.6 with a rate limiter.

$$\frac{Y(s)}{U(s)} = \frac{\omega_v^2}{s^2 + 2\zeta_v \omega_v s + \omega_v^2} \qquad \text{Eq. 4.6}$$

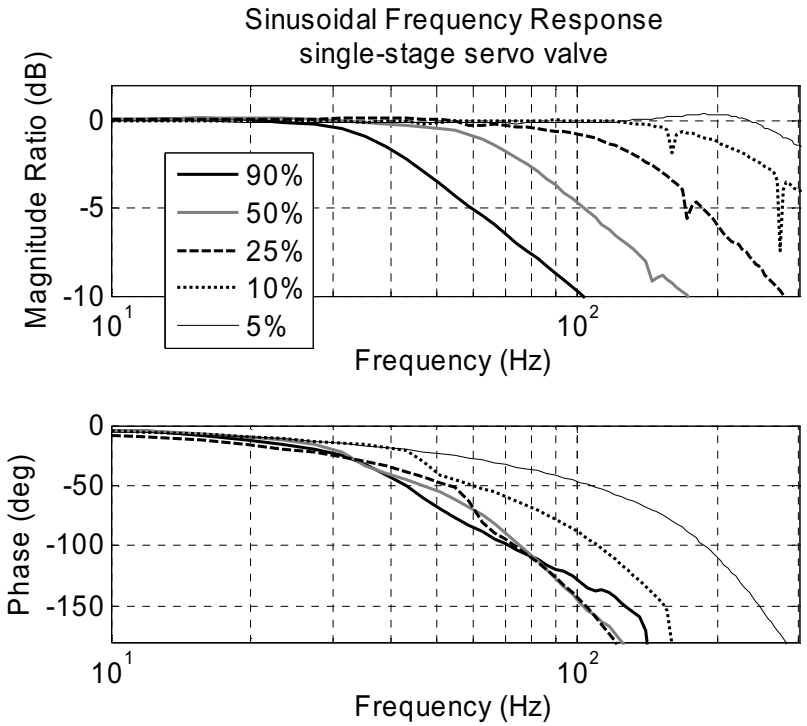

Figure 4.2 Bode plot of valve spool dynamic response

The rate of pressure change in the control cylinder chambers depends on the flow rates in or out and the piston motion, as given by the continuity equations Eq. 4.7 and Eq. 4.8.

$$\dot{p}_{p,A} = \frac{K_{oil}}{V_{p,A}}\left(Q_{p,A} - A_p\dot{x}_p - k_{L,p}p_{p,A}\right) \qquad \text{Eq. 4.7}$$

$$\dot{p}_{p,B} = \frac{K_{oil}}{V_{p,B}}\left(Q_{p,B} + A_p\dot{x}_p - k_{L,p}p_{p,B}\right) \qquad \text{Eq. 4.8}$$

Figure 4.1 shows the pump's internal geometry, with the shaft and bearings removed for clarity. The swash plate angle β is measured from the centered position and can be either positive or negative. With some simple kinematic relationships, the equation of motion for the swash plate Eq. 4.11 can be written

as a function of the control piston forces. Frictional effects from the swash plate bearing and cylinders are lumped together and assumed to be linear with viscous coefficient $f_{v,p}$. The moment M_x acts as a disturbance on the pump adjustment system and will be explained in the next sub-section. The model derived here closely follows the work of Grabbel (2004).

$$x_p = r_p \sin\beta \qquad \text{Eq. 4.9}$$

$$\dot{x}_p = r_p \dot{\beta} \cos\beta \qquad \text{Eq. 4.10}$$

$$I_p \ddot{\beta} = \left(A_p \left(p_{A,p} - p_{B,p} \right) - 2k_x r_p \sin\beta - 2 f_{v,p} r_p \dot{\beta} \cos\beta \right) r_p \cos\beta + M_x \qquad \text{Eq. 4.11}$$

The pump flow rate is a function of the derived displacement volume V_i (Ivantysyn and Ivantysynova, 2001). For the purpose of control design, V_i can be assumed to be proportional to β. The pump's effective discharge flow rate is reduced by volumetric losses Q_s (see Eq. 3.3).

$$\begin{aligned} Q_1 &= n_p V_i - Q_s = Q \qquad V_i \geq 0 \\ Q_2 &= n_p V_i \end{aligned} \qquad \text{Eq. 4.12}$$

$$\begin{aligned} Q_1 &= n_p V_i \qquad V_i < 0 \\ Q_2 &= n_p V_i + Q_s \end{aligned} \qquad \text{Eq. 4.13}$$

For positive β and V_i, Q_1 is the flow rate from the outlet port and Q_2 is the flow rate at the inlet. When the swash plate moves overcenter and $\beta<0$, the flow direction is reversed. The direction of shaft rotation remains constant.

4.1.2. Swash Plate Control Moment

Pistons in the rotating cylinder block exert forces F_N on the swash plate due to the pressure of the fluid being pumped as well as friction and inertia. The normal forces can be resolved into axial and tangential components F_A and F_T. The

resultant piston forces produce moments about each of the coordinate axes, as expressed in the following equations (Ivantysyn and Ivantysynova, 2000).

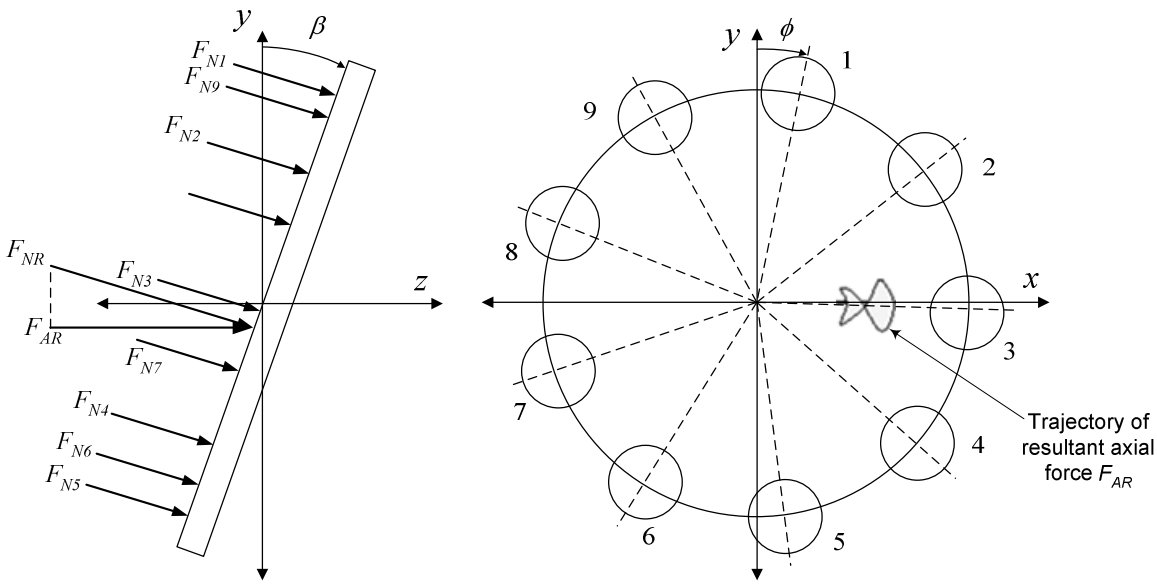

Figure 4.3 Piston forces and resultant axial force

$$M_x = \frac{r_p}{\cos^2(\beta)} \sum_{i=1}^{k} F_{A_i} \cos\phi_i \qquad \text{Eq. 4.14}$$

$$M_y = -r_p \sum_{i=1}^{k} F_{A_i} \sin\phi_i \qquad \text{Eq. 4.15}$$

$$M_z = -r_p \left(\sum_{i=1}^{k} F_{T_i} + \tan\beta \sum_{i=1}^{k} F_{A_i} \sin\phi_i \right) \qquad \text{Eq. 4.16}$$

Moments M_y and M_z are supported by the swash plate bearing. M_x acts about the swash plate's axis of rotation and is supported by the control cylinders. Hence, M_x is an important parameter in the design of the pump adjustment system. M_x must also be considered when designing the pump valve plate, since the valve plate geometry determines the instantaneous cylinder pressure and the

resulting piston forces (Ivantysynova, Grabbel and Ossyra 2002). Because of the rather complicated interactions that contribute to the instantaneous cylinder pressures and the difficulty of measuring these pressures directly, the control moment M_x is best determined by numerical simulation. The CASPAR simulation tool developed by Wieczorek, Ivantysynova and others (2000) allows M_x to be determined for any operating condition.

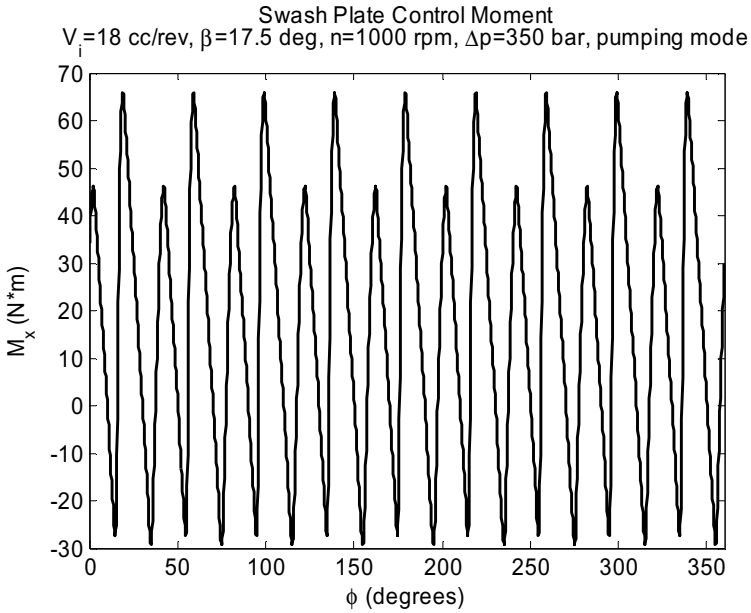

Figure 4.4 Swash plate control moment from CASPAR simulation

Figure 4.4 is a graph of M_x over one shaft revolution for a pump with nine pistons. The period of oscillation is 360°/9 = 40°. At 1000 rpm, the period is 2.2 ms, corresponding to a frequency of 150 Hz. Since there are two peaks per period, the principal frequency component is at roughly 300 Hz. At this frequency, the oscillating moment produces mechanical vibration and audible noise, but the change in swash plate position is negligible. Rather, it is the mean value of M_x that is important to consider for designing the pump adjustment and control systems.

The control moment acts as a disturbance on the pump control system, tending to move the swash plate away from the desired position. For the purpose of simulating swash plate control, it is desirable to create a model that includes M_x at varying operating conditions (i.e. displacement, speed and pressure). To obtain such a model, the pump is simulated with CASPAR at different points across its operating range. A polynomial regression model is then fitted to the simulated M_x data as a function of the operating point. Surface plots of a control moment polynomial are shown in Figure 4.5.

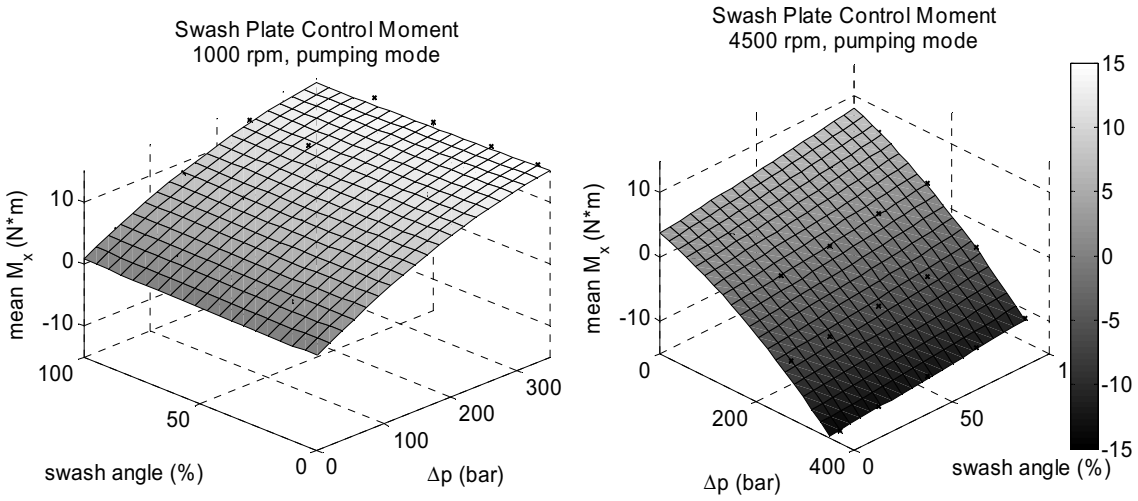

Figure 4.5 Mean control moment over range of pump operating conditions

4.1.3. Simulation and Measurement of Variable Displacement Pump

To validate the model, the frequency response of a pump adjustment system was simulated and measured. Results are plotted in Figure 4.6 and Figure 4.7. In these experiments, the input is a sinusoidal voltage signal to the control valve, and the output is the swash plate position. The pump response was measured at 0 rpm. For visual clarity, the magnitude ratio in dB is calculated relative to 100% displacement, as in Eq. 4.17. As is evident from the figures, there is good agreement between the model and the experimental results.

$$G_{dB}(\omega) = 20\log_{10}\left(\frac{\|u\|_{\infty}}{100}G(\omega)\right) \qquad \text{Eq. 4.17}$$

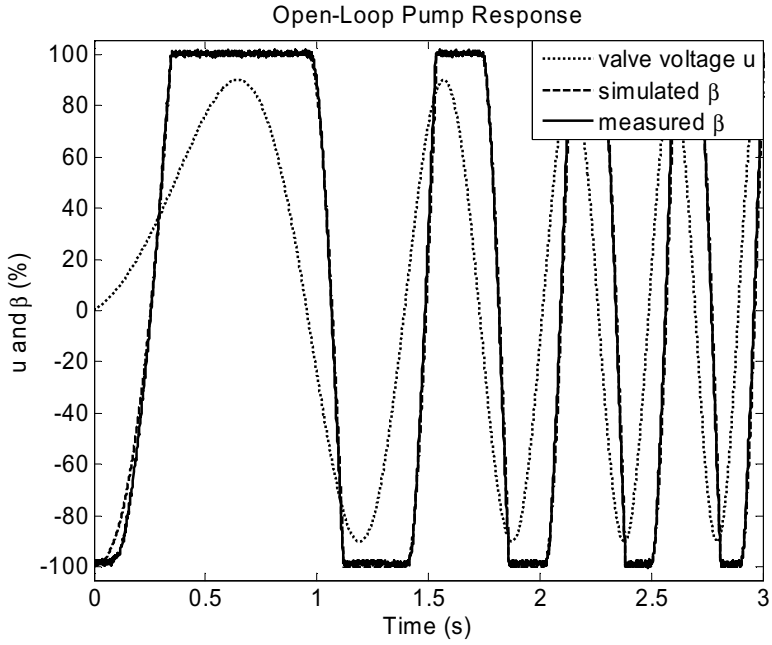

Figure 4.6 Time domain comparison of pump simulation and experiment

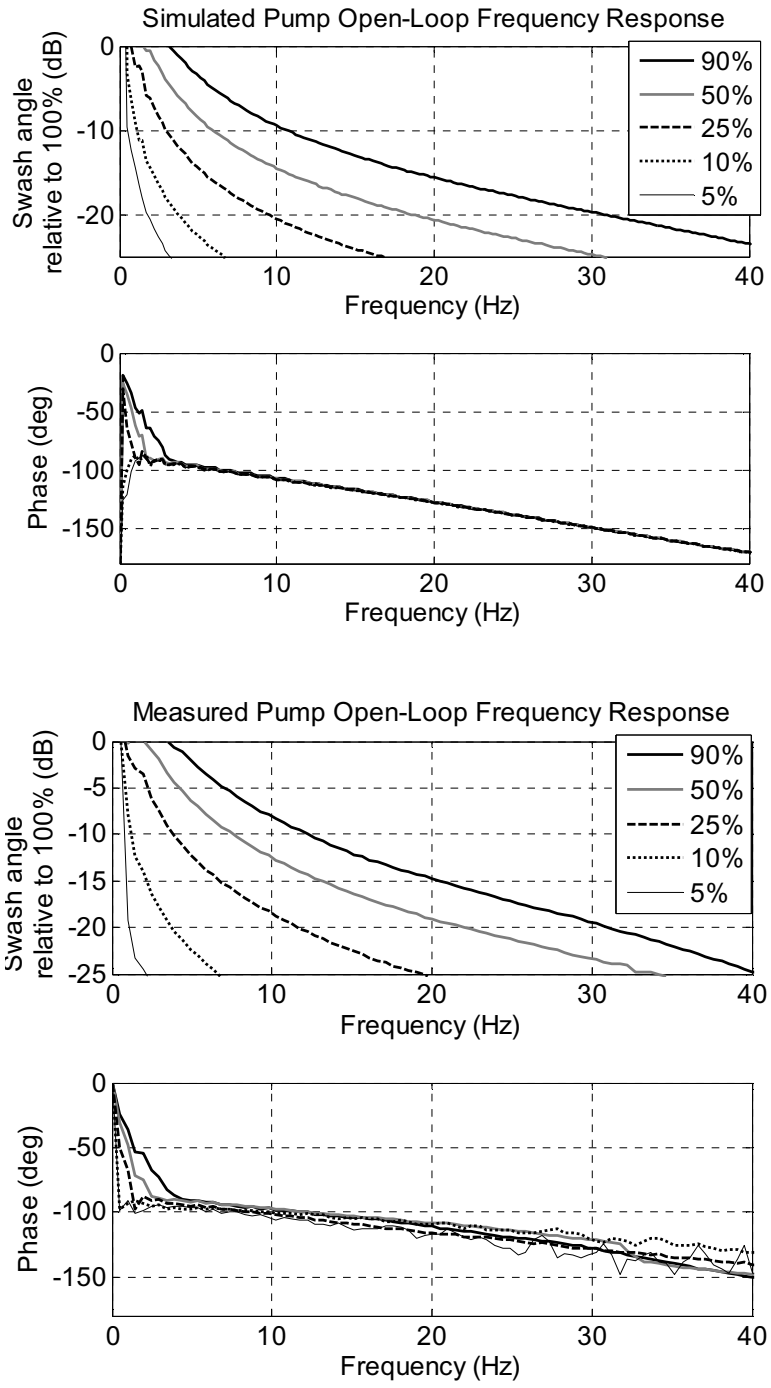

Figure 4.7 Simulated (above) and measured (below) Bode plots of pump adjustment system frequency response

4.2. Linear Actuator

Linear hydraulic actuators of the type shown in Figure 4.8 are very common in mobile applications. The DC excavator is equipped with six such actuators. The dynamic equations for these actuators are similar to the control cylinders in the previous subsection, with Eq. 4.18 and Eq. 4.19 for calculating the pressure rise and Eq. 4.20 for the net actuator force.

$$\dot{p}_A = \frac{K_{oil}}{V_A}\left(Q_A - A_A\dot{x}_{act} - Q_L\right) \qquad \text{Eq. 4.18}$$

$$\dot{p}_B = \frac{K_{oil}}{V_B}\left(-Q_B + A_B\dot{x}_{act} + Q_L\right) \qquad \text{Eq. 4.19}$$

$$F_{act} = p_A A_A - p_B A_B - F_f - F_L \qquad \text{Eq. 4.20}$$

The leakage and friction characteristics of the actuator seals affect the actuator system dynamics. Internal leakage Q_L across the piston seal is modeled by Eq. 4.21 as a function of relative pressure and velocity.

$$Q_L = k_L\left(p_A - p_B\right) - k_{Lv}\dot{x}_{act} \qquad \text{Eq. 4.21}$$

$$F_f = f_s e^{-\tau_s|v|}\operatorname{sgn}(v) + f_C\operatorname{sgn}(v) + f_v v \qquad \text{Eq. 4.22}$$

$$F_f = f_s e^{-\tau_s|\dot{x}_{act}|}\tanh(\gamma\dot{x}_{act}) + f_C\left(p_A + p_B\right)\tanh(\gamma\dot{x}_{act}) + f_v\dot{x}_{act} \qquad \text{Eq. 4.23}$$

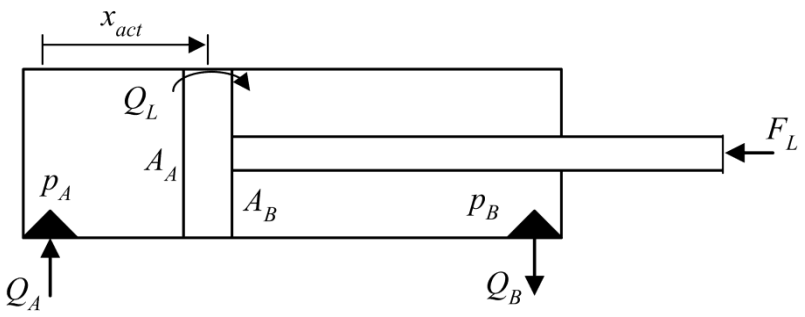

Figure 4.8 Single-rod, double-acting hydraulic cylinder

The well-known Stribeck equation (Eq. 4.22) models mixed friction with static, Coulomb and viscous terms. Friction curves for hydraulic actuator seals follow a similar trend, although friction force is a function of fluid pressure as well. Eq. 4.23 adapts the Stribeck curve to the present application with pressure-dependent Coulomb force and the hyperbolic tangent function as a continuous approximation of sgn(v). Friction coefficients are identified experimentally (Williamson and Ivantysynova, 2009).

4.3. Rotary Actuator

Hydraulic motors are modeled similar to the linear actuators. Internal leakage is proportional to the differential pressure $\Delta p = p_A - p_B$, and external leakage is proportional to absolute pressure. Motor friction is also modeled similar to the linear actuator, with viscous and Coulomb terms. The net actuator torque is given by Eq. 4.25.

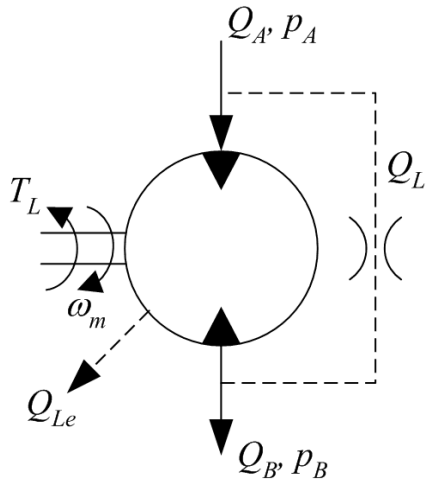

Figure 4.9 Schematic diagram of hydraulic motor

$$\dot{p}_A = \frac{K_{oil}}{V_A}\left(Q_A - n_m V_m - k_{L,m}\Delta p - k_{Le,m} p_A\right)$$

$$\dot{p}_B = \frac{K_{oil}}{V_B}\left(-Q_B + n_m V_m + k_{L,m}\Delta p - k_{Le,m} p_B\right)$$

Eq. 4.24

$$T_m = \frac{V_m \Delta p}{2\pi} - f_{v,m}\omega_m - f_{C,m}\,\mathrm{sign}(\omega) - T_L$$

Eq. 4.25

4.4. Transmission Lines

Pressure losses in the transmission lines between the pumps and actuators are modeled in the way with lumped resistances. Pressure drop due to viscous friction for laminar flow through hoses is calculated with Eq. 4.26. Losses due to the change of fluid momentum in fittings, bends and other restrictions are calculated with Eq. 4.27, where ξ is the drag coefficient associated with each component. The individual coefficients can be lumped into a single coefficient C_D which is identified experimentally.

$$\Delta p = \left(\frac{64}{\mathrm{Re}}\right)\left(\frac{l}{d}\right)\left(\frac{\rho}{2}\right)v^2 = \frac{128\mu l}{\pi d^4}Q \qquad \text{Eq. 4.26}$$

$$\Delta p = \sum \xi \left(\frac{\rho}{2}\right)v^2 = \left(\frac{8\rho}{\pi^2}\right)Q^2 \sum \frac{\xi}{d^4} = C_D Q^2 \qquad \text{Eq. 4.27}$$

Transient flow effects due to hydraulic inductance are modeled with Eq. 4.28. In the case of the prototype excavator system, the effect of hydraulic inductance is negligible for the swing and boom functions. However, the hoses to the stick and bucket cylinders are long enough that inductance does have a small but noticeable effect (5 to 10 bar) on actuator pressures for transient flows.

$$\Delta p = \frac{\rho l}{A}\dot{Q} \qquad \text{Eq. 4.28}$$

4.5. Multi-body Dynamics

In addition to the hydraulic system, the multi-body dynamics of the multi-actuator machine must also be considered. An analytical model based on the classical Lagrange-Euler method is described here. The Lagrange-Euler formulation of multi-body equations of motion is based on the mechanical energy of the machine. In Eq. 4.29, L is the Lagrangian function, K represents the system's kinetic energy, and P is its potential energy. The Lagrange-Euler formula (Eq. 4.30) relates the Lagrangian function to the torques τ at each joint. The relative angles between joints are θ, and $\mathbf{r}_{0,i}$ is the position vector from coordinate frame 0 to the mass center of body i.

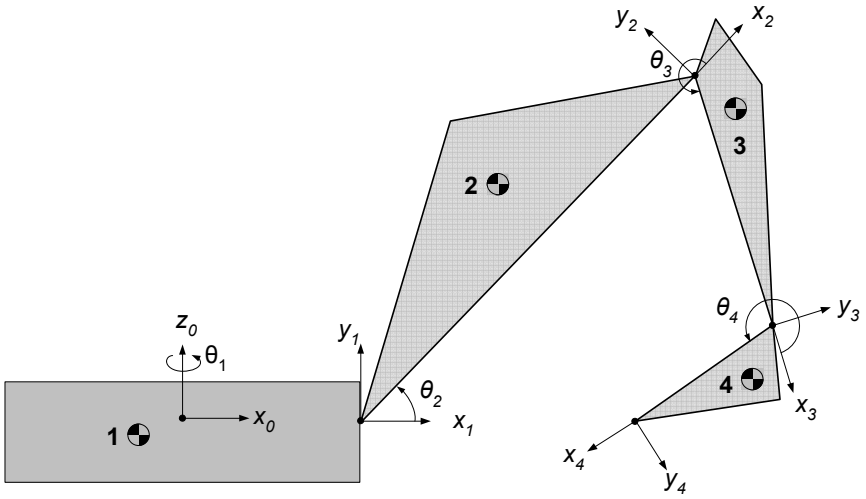

Figure 4.10 Example definition of machine linkage and coordinate reference frames

$$L = K - P = \frac{1}{2}\dot{\boldsymbol{\theta}}^T \mathbf{M}\dot{\boldsymbol{\theta}} + \sum_{i=1}^{n} m_i \mathbf{g}^T \mathbf{r}_{0,i} \qquad \text{Eq. 4.29}$$

$$\frac{d}{dt}\left(\frac{\partial L}{\partial \dot{\theta}_i}\right) - \frac{\partial L}{\partial \theta_i} = \tau_i \qquad \text{Eq. 4.30}$$

After calculating the partial derivatives and gathering terms, Eq. 4.30 can be rewritten as a matrix equation Eq. 4.31 where **M** is the symmetric inertial matrix, **V** contains centripetal and coriolis terms and **G** represents torques due to gravitational acceleration. The torque vector **τ** is the net torque applied to each joint by the actuator. For rotary actuators, the net torque is simply T_m from Eq. 4.25 multiplied by a gear ratio (if applicable), i.e. $\tau_1 = i_1 T_m$. For the other joints, joint torque is calculated from linear actuator force with the kinematic Jacobian $dx/d\theta$ as in Eq. 4.32. Hence, the right side of Eq. 4.31 is the sum of torques due to friction, load, and actuator pressure, and the left side contains products of inertia and acceleration. For solving forward dynamics or writing state equations, Eq. 4.31 is rearranged to form Eq. 4.33.

$$\mathbf{M}(\boldsymbol{\theta})\ddot{\boldsymbol{\theta}}+\mathbf{V}\left(\boldsymbol{\theta},\dot{\boldsymbol{\theta}}\right)+\mathbf{G}(\boldsymbol{\theta})=\boldsymbol{\tau} \qquad \text{Eq. 4.31}$$

$$\tau_i=\frac{\partial x}{\partial \theta}F_{act,i} \qquad \text{Eq. 4.32}$$

$$\ddot{\boldsymbol{\theta}}=\mathbf{M}^{-1}\left(\boldsymbol{\tau}-\mathbf{G}-\mathbf{V}\right) \qquad \text{Eq. 4.33}$$

4.6. Simulation and Measurement of a Multi-Actuator Machine

The equations in the preceding sections model the dynamic behavior of a generic multi-actuator machine. As an example, a compact excavator has been modeled with Mathworks Matlab/Simulink software (Zimmerman, 2008). The multi-body dynamics were modeled with commercial code (SimMechanics) rather than the analytical method described in section 4.5 for reduced computation time. The hydraulic system was modeled with the equations in sections 4.1 through 4.4. Simulation results can be visualized with a 3D animation (Figure 4.11). Duty cycles are defined by actuator positions and loads, which are derived from measured positions and pressures on a real excavator (Zimmerman, 2008).

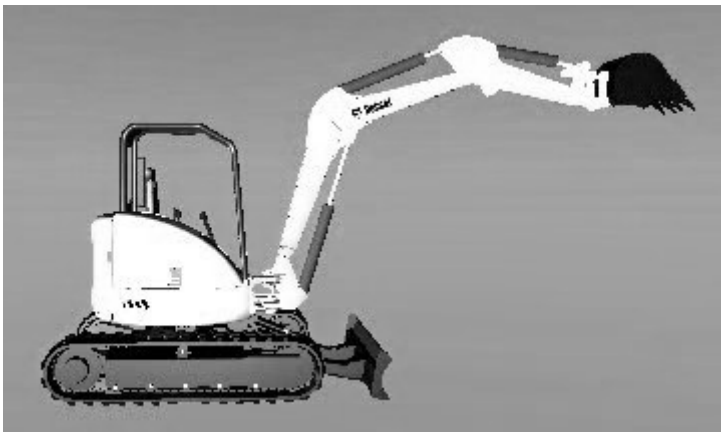

Figure 4.11 Screen view of excavator animation

Simulated and experimental results are compared for a truck loading cycle. The duty cycle was measured with a professional operator over an interval of 197 seconds (3.3 minutes), in which 20 buckets of loose soil were loaded into a truck located 90° from the excavation. Actuator position s and pressures are plotted in Figure 4.13 through Figure 4.12 for a portion of the cycle (t = 10 to 30 seconds). The mean error between measured and simulated actuator positions was <3% of full scale for all actuators. Mean pressure error was <7% for the linear actuators and 28% for the swing motor. The mean error in engine speed was <3%. The mass of fuel combusted during the simulated cycle was 311 g. Measured fuel consumption was 295±2.5 g, a difference of 5.1%.

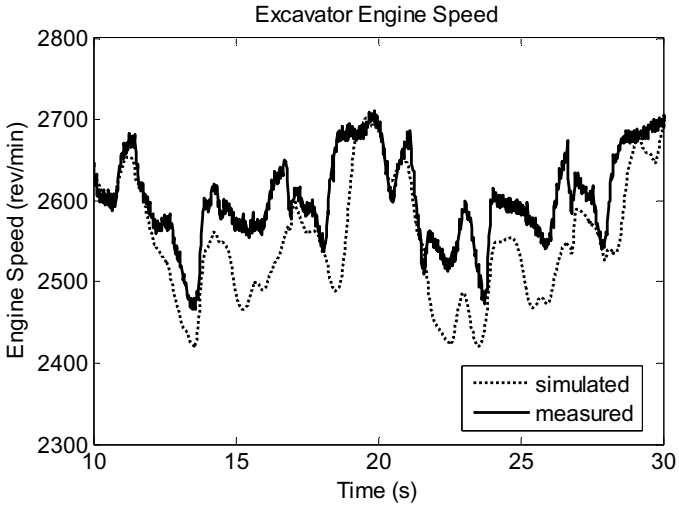

Figure 4.12 Engine speed, comparison of model and experiment

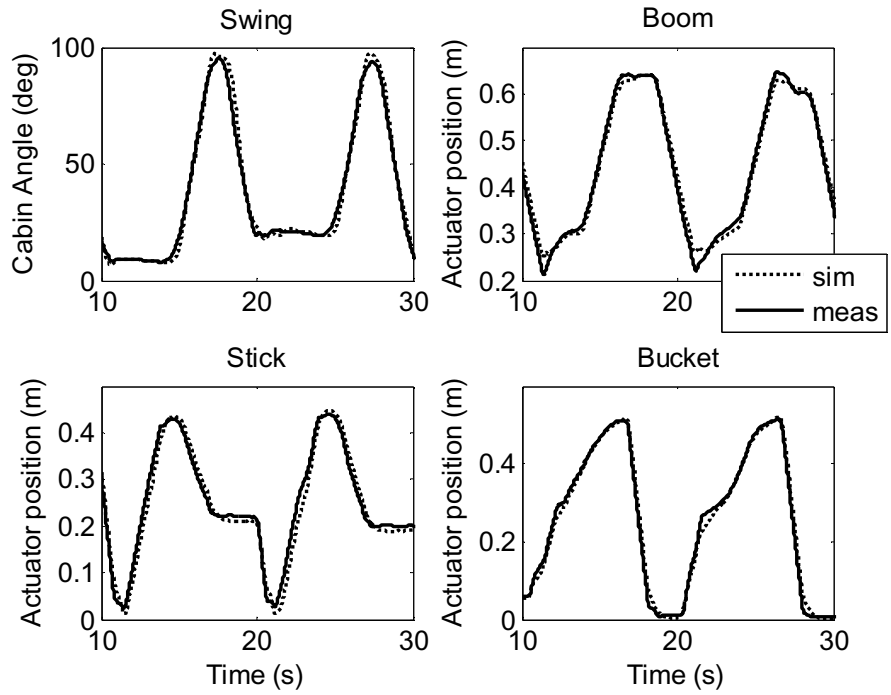

Figure 4.13 Actuator positions, comparison of model and experiment

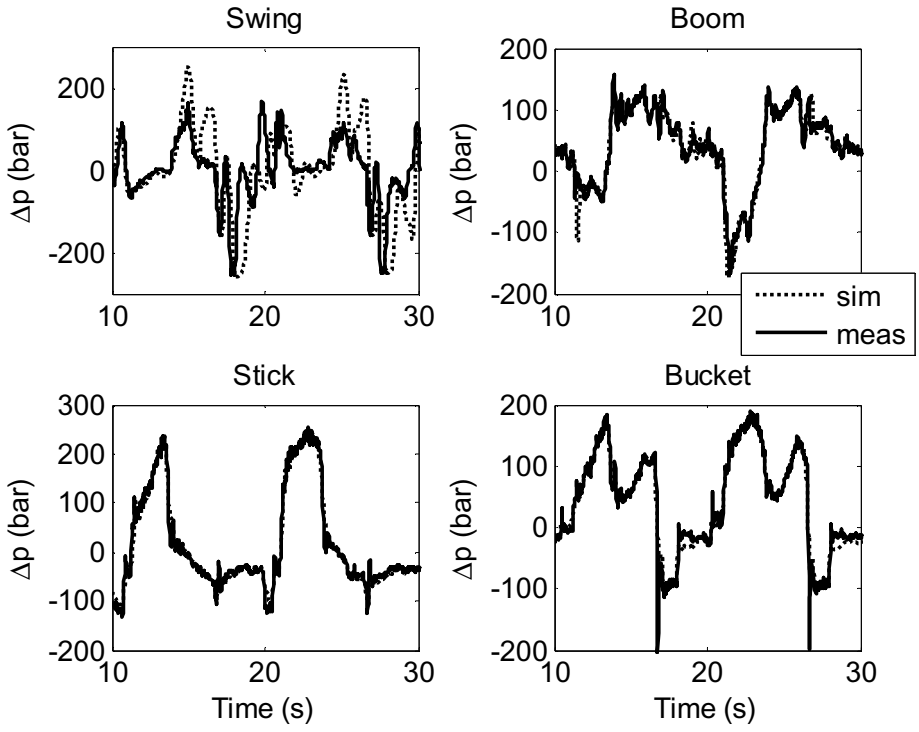

Figure 4.14 Actuator differential pressure, comparison of model and experiment

4.7. Chapter Summary

- A mathematical model was derived to describe the dynamics of a multi-actuator machine with DC hydraulic actuators. Nonlinear ordinary differential equations model the dynamics of variable displacement pumps, linear actuators, rotary actuators, transmission lines and mechanical linkages.
- Simulations and measurements of an excavator are compared to provide confidence in the accuracy of the model. The deviation between measured and predicted fuel consumption was 5.1%. Simulated actuator positions and pressures also correlated well with the experiments.
- The mathematical models in this chapter are included for completeness and are not intended to be an original research contribution. Instead, the models support the development of new system-level and component-level control methods which are the subject of the present work.

CHAPTER 5 CONTROL DESIGN AND ANALYSIS

As explained in chapter 3, power management in DC multi-actuator machines relies on control laws at the sub-system and component levels to realize the desired system trajectory. Chapter 5 focuses on the design and analysis of control laws for electro-hydraulic variable displacement pumps and displacement controlled linear actuators. The work of previous researchers is presented, and shortcomings are pointed out that necessitate novel contributions. In section 5.1, a new swash plate control law is proposed that is robust to variations in supply pressure and control moment. In section 5.2, new analysis and experiments demonstrate that the DC actuator is unstable under certain conditions. Solutions are presented for stabilizing the actuator system by passive design and active control.

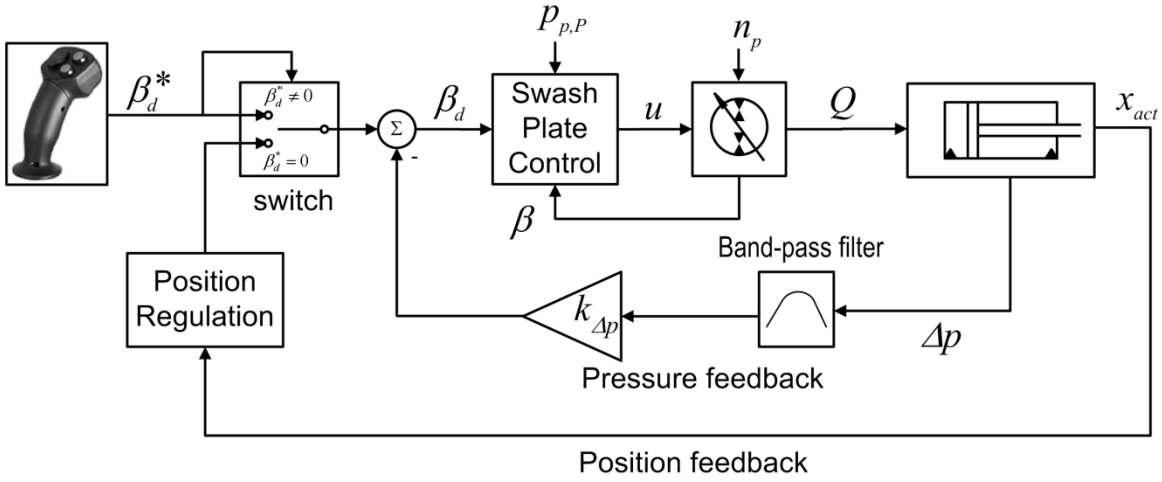

Figure 5.1 Overview of DC actuator control system

Figure 5.1 describes the DC excavator control system in block diagram form. The control system is structured in three nested feedback loops. The pump displacement control is the innermost subsystem and is responsible for controlling the swash plate position β. A pressure feedback loop increases the actuator stability. The outer loop is a switched actuator position and velocity control (Rahmfeld, 2002). When the operator input (joystick angle) is nonzero, the control system operates in an open-loop velocity mode where the operator input is interpreted as a pump displacement reference signal. In this mode, the operator closes the loop around the actuator velocity and position. When the joystick signal is zero, a closed-loop position control law holds the current actuator position.

5.1. Pump Displacement Control

5.1.1 Nonlinear Pump Model

To begin, a simplified model is derived based on the pump dynamic model from section 4.1 (Grabbel, 2004). The dynamic equations for the control valve (Eq. 5.1) and the control piston pressures (Eq. 5.2) are repeated here for convenience.

$$\frac{Y(s)}{U(s)} = \frac{\omega_v^2}{s^2 + 2\zeta_v \omega_v s + \omega_v^2} \qquad \text{Eq. 5.1}$$

$$\dot{p}_{p,A} = \frac{K_{oil}}{V_{p,A}}\left(Q_{p,A} - A_p \dot{x}_p - k_{Lp} p_{p,A}\right) \qquad \text{Eq. 5.2}$$

$$\dot{p}_{p,B} = \frac{K_{oil}}{V_{p,B}}\left(Q_{p,B} + A_p \dot{x}_p - k_{Lp} p_{p,B}\right)$$

Assuming that $V_{p,A} = V_{pB} = V_p$ and $Q_{p,A} = -Q_{p,B}$, the two pressure states can be combined into a single differential pressure $\Delta p_p = p_{p,A} - p_{p,B}$.

$$\Delta\dot{p} = \frac{K_{oil}}{V_p}\left(2Q_p - 2A_p\dot{x}_p - k_{Lp}\Delta p_p\right) \qquad \text{Eq. 5.3}$$

With the same assumption of equal flow rates $Q_{p,A} = -Q_{p,B}$, the equations for the valve's four metering orifices can also be reduced to a single equation, Eq. 5.4.

$$Q_p = C_v y\sqrt{\frac{1}{2}\left(p_{p,P} - \Delta p_p\right)} \qquad \text{Eq. 5.4}$$

The equation of motion for the swash plate and control pistons (Eq. 4.11) is repeated here as Eq. 5.5.

$$I_p\ddot{\beta} = \left(A_p\left(p_{A,p} - p_{B,p}\right) - 2k_x r_p \sin\beta - 2f_{v,p}r_p\dot{\beta}\cos\beta\right)r_p\cos\beta + M_x \qquad \text{Eq. 5.5}$$

Since the maximum range of β for swash plate type pumps is less than ±21°, a small-angle approximation is acceptable. Let $\sin\beta = \beta$ and $\cos\beta = 1$, which yields Eq. 5.6.

$$I_p\ddot{\beta} = \left(A_p\Delta p_p - 2k_x r_p\beta - 2f_{v,p}r_p\dot{\beta}\right)r_p + M_x \qquad \text{Eq. 5.6}$$

The preceding equations can now be assembled into a nonlinear state-space model of the pump adjustment system, Eq. 5.7. There is a second order transfer function between u and y_v. Hence, the pump is a fifth order SISO system from u to β, or the relative degree between u and β is 4.

$$\begin{aligned}
\dot{x}_1 &= \Delta\dot{p}_p = \frac{K_{oil}}{V_p}\left(2C_v y_v\sqrt{\frac{1}{2}\left|p_{p,P} - \Delta p_p\right|} - 2A_p r_p\dot{\beta} - k_{L,p}\Delta p_p\right) \qquad \text{Eq. 5.7}\\
\dot{x}_2 &= \ddot{\beta} = \frac{1}{I_p}\left(\left(A_p\Delta p_p - 2k_x r_p\beta - 2f_{v,p}r_p\dot{\beta}\right)r_p + M_x\right)\\
\dot{x}_3 &= \dot{\beta} = x_2
\end{aligned}$$

5.1.2 Linear Reduced Order Pump Model

If the state equations Eq. 5.7 are linearized and the eigenvalues are calculated, it has been shown that the eigenvalues corresponding to the valve dynamics are much slower than those from the pump adjustment system (Grabbel and Ivantysynova, 2005). For the variable displacement pumps on the DC excavator, the swash plate has a resonant frequency between 750 and 900 Hz. In comparison, the bandwidth of single stage servo valves is <300 Hz for small amplitudes and <100 Hz for the large amplitudes required at typical supply pressure levels.

Slower poles dominate, so the pump response is primarily determined by the valve dynamics. The model Eq. 5.7 can be then simplified to neglect swash plate inertia and oil compressibility. With these assumptions, the swash plate velocity is proportional to the flow rate through the control valve (Eq. 5.8). Dividing by the control cylinder stroke $x_{p,max}$ normalizes the velocity.

$$\dot{\beta} = \frac{Q_p}{A_p x_{p,max}} \qquad \text{Eq. 5.8}$$

The pump model can be further simplified by assuming small motions. Then limits (saturations) on swash plate position and velocity are neglected, and the valve flow rate varies linearly with spool position: $Q_p = y_v C_q$.

$$\dot{\beta} = \frac{y_v C_q}{A_p x_{p,max}} = c_p y_v \qquad \text{Eq. 5.9}$$

$$\frac{\beta(s)}{U(s)} = \frac{c_p}{s} \cdot \frac{\omega_v^2}{s^2 + 2\zeta_v \omega_v s + \omega_v^2} \qquad \text{Eq. 5.10}$$

Combined with the valve dynamics (Eq. 5.1), the linearized pump adjustment system model can be written as a third order transfer function, Eq. 5.10. A linear control law (e.g., transfer function) can then be designed based on this plant

model. This is the approach that has been used in prior work. For robustness, Grabbel and Ivantysynova considered variation in the servo valve parameters ζ_v and ω_v (2005). Dean and Fales considered uncertainty in the bulk modulus K_{oil} and the valve flow coefficient C_v (2007).

5.1.3 Nonlinear Reduced Order Pump Model

In the previous two sub-sections, plant model simplifications and control design have been based on previous work by other authors. The resulting control law is simple to implement and considers variation in some of the plant parameters. It also offers better performance than traditional PID control. However, there are some limitations. First, like all fixed-gain robust controllers, the design must be conservative. Guaranteeing stability for the worst-case parameter values usually means reduced performance for typical values. Second, the previous approach neglects the control moment M_x and variations in control valve supply pressure, which act as disturbances on the pump control system. A nonlinear control law which considers these effects may offer better robustness.

One of the basic approaches to nonlinear control design is feedback linearization. That is, designing a model-based control law so that the input cancels the nonlinear terms of the system. The difficulty with the pump adjustment system Eq. 5.7 is that the nonlinear terms are mismatched, separated from the input channel by integration. For example, the input u is integrated three times before reaching the state equation containing M_x. Mismatching can be overcome by integrator backstepping, inputting the derivative of the term to be compensated (Khalil, 2007). However, numerical derivatives of measured signals are often noisy, and higher order derivatives like $\dddot{p}_{p,P}$ and $\ddddot{M}_x$ could be very difficult to implement in practice. Therefore, a reduced order model is still desirable.

In order to design a robust, nonlinear pump control law, a new method for simplifying the pump dynamic model will now be presented. To begin, consider Eq. 5.8, derived in the previous subsection. Rather than linearizing the relationship between u and Q_p, a nonlinear model can be derived that includes the aforementioned disturbances while preserving the desired low model order. Previously, the model order was reduced from five to three by neglecting the effects of swash plate inertia and fluid compressibility. This assumption does not imply that all forces and moments on the swash plate are constant or zero, only that the swash plate remains in static equilibrium. By setting $I_p = 0$, Eq. 5.6 becomes Eq. 5.11, and it is apparent that the pressures in the control cylinders must be sufficient to balance forces from spring stiffness, friction and control moment M_x. Neglecting viscous friction (which is smaller than the other forces) and rearranging the equation gives Eq. 5.12.

$$\left(A_p\left(p_A - p_B\right) - 2k_x r_p \beta - 2f_{v,p} r_p \dot{\beta}\right) r_p + M_x = 0 \qquad \text{Eq. 5.11}$$

$$p_A - p_B = \frac{2k_x r_p^2 \beta - M_x}{A_p r_p} \qquad \text{Eq. 5.12}$$

Now return to the nonlinear valve flow equations Eq. 4.2 and Eq. 4.3 and solve for pressure. It may be noted that these are static equations, unrelated to fluid compressibility.

$$Q_A = y_v C_v \sqrt{p_{p,P} - p_A} \quad \rightarrow \quad p_{p,P} - p_A = \left(\frac{Q_A}{y_v C_v}\right)^2 \qquad \text{Eq. 5.13}$$

$$Q_B = y_v C_v \sqrt{p_B} \quad \rightarrow \quad p_B = \left(\frac{Q_B}{y_v C_v}\right)^2$$

The assumption of an infinitely stiff fluid implies that $Q_A = -Q_B = Q_p$, so Eq. 5.12 and Eq. 5.13 can be substituted into Eq. 5.14 and rearranged to solve for Q_p (Eq. 5.15).

$$p_{p,P} = \left(p_{p,P} - p_A\right) + \left(p_A - p_B\right) + p_B \qquad \text{Eq. 5.14}$$
$$= 2\left(\frac{Q_p}{y_v C_v}\right)^2 + \frac{2k_x r_p^2 \beta - M_x}{A_p r_p}$$

$$Q_p = y_v C_v \sqrt{\frac{1}{2}\left(p_{p,P} - \frac{2k_x r_p \beta}{A_p} + \frac{M_x}{A_p r_p}\right)} \qquad \text{Eq. 5.15}$$

Substituting this expression into Eq. 5.8 gives a nonlinear, reduced-order model of the pump dynamics.

$$\dot{\beta} = \frac{Q_p}{A_p x_{p,max}} = \frac{y_v C_v}{A_p x_{p,max}} \sqrt{\frac{1}{2}\left(p_{p,P} - \frac{1}{A_p}\left(2k_x r_p \beta - \frac{M_x}{r_p}\right)\mathrm{sgn}\left(y_v\right)\right)} \qquad \text{Eq. 5.16}$$

When making this substitution, it is necessary to insert the signum (sign) function sgn(y_v), since $x \cdot \mathrm{sgn}(x) > 0$. In this way, the direction of the centering spring and control moments is independent of the valve position, as they should be. The additional term must be added to correct for the fact that there are two sets of valve flow equations, depending on the sign of y_v.

Eq. 5.16 can be understood intuitively by recognizing that the pressures in the control cylinders must counter forces from the centering springs and the control moment. Flow rate is determined by pressure, so forces on the swash plate change the available flow rate through the control valve and the corresponding swash plate velocity. The centering springs reduce velocity while stroking the swash plate and increase velocity while de-stroking the swash plate. The control moment effectively decreases swash plate velocity in one direction and increases it in the other.

The reduced-order model derived here is a good step toward the stated goal of designing a linearizing control law without integrator backstepping. However, the control input and the nonlinear terms to be compensated are still separated by the valve dynamics, Eq. 5.1. To avoid this obstacle, consider the frequency

content of the terms to be compensated. In DC hydraulic systems, the control supply pressure $p_{p,P}$ is provided by a fixed displacement charge pump and a low pressure accumulator, which also supply fluid to compensate for the differential cylinder volumes in each actuator circuit (see Figure 3.3). A cooling fan and other auxiliary functions may also be connected to the same low pressure supply line. Consequently, the control pressure fluctuates according to the actuator motion and the auxiliary requirements, which is less than 10 Hz in frequency. Similarly, the control moment M_x is primarily a function of shaft speed (<2 Hz) and pump pressure (which is related to the cylinder eigenvalues, also <10 Hz). In comparison, the valve poles are at 50 – 300 Hz. Therefore, for the purposes of feedback linearization, the valve dynamics can be neglected by letting $u = y_v$. The pump adjustment system then reduces to a first order differential equation, Eq. 5.17, and all of the terms are matched to the input.

$$\dot{\beta} = \frac{uC_v}{A_p x_{p,max}} \sqrt{\frac{1}{2}\left(p_{p,P} - \frac{1}{A_p}\left(2k_x r_p \beta - \frac{M_x}{r_p} \right) \mathrm{sgn}(u) \right)} \qquad \text{Eq. 5.17}$$

A few comments may be helpful to clarify the purpose of the simplified pump model which has just been derived. The state-of-the-art approach to servo pump control outlined in the previous sub-section is based on the assumption that the swash plate response is primarily determined by the control valve characteristics, and other effects are of secondary importance. This assumption is valid in many cases, such as when the valve bandwidth is relatively low (e.g. a proportional valve) and the control supply pressure is nearly constant (such as in an industrial installation). In other situations, the control valve response may have less effect than other factors, and the previous assumption is invalid. Supply pressure may vary more in a mobile hydraulic system, for example. Or the pump design may be such that the control moment M_x and the centering springs required to

overcome it may substantially affect the pump's dynamic response. In such cases, the new method proposed here is more appropriate.

5.1.4 Swash Plate Position Control Law

A nonlinear sliding mode control (SMC) is proposed, with explicit compensation for variations in the pump supply pressure and control moment. For notational clarity, the state equation Eq. 5.17 is rewritten in terms of a vector of known functions φ, uncertain parameters θ_p and unmodeled quantities Δ.

$$\dot{\beta} = u b_p \sqrt{\varphi^T \theta_p + \Delta} \qquad \text{Eq. 5.18}$$

$$\varphi^T = \begin{pmatrix} p_{p,P} & \beta \operatorname{sgn}(u) & \operatorname{sgn}(u) \end{pmatrix} \qquad \text{Eq. 5.19}$$

$$\theta_p = \begin{pmatrix} 1 & -\dfrac{2k_x r_p}{A_p} & -\dfrac{M_x}{A_p r_p} \end{pmatrix}$$

The control input u has two parts: a feedforward term u_{ff} for compensating for known dynamics and a feedback term u_{fb} for overcoming uncertainty, Eq. 5.20. $\hat{\theta}_p$ is a vector of parameter estimates, β_d is the desired swash plate angle, and e is the position error $e = \beta - \beta_d$.

$$u = u_{ff} + u_{fb} \qquad \text{Eq. 5.20}$$

$$u_{ff} = \frac{\dot{\beta}_d}{\hat{b}_p \sqrt{\varphi^T \hat{\theta}_p}}$$

$$u_{fb} = -H \cdot \operatorname{sgn}(e)$$

Applying the control input to the system state equation, the error dynamics can be calculated in Eq. 5.21.

$$\begin{aligned}\dot{e} &= \dot{\beta} - \dot{\beta}_d \\ &= \left(u_{ff} + u_{fb}\right) b_p \sqrt{\varphi^T \theta_p + \Delta} - \dot{\beta}_d \\ &= \dot{\beta}_d \left(\frac{\sqrt{\varphi^T \theta_p + \Delta}}{\sqrt{\varphi^T \hat{\theta}_p}} - 1 \right) - H \cdot \mathrm{sgn}(e) \cdot b_p \sqrt{\varphi^T \theta_p + \Delta}\end{aligned} \qquad \text{Eq. 5.21}$$

The idea is to choose a value for the switching gain *H* such that $\dot{e} < 0$ and $\lim_{t \to \infty}(e) = 0$. Applying this condition in Eq. 5.22, a suitable expression for *H* is obtained in Eq. 5.23.

$$\dot{\beta}_d \left(\frac{\sqrt{\varphi^T \theta_p + \Delta}}{\sqrt{\varphi^T \hat{\theta}_p}} - 1 \right) - H \cdot \mathrm{sgn}(e) \cdot b_p \sqrt{\varphi^T \theta_p + \Delta} < 0 \qquad \text{Eq. 5.22}$$

$$H \cdot \mathrm{sgn}(e) > \dot{\beta}_d \frac{\left(\frac{\sqrt{\varphi^T \theta_p + \Delta}}{\sqrt{\varphi^T \hat{\theta}_p}} - 1 \right)}{b_p \sqrt{\varphi^T \theta_p + \Delta}}$$

$$H > \frac{\left\| \dot{\beta}_d \right\|_\infty}{b_p} \left| \frac{1}{\sqrt{\varphi^T \hat{\theta}_p}} - \frac{1}{\sqrt{\varphi^T \theta_p + \Delta}} \right| \qquad \text{Eq. 5.23}$$

Because the control valve has a limited bandwidth, it is advantageous to make the switching feedback continuous with a boundary layer *Φ* to avoid chattering, as in Eq. 5.24. The saturation function is illustrated in Figure 5.2.

$$u_{fb} = -H \cdot \mathrm{sat}\left(\frac{e}{\phi} \right) \qquad \text{Eq. 5.24}$$

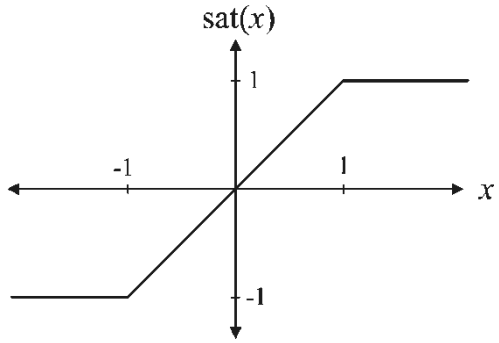

Figure 5.2 Definition of saturation function

Combining the feedforward and feedback terms, the control law is Eq. 5.25. The control law supplies a feedforward reference trajectory and compensates for variations in control pressure, spring force and control moment. Robust switching feedback overcomes model uncertainty and unmodeled quantities like friction.

$$u = \frac{\dot{\beta}_d}{\hat{b}_p}\left(p_{p,P} - \left(\frac{2\hat{k}_x r_p}{A_p}\beta + \frac{\hat{M}_x}{A_p r_p} \right) \mathrm{sgn}\left(y_v\right) \right)^{-1/2} - H \cdot \mathrm{sat}\left(\frac{e}{\phi}\right) \qquad \text{Eq. 5.25}$$

5.1.5 Simplified Swash Plate Control Law

As discussed in the preceding sub-section, the sliding mode control law offers the advantages of good disturbance rejection and zero steady-state error. On the other hand, its requirements in terms of sensor signals and valve performance are relatively high. Measurements of swash plate angle and control pressure are fed back directly, and the pump port pressures and shaft speed must be measured to estimate the control moment. The switching control works best with a high speed proportional valve or single stage servo valve in the pump adjustment system. While these requirements are met on the DC excavator, the cost of a high performance valve and additional sensors is likely too high for a

general construction machine. In this case, the nonlinear control can be adapted for use with a slower, low-cost valve.

As an alternative control law, Eq. 5.26 retains the same feedforward term as Eq. 5.20, except that only changes in the control pressure are compensated. For feedback, the switching term from Eq. 5.20 is replaced with proportional and integral terms. A similar approach has been published previously (Du, 2002).

$$u = u_{ff} + u_{fb} = \frac{\dot{\beta}_d}{b_p\sqrt{p_{p,P}}} - K_p e - K_i \int (e) dt \qquad \text{Eq. 5.26}$$

5.1.6 Pump Control Simulations

The variable displacement pump was simulated with three control laws. A PI controller is the baseline; K_p = 3.5 and K_i = 0.5 with normalized signals. Proportional-Integral feedback with feedforward compensation (Eq. 5.26), is the second control law labeled PI+FF. The third control law is the nonlinear sliding mode control Eq. 5.25. Two operating conditions are simulated: nominal and extreme. The nominal condition is at moderate speed, maximum control pressure and minimum pump pressure in pumping mode. In this condition, M_x exerts the least disturbance on the swash plate position. The extreme condition is at maximum speed, minimum control pressure, and maximum pump pressure in motoring mode. M_x is largest at this condition.

Simulation results are plotted in Figure 5.3 through Figure 5.6. As intended, SMC has better robustness at the extreme operating condition than the other two control laws. Compared to PI+FF, SMC reduces tracking error by about 40% for a sinusoidal reference signal and steady-state error by more than 50% for a step reference input. The improvement over PI control is even more dramatic. SMC also shows better accuracy at the nominal operating condition.

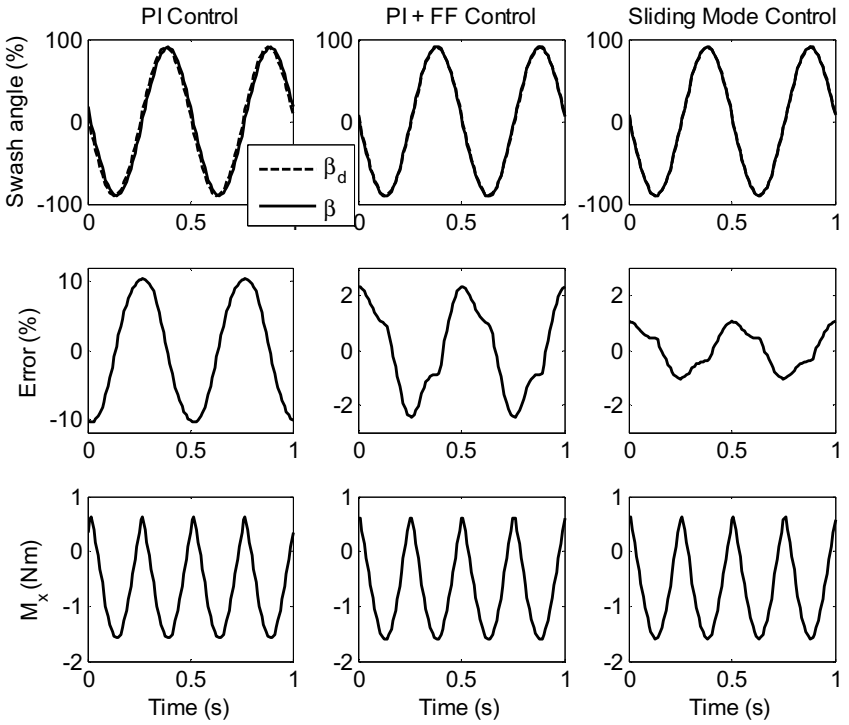

Figure 5.3 Pump control simulation, nominal (2500 rpm, Δp=0 bar, $p_{p,P}$=30 bar)

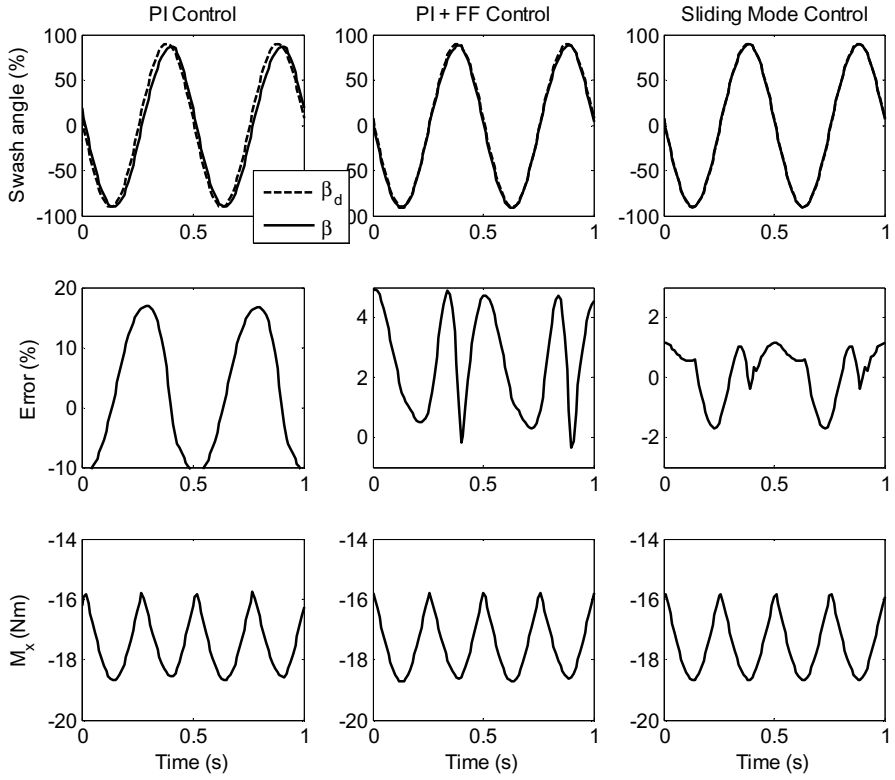

Figure 5.4 Pump control simulation, extreme (4500 rpm, Δp=350 bar, $p_{p,P}$=20bar)

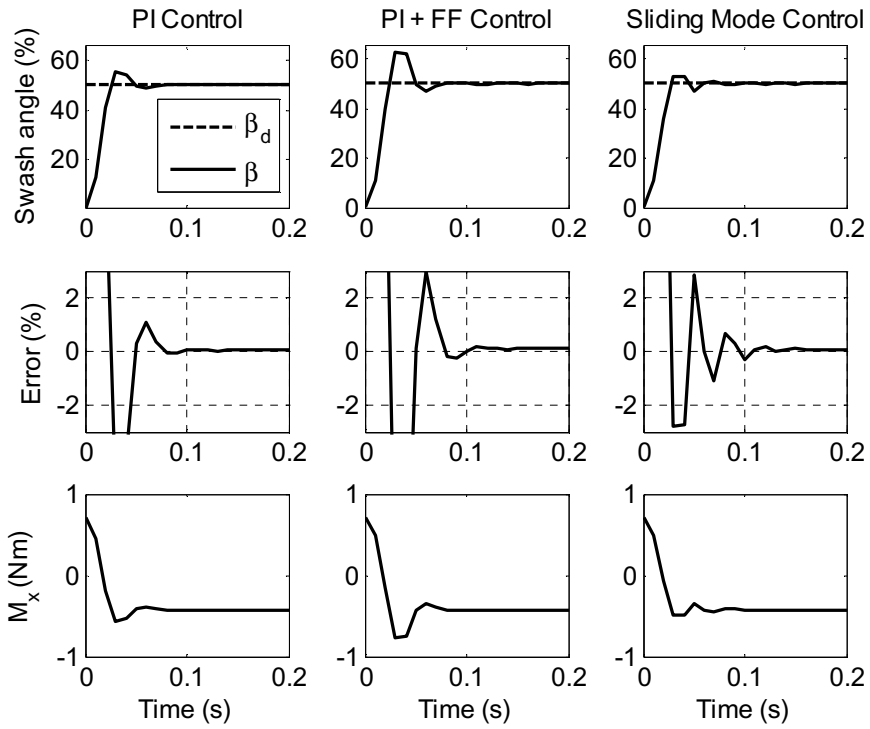

Figure 5.5 Pump control simulation, nominal (2500 rpm, Δp=0 bar, $p_{p,P}$=30 bar)

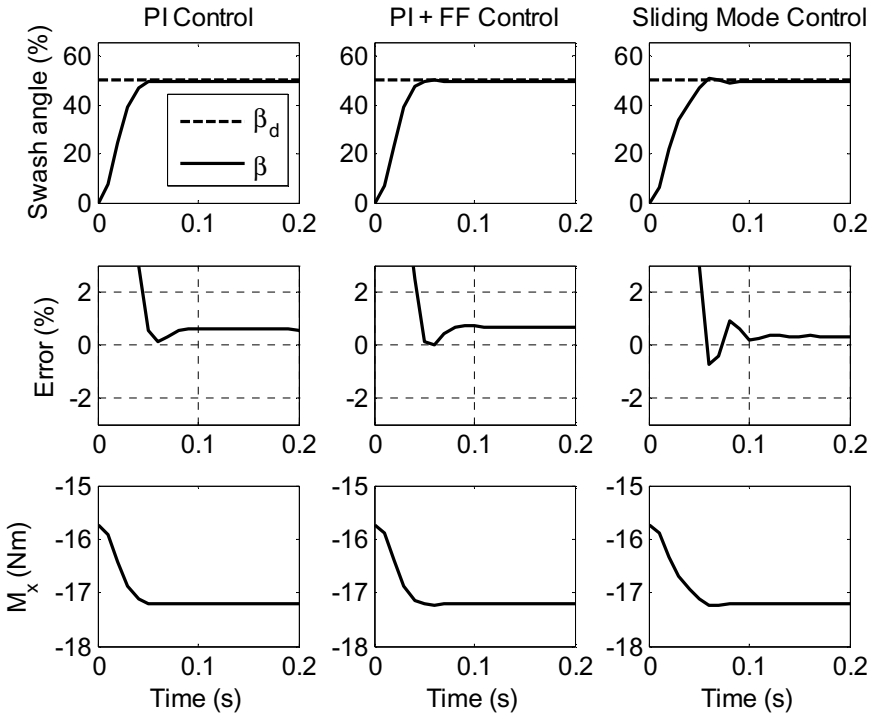

Figure 5.6 Pump control simulation, extreme (4500 rpm, Δp=350 bar, $p_{p,P}$=20bar)

5.2. Actuator Control

5.2.1. Four-Quadrant Operation

Figure 5.7 shows a DC circuit for a single actuator. Relief valves and the low pressure system (charge pump, accumulator, reservoir, etc.) have been omitted for clarity. The servo pump can operate in both pumping and motoring modes, depending on the actuator load. When the directions of the load force and the cylinder velocity are opposite, the circuit is in pumping mode. When they are the same (i.e. an overrunning load), the pump runs as a motor. The DC actuator's operating space can be visualized as a plane (Figure 5.8) with the differential pump pressure on the horizontal axis and the actuator velocity on the vertical axis (Rahmfeld, 2002). The axes divide the pumping and motoring modes into four quadrants. As shown in Figure 5.8, the maximum velocity is higher in the left half-plane than the right. The difference is due to the geometry of the single-rod cylinder. When the pump supplies fluid to the rod-side volume (left half-plane; valve d_1 is open, valve d_2 is closed), the actuator velocity is higher than when the pump is connected to the piston-side volume (right half-plane; valve d_1 is closed, valve d_2 is open). The transition between the left and right regions occurs when the pump pressures are equal, $p_1 = p_2 = p_{cp}$ or $\Delta p = (1-\alpha)p_{cp}$, where p_{cp} is the charge pressure. The ratio of cylinder volumes (and consequently, cylinder velocities) is defined by Eq. 5.27.

$$\alpha = \frac{A_B}{A_A} \qquad \text{Eq. 5.27}$$

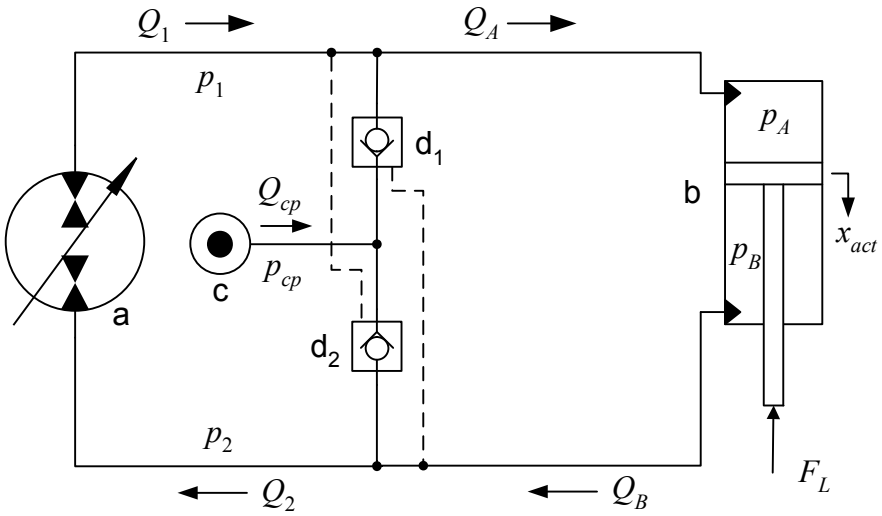

Figure 5.7 Basic displacement controlled actuation circuit

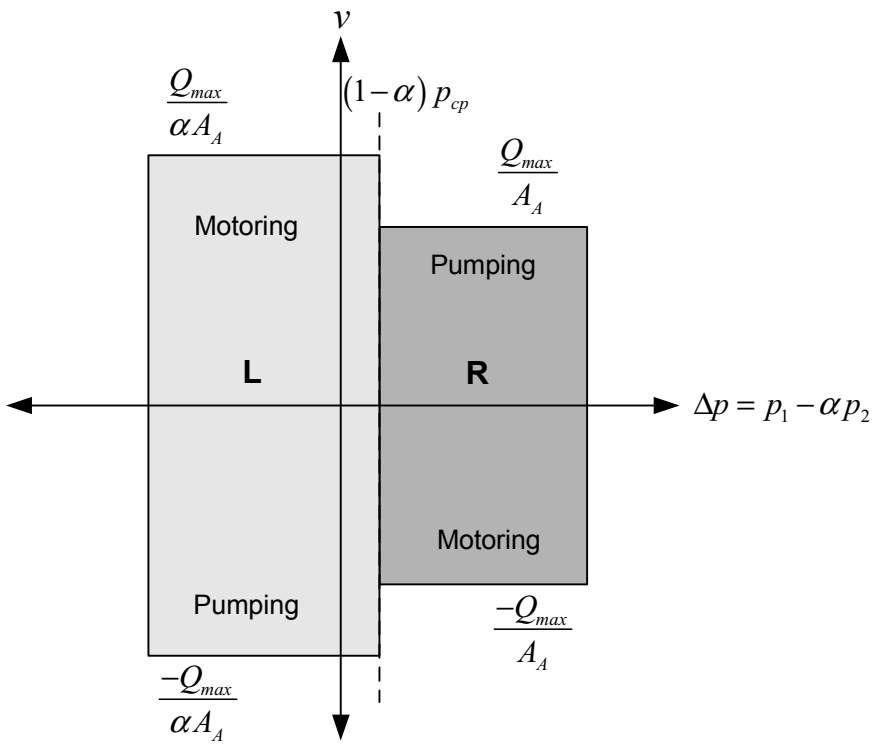

Figure 5.8 DC circuit operating plane and maximum velocity in each quadrant

Should the net force on the actuator change direction while the velocity is nonzero, the cylinder velocity will quickly increase or decrease by a factor of 1/*α*. Since *α* values are typically in the range of 0.4 to 0.8, the change in velocity may be quite significant. Worse still, the circuit may switch repeatedly between the left and right regions, resulting in a loss of velocity control (Williamson and Ivantysynova, 2008). Mode switching instability in DC actuator circuits is analyzed for the first time in this work. Design criteria and control solutions for stabilizing the actuator will be presented hereafter.

5.2.2. Simplified Actuator Model

Multi-actuator machines commonly use cylinders to actuate a rotary joint. The equation of motion for the cylinder can be written equivalently in terms of angular motion at the joint Eq. 5.28 or the linear motion of the cylinder Eq. 5.29. The equivalent mass m_{eq} "seen" by the cylinder due to linear and rotational inertia is defined in Eq. 5.30.

$$F_{act}\frac{\partial x_{act}}{\partial \theta} = I\ddot{\theta} \qquad \text{Eq. 5.28}$$

$$F_{act} = m_{eq}\ddot{x}_{act} \qquad \text{Eq. 5.29}$$

$$m_{eq} = I\frac{\ddot{\theta}}{\ddot{x}_{act}}\frac{\partial \theta}{\partial x_{act}} \qquad \text{Eq. 5.30}$$

Eq. 5.29 can then be combined with Eq. 4.20 to form Eq. 5.31, which is the cylinder's equation of motion.

$$\ddot{x}_{act} = \frac{1}{m_{eq}}\left(p_A A_A - p_B A_B - F_f - F_L\right) \qquad \text{Eq. 5.31}$$

Previously, the pilot-operated check valves have been modeled as orifices whose open area was determined by the balance of pressures on the valve poppet (Rahmfeld, 2002). Since the dynamic response of the check valves is much faster than the other system poles, the check valves are modeled here as discrete states—either open or closed. Moreover, the cracking pressure and flow restriction of the check valves is rather low, so the pressure drop across an open valve is neglected.

The actuator model is now linearized to facilitate a clearer analysis. Separate linear models are derived for each half of the operating plane, beginning with the right region. The actuator's pressure build-up equations (Eq. 4.18 and Eq. 4.19) are linearized by taking the volumes V_1 and V_2 to be constant at mid-stroke, $x_{act} = h/2$. Hydraulic capacitances are defined in Eq. 5.32. Because line 2 is connected to the charge line by valve (d_2), its capacitance is increased (see Figure 5.7). The expression for C_a (Eq. 5.33) is the capacitance of a hydropneumatic accumulator with volume V_0 and pre-charge pressure p_0 based on the ideal gas law, pV^N = constant.

$$C_{H1,R} = \frac{V_1}{K_{oil}} \qquad C_{H2,R} = \frac{V_2}{K_{oil}} + C_a \qquad \text{Eq. 5.32}$$

$$C_a = \frac{V_0 p_0^{1/N}}{N p_{cp}^{N+1/N}} \qquad \text{Eq. 5.33}$$

Pressure losses in the line are assumed to be linearly dependent on flow rate, as in Eq. 5.36. The pump pressures p_1 and p_2 can be combined into a single differential pressure $\Delta p = p_1 - \alpha p_2$. In region R (the right half-plane), $Q_1 = Q_2 = Q_A$. With the approximation $Q_B = \alpha Q_A$ and combined capacitances (Eq. 5.35), the model is reduced to a second order linear system (Eq. 5.37). The leakage coefficient k_L is replaced with k_L^* to account for $\Delta p \neq p_A - p_B$.

$$C_{Hr} = \left(\frac{1}{C_{H1,R}} + \frac{\alpha}{C_{H2,R}} \right)^{-1} \quad \text{Eq. 5.34}$$

$$C_{HR} = \left(\frac{1}{C_{H1,R}} + \frac{\alpha^2}{C_{H2,R}} \right)^{-1} \quad \text{Eq. 5.35}$$

$$p_1 = p_A + C_L Q_A$$
$$p_2 = p_B - C_L Q_B \quad \text{Eq. 5.36}$$

$$\begin{pmatrix} \dot{v} \\ \Delta\dot{p} \end{pmatrix} = \begin{pmatrix} -f_v / m_{eq} & A_A / m_{eq} \\ -A_A / C_{HR} & -k_L^* / C_{Hr} \end{pmatrix} \begin{pmatrix} v \\ \Delta p \end{pmatrix} + \begin{pmatrix} -\left(1+\alpha^2\right) C_L A_A / m_{eq} \\ 1/C_{HR} + \dfrac{k_L C_L (1+\alpha)}{C_{Hr}} \end{pmatrix} Q_1 + \begin{pmatrix} -F_{load} \\ 0 \end{pmatrix} \quad \text{Eq. 5.37}$$

The system model is structurally identical in the left half of the operating plane, but the coefficients are different. The charge line is now connected to the side 1, so the hydraulic capacitances must be redefined. In region L, $Q_1 = Q_2 = Q_B = Q_A/\alpha$. The $1/\alpha$ term in the input matrix means that the flow rates to and from the cylinder are much higher in left half of the operating plane. This characteristic has important implications for stability, as will be shown in the next section.

$$C_{H1,L} = \frac{V_1}{K_{oil}} + C_c \qquad C_{H2,L} = \frac{V_2}{K_{oil}} \quad \text{Eq. 5.38}$$

$$C_{HL} = \left(\frac{1}{C_{H1,L}} + \frac{\alpha^2}{C_{H2,L}} \right)^{-1} \quad \text{Eq. 5.39}$$

$$\begin{pmatrix} \dot{v} \\ \Delta\dot{p} \end{pmatrix} = \begin{pmatrix} -f_v / m_{eq} & A_A / m_{eq} \\ -A_A / C_{HL} & -k_L^* / C_{HL} \end{pmatrix} \begin{pmatrix} v \\ \Delta p \end{pmatrix} + \begin{pmatrix} -\left(1+\alpha^2\right) C_L A_A / m_{eq} \\ 1/\alpha C_{HL} + \dfrac{k_L C_L (1+\alpha)}{\alpha C_{Hl}} \end{pmatrix} Q_1 + \begin{pmatrix} -F_{load} \\ 0 \end{pmatrix} \quad \text{Eq. 5.40}$$

5.2.3. Stability Analysis

Modeled in this way, the DC actuator is a hybrid dynamic system composed of two linear systems, $\dot{x} = A_R x + B_R u + F_L$ (Eq. 5.37) in the right half of the operating plane and $\dot{x} = A_L x + B_L u + F_L$ (Eq. 5.40) in the left half-plane. The switching condition between the two is state-dependent, $\Delta p = p_c (1 - \alpha)$. For any 2x2 square matrix A, the eigenvalues are given by Eq. 5.41, where τ is the trace of A, and Δ is the determinant of A. Let $D = \tau^2 - 4\Delta$.

$$\lambda_{1,2} = \frac{\tau \pm \sqrt{\tau^2 - 4\Delta}}{2} \qquad \text{Eq. 5.41}$$

By inspection of A_R and A_L, it is clear that the traces τ_R and τ_L are always negative, and the determinants Δ_R and Δ_L are always positive. Thus, for both of these matrices, when the eigenvalues λ are complex ($D < 0$), they have real parts that are negative. When eigenvalues are real ($D > 0$), they are still both negative. As a result, each linear system (on either side of the switching condition) is stable by itself. Any instability in the system must be due to the non-linearity introduced in switching modes.

To illustrate mode switching instability, the previously derived model is simulated with parameters taken from the DC excavator boom cylinder. Figure 5.9 shows the DC actuator system with no load force and zero initial conditions. As a negative step input is applied, the state trajectory moves into the left half plane and begins to spiral toward the left-system equilibrium point marked by the lower triangle. When the switching condition is reached at the vertical axis (p_{cp} is taken to be zero), the trajectory spirals around the right-system equilibrium point marked by the center triangle. Because of the relative locations of the equilibrium points, each time the system switches it moves to a larger spiral in the other half-plane. The result is that the oscillations grow until the spirals are the same size and the system settles into a limit cycle of repeated oscillations.

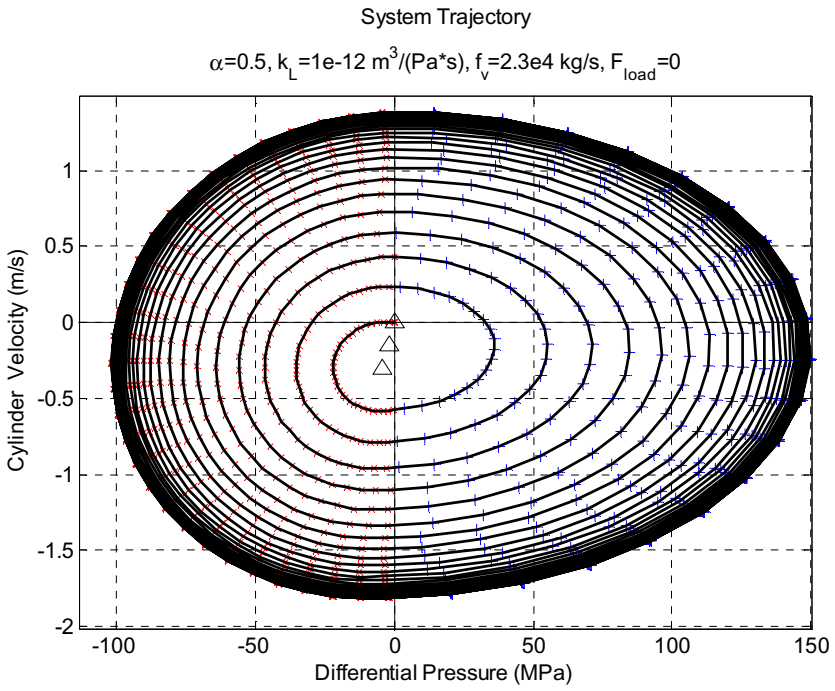

Figure 5.9 Simulation of system with low damping and no load showing unstable mode switching

To provide more confidence in the validity of the simplified actuator model and the preceding analysis, results of measurement and simulation are compared side by side in Figure 5.10. The measurements are from the DC mini excavator while rapidly retracting the boom cylinder. Due to the many simplifications in the model, the curves do not match exactly. However, the size of the spirals are similar and the oscillation between operating modes is clearly evident in the experiment. The frequency of oscillation is also approximately the same at about 2.5 cycles per second. In Figure 5.10, the cylinder damping is high enough that the spirals slowly converge toward equilibrium instead of increasing to a limit cycle, as in Figure 5.9. Although the system is stable in a theoretical sense, the rate of convergence is unacceptably slow.

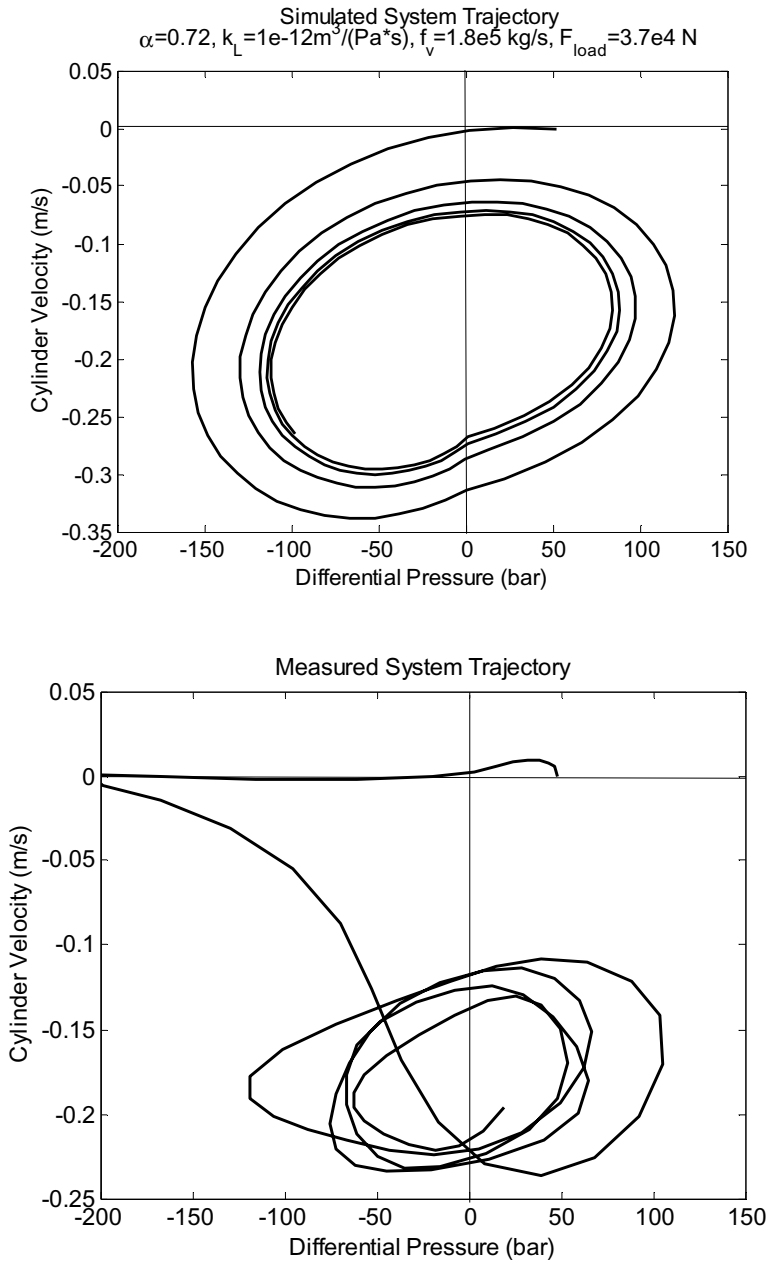

Figure 5.10 Comparison of simulated and measured mode switching

Considering the system dynamics, there are three ways to avoid instability (growing spirals). The trivial solution is that the equilibrium points for both the left and right systems are at the same location, i.e. α=1, a double-rod cylinder. Another solution is to increase the system damping so that the system trajectory

approaches the equilibrium point without switching modes. Figure 5.11 illustrates the second case, where the leakage and friction coefficients have been greatly increased and the eigenvalues are real (D>0). The system shows a damped response, approaching the equilibrium point asymptotically without oscillation. The system could also be stable with complex eigenvalues so long as the trajectory converges quickly enough that the spirals do not cross the switching boundary. A third solution is to increase the load force, forcing the equilibrium points farther away from the switching condition. The third case is depicted in Figure 5.12. The equilibrium points are now in the right half-plane, sufficiently far from the vertical axis to avoid switching modes. The system shows an underdamped response; oscillations settle out with time.

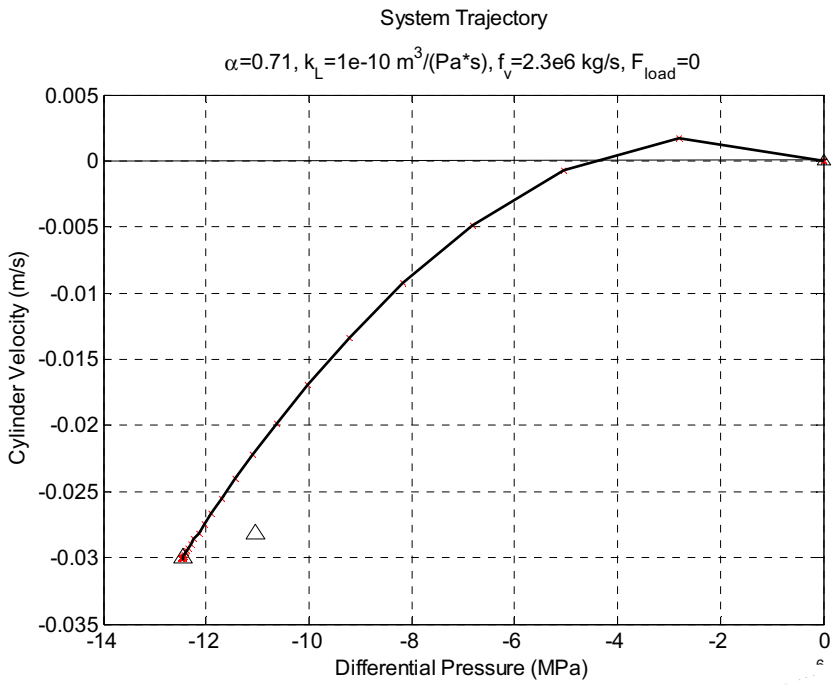

Figure 5.11 Simulation of system with high damping and no load showing a stable trajectory

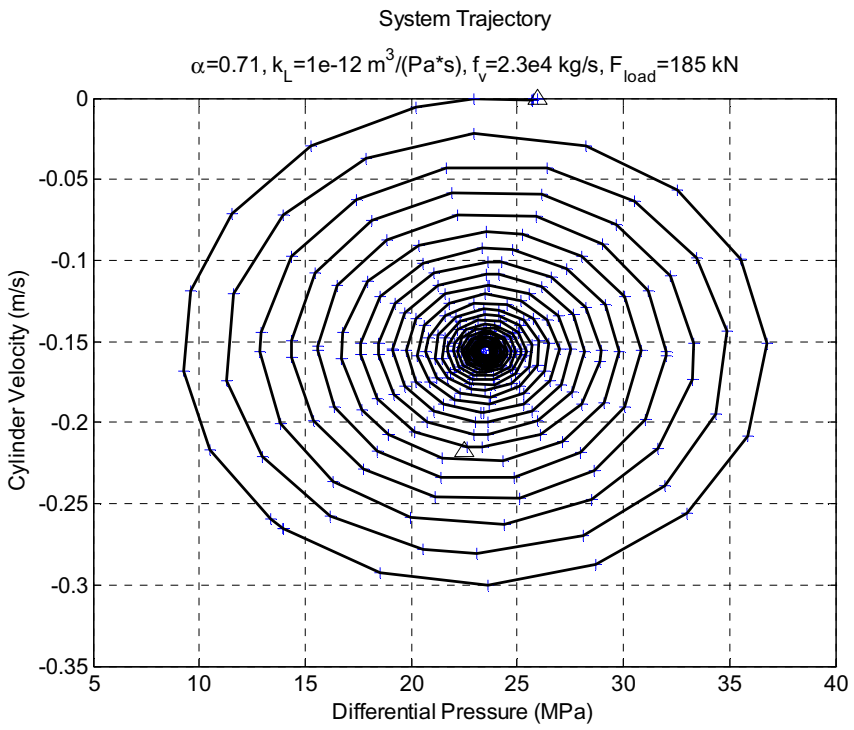

Figure 5.12 Simulation of system with low damping and high load showing stable underdamped oscillations and no mode switching

A simple stability criterion for the third case can be obtained from Eq. 5.31. Substituting for p_A and p_B and rearranging,

$$F_L = \left(p_1 + C_L Q_1\right) A_A - \left(p_2 - C_L Q_1\right) A_B - F_f - m_{eq}\ddot{x}_{act} \qquad \text{Eq. 5.42}$$

At the switching boundary, $p_1=p_2=p_{cp}$ and the equation becomes

$$F_L = \left(1-\alpha\right) A_A p_c - \left(1+\alpha\right) A_A C_L Q_1 - F_f - m_{eq}\ddot{x}_{act} \qquad \text{Eq. 5.43}$$

If the '=' sign is changed to '>' then the system trajectory cannot reach the switching boundary, and the system is stable.

5.2.4. Actuator Control Law

Unfortunately, it is often impractical to design a multi-actuator system that meets one of the three sufficient conditions for stability. In the first case, single-rod actuators are preferred over double-rod actuators because of their superior compactness (shorter total length for the same stroke). In the second case, increased damping is due to increased energy dissipation, which would eliminate the motivation for DC actuators: saving energy. The third case may be feasible for actuators that always act opposite the direction of gravity (such as lifting and lowering a boom), but cannot be satisfied in general.

If the stability conditions cannot be met by design, DC actuators can also be stabilized by feedback control (Williamson and Ivantysynova, 2010, 2). The control law must simply increase the damping of the closed-loop system so that the eigenvalues of A-BK are real and negative. This is not a new problem; fluid power actuators are often underdamped, and several classical techniques for increasing damping have been known for decades. Among these are pressure feedback and state feedback (Lewis and Stern, 1962; Merritt, 1967). Force and acceleration are closely related to pressure and can also be controlled to increase damping (Jelali and Kroll, 2003). Such techniques have been investigated previously for DC actuators, though not with regard to mode switching (Grabbel, 2004).

A block diagram with stabilizing pressure feedback was already presented in Figure 5.1. Actuator pressure is controlled by adjusting the pump flow rate. A band-pass filter removes the steady-state component of the pressure signal that is due to static load. Hence, only pressure transients are penalized. The filter passband should be designed so as to include the actuator's resonant frequency but not the frequencies characteristic of the load force. Where this is not possible, a loop-shaping filter design may be appropriate. Acceleration feedback may also be preferable because of reduced load effects.

Stabilizing the DC actuator by active control requires a relatively fast pump response. Suitable bandwidth can be achieved with an appropriately designed swash plate adjustment mechanism including a properly sized control valve (Grabbel and Ivantysynova, 2005). In an alternate circuit configuration, a proportional valve between the two high pressure lines could be used to regulate pressure transients. The actuator motion would then be determined by pump control and valve control simultaneously. Such a configuration may be advantageous where the pump response is too slow for active damping. However, this approach requires additional control effort and may increase the cost of components.

5.2.5. Simulation Results

To demonstrate the effectiveness of the proposed control law, the DC actuator system is simulated with the nominal parameter values (α=0.71, k_L=1e-12 $m^3/(Pa \cdot s)$, f_v=2.3e4 kg/s, F_L=37 kN) and pressure feedback ($k_{\Delta p}$=2). Figure 5.13 shows that the system trajectory makes a stable mode switch and converges quickly to an equilibrium point. The control input and system states are also plotted in the time domain as an alternate representation of the system behavior. Corresponding measurements may be found in section 6.4.

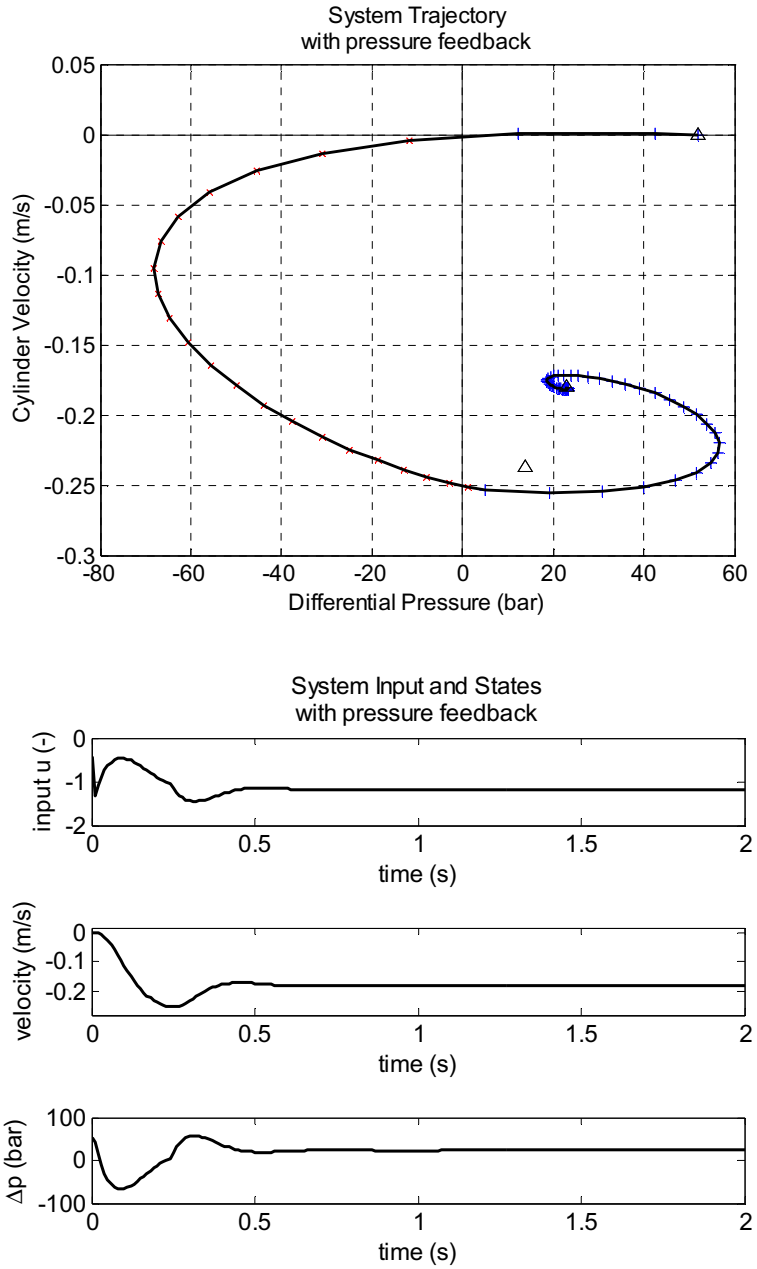

Figure 5.13 Simulation of DC actuator with stabilizing pressure feedback

5.3. Summary

- Chapter 5 covers the design and analysis of control systems for electro-hydraulic variable displacement pumps and displacement controlled linear actuators.
- The pump adjustment system dynamics are reduced to a first order model with nonlinear terms included. Based on the simplified model, a sliding mode control law is proposed which compensates for variation and uncertainty in the supply pressure, centering spring force and control moment. Robust performance is demonstrated by simulation.
- Pump-controlled circuits operate in two different modes, depending on the direction of the net force on the actuator. The actuator can switch repeatedly between modes, causing oscillations in velocity.
- DC actuator stability is analyzed. Mode switching limit cycles are caused by nonlinear state-dependent switching between two linear systems which by themselves are stable. This phenomenon is studied for the first time within this research.
- Design criteria for actuator stability are determined. A method for actively stabilizing the actuator by pump control is also proposed. Simulations of each case are presented.

CHAPTER 6 EXPERIMENTAL INVESTIGATIONS

6.1. Description of Multi-Actuator Machine Prototype

Developing a prototype was a major part of the research project. The author was a primary contributor to the effort, being solely responsible for designing and implementing the electronic controls. The author also contributed cooperatively in various aspects of simulation, prototype assembly and experimentation. The DC system architecture was implemented on a 5-ton mini excavator, shown in Figure 6.1. The DC excavator, used for validation in this study, has a mass of approximately 4800 kg; the maximum engine power is 36.5 kW. Additional specifications are listed in Appendix A. This machine was selected for the current research because its size and cost are suitable for a laboratory environment, yet the machine kinematics and hydraulics are similar to larger machines.

The excavating arm is typical of excavators and backhoes, with a serial linkage consisting of three links (boom, stick and bucket). The relative angles between the links are controlled by single-rod cylinders. Cabin rotation (called swing or slew) is achieved with a hydraulic motor. Digging tasks involve these four primary functions. Secondary functions include a blade for backfilling excavations, boom offset (which changes the angle of the arm with respect to the cabin) and two tracks for travelling.

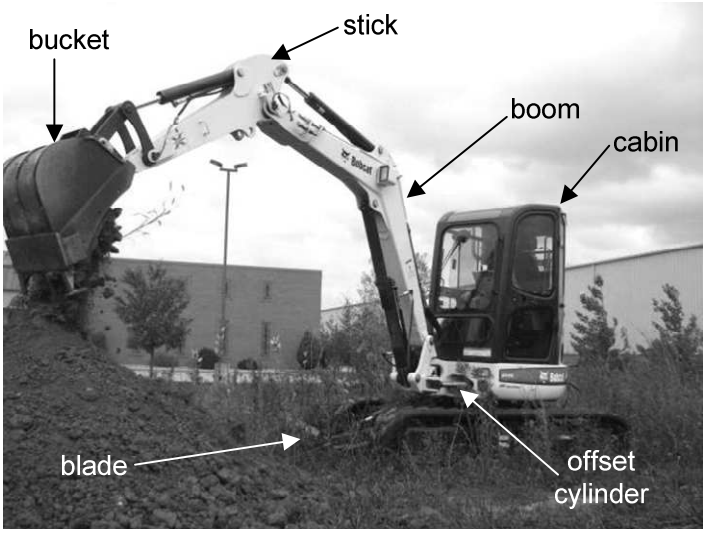

Figure 6.1 Displacement controlled mini excavator

The DC hydraulic circuit is shown in . The system design is based on the basic DC circuit developed by Rahmfeld (2002). For clarity, drain lines from the pump and motor cases have been omitted, and the pump swash plate controls are represented by boxes labeled C. Figure 4.1 shows the pump configuration in more detail. There are four 18 cc/rev variable displacement pumps which can be connected via two-way valves to either the primary or secondary actuators. These pumps are of the axial piston swash plate type with electro-hydraulic valves for adjusting the pump displacement. A gear-type charge pump supplies the pump displacement controls, provides volumetric compensation for the actuator circuits, and powers a cooling fan for the engine and hydraulic heat exchangers. Detailed specifications are given in Appendix A.

The DC excavator was fully instrumented with sensors for control and measuring energy distribution throughout the hydraulic system and machine structure. Figure 6.3 shows the placement of these sensors. Fluid pressure is measured at the pump and cylinder ports with strain-gauge type transducers. Pressure levels are also measured at the cooling fan motor, the swash plate control supply line and the low pressure charge line. Engine shaft speed is measured at the

flywheel with a Hall effect tachometer. Each pump includes a rotary Hall effect type position sensor for measuring swash plate angle. Linear position sensors are integrated into the hydraulic cylinders for the boom, stick and bucket functions. The cylinder position sensors are of the magnetostrictive type and are coaxial with the piston rod. The operator joysticks also have integrated position sensors. An angular sensor (also contactless Hall effect type) measures the swing motor position. The engine speed setpoint is controlled by an electric ball screw actuator with integrated position sensing (a potentiometer). Sensor characteristics are tabulated in Appendix A. An embedded PC running Mathworks xPC Target real-time operating system is used for control and data acquisition.

Although the excavator is pump controlled, there are still various valves required for operation. Perhaps the most important of these are the control valves for adjusting the pump displacements. Relatively high bandwidth and linear flow characteristics are required, so Moog D636 single-stage servo valves were selected. The 18 cc/rev piston pumps were custom made by Parker Hannifin for the DC prototype.

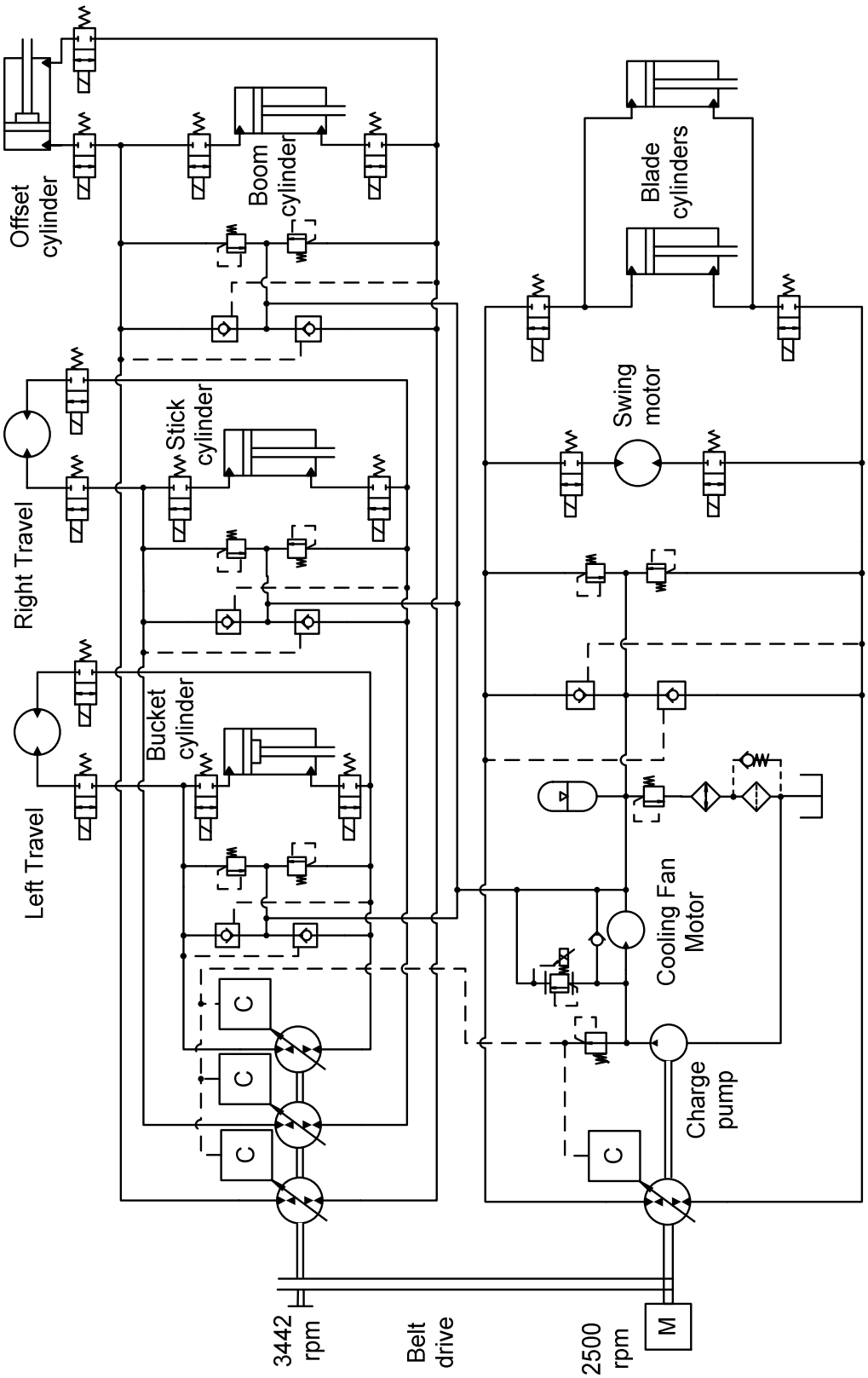

Figure 6.2 DC excavator hydraulic circuit

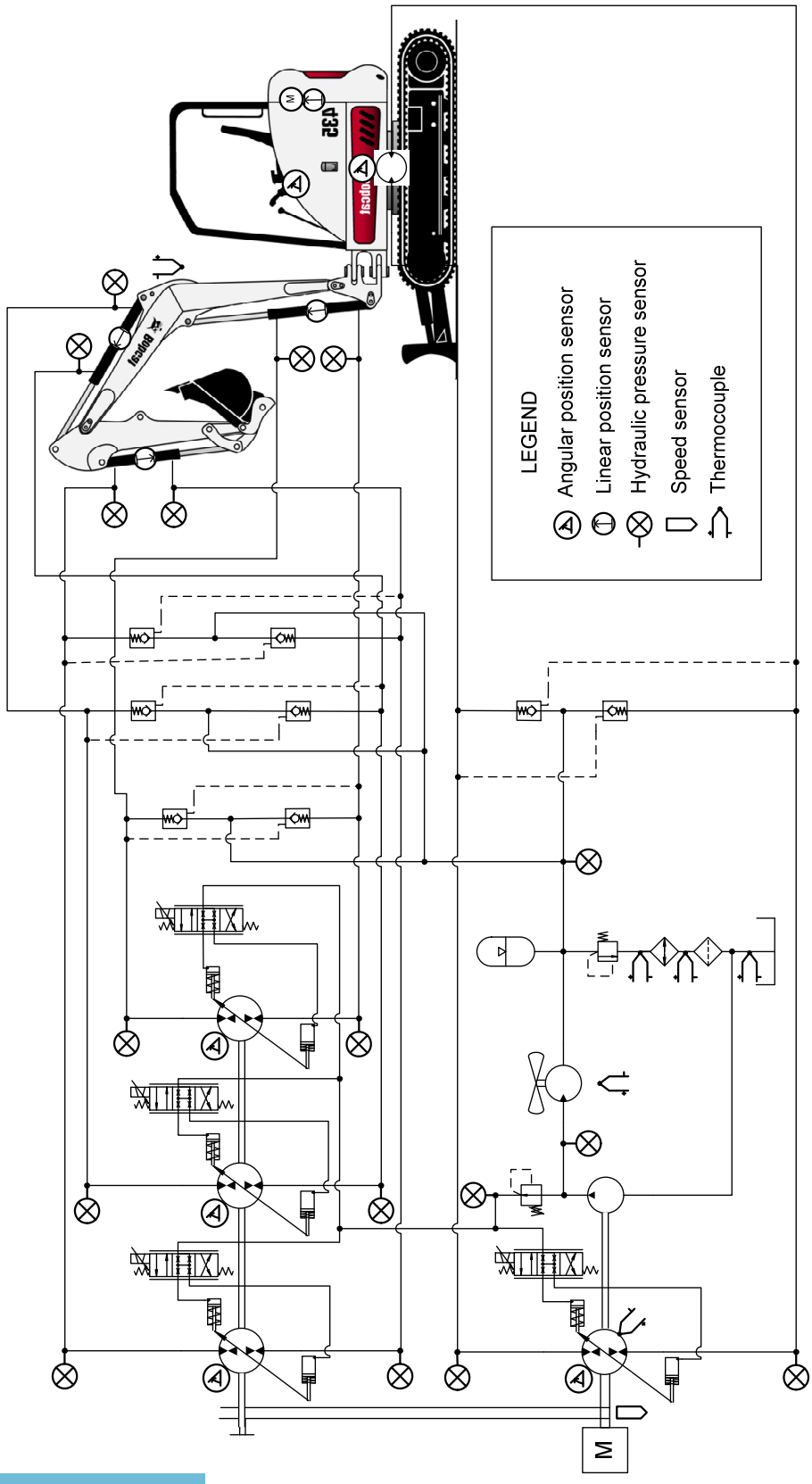

Figure 6.3 Excavator diagram showing hydraulic and electrical components

6.2. Measurement of Optimal Power Management

A fuel efficiency test was conducted to evaluate the proposed optimal power management algorithm. The duty cycle consisted of moving a 250 kg mass suspended from the bucket on a chain. Targets were placed on either side of the excavator. While rotating the cabin 180°, the weig ht was raised from one target and then lowered onto the other. Each trial consisted of 20 repetitions, after which an external fuel tank was weighed to determine the fuel mass consumed. Five trials each were conducted with and without power management. In the latter case, the engine speed was set to high idle (~2700 rev/min).

Figure 6.4 Power management fuel test setup

Results are tabulated in Table 2. Mean values are listed along with 95% confidence intervals based on a two sided t-distribution. The same test cycle was also simulated with the excavator dynamic model, and the simulation results are summarized in Table 3 for comparison. Although there is significant discrepancy between simulation and measurement in terms of fuel mass consumed, the relative difference with and without power management is quite similar (< 7%). The error in the simulated fuel consumption is primarily due to

the nature of the duty cycle; the machine operates at low power on the edge of the measured engine fuel map.

Table 2. Power management test results, average of five trials

	Fuel consumed (g)	Cycle time (s)	Fuel rate (kg/h)
Constant engine speed	270 ±32	15.9 ±0.7	3.030 ±0.259
Power management	118 ±37	15.3 ±2.3	1.383 ±0.254
Difference	-56.4%	-3.5%	-54.4%

Two test cycles are plotted in Figure 6.5. It is apparent that with power management, the engine operates at a lower speed and the pumps operate at higher displacement. In this way, the same actuator motion is attained more efficiently. The measured duty cycle was intentionally selected because it requires slow, careful motions to prevent the weight from swinging. The cycle is comparable to pipe laying or other realistic tasks for an excavator. In a more demanding cycle, there would be less opportunity for reducing engine speed and fuel consumption. It is fair to say that the duty cycles in section 6.1 (truck loading) and this section (positioning a suspended weight) bracket the operational extremes for an excavator. The former cycle requires high speed and power nearly continuously, while the power and speed requirements of the latter cycle are consistently low.

Table 3. Power management test results, simulations of measured cycle

	Fuel consumed (g)	Cycle time (s)	Fuel rate (kg/h)
Constant engine speed	318	15.9	3.85 kg/h
Power management	160	15.9	1.94 kg/h
Difference	-49.7%	0%	49.7%

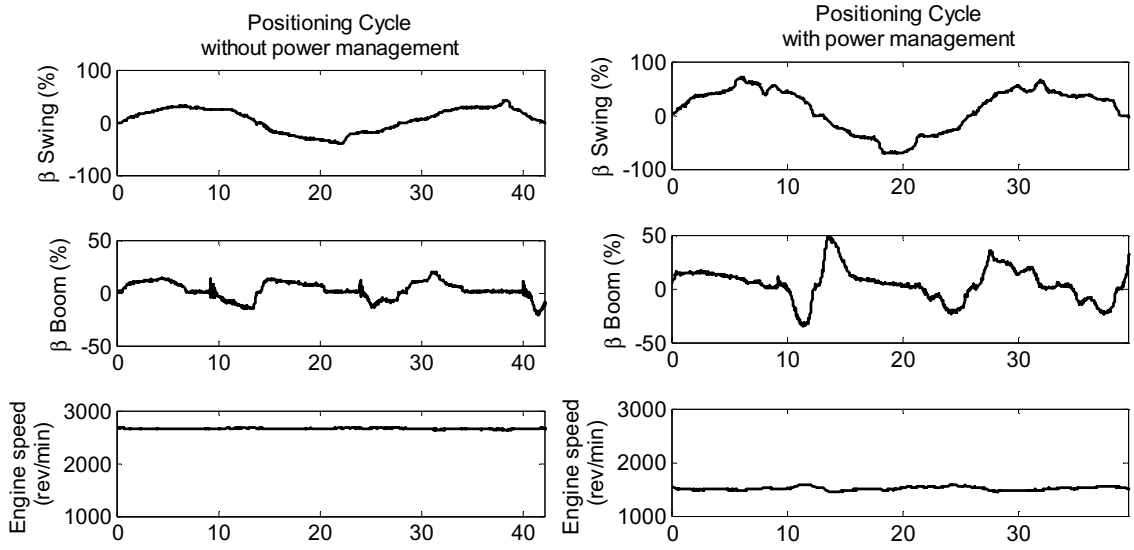

Figure 6.5 Pump and engine operation during power management test

During the power management fuel test, the operator inputs and states vary slowly. Such a quasi-steady-state cycle was selected intentionally for repeatability. However, the power management method also works well with a more dynamic duty cycle such as the digging cycle simulated in Chapter 3. Measurements of the system states with dynamic inputs are plotted in Figure 6.6.

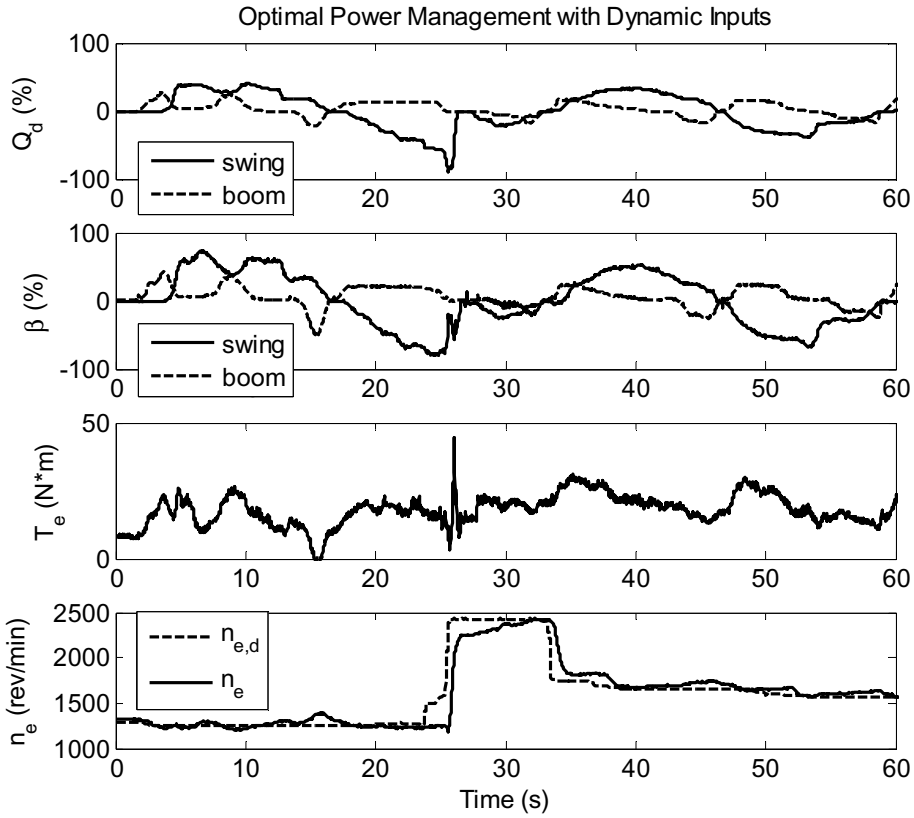

Figure 6.6 Measured system states with dynamic operator inputs

6.3. Measurement of Pump Displacement Control

The pump swash plate position control laws described in section 5.1 were implemented and tested on the DC excavator. Three control laws were compared: a conventional PI control, PI control plus a feedforward signal (PI+FF) with the reference signal velocity and compensation for variations in control pressure, and a nonlinear sliding mode control law (SMC) with compensation for control pressure, control moment, and spring force. In the first two cases, the feedback gains were K_p = 2.0 and K_i = 0.3 with normalized signals. Detailed specifications for the control valves and position sensors are tabulated in Appendix A. The sliding mode control law was implemented as an embedded

Matlab function; the code is included in Appendix B. The sampling rate for all control tests was 500 Hz.

Pump ramp response is plotted in Figure 6.7. Ramp reference input signals were obtained from joystick positions. Measurements were obtained from the pump connected to the stick cylinder and left travel motor. On the left, the pump response was measured at approximately 3700 rpm, high pump pressure (up to 250 bar) and 25-30 bar control pressure. On the right, the pump operating condition was approximately 2000 rpm, zero pump pressure, and 17-20 bar control pressure. When the control moment disturbance is low (right side), the pump response is very similar with all three control laws, although rise time for a 10% step is 21% faster with SMC. When the pump pressure is high (left side), the control moment acts as a disturbance that tends to center the swash plate. In this case, SMC visibly reduces the steady-state error, particularly at 10% and 25% swash plate angles.

Sinusoidal frequency response results are given in Figure 6.8. All measurements shown are at high idle with low load (n_p = 3700 rpm, $p_{p,P}$ = 30 bar, Δp =0). The time domain plots on the left show the tracking error for sine wave of 90% amplitude and and increasing frequency. The PI+FF and SMC control laws reduce the tracking error by a factor of 4 compared to conventional PI control. Looking at the bode plots on the right, the -3 dB bandwidth is significantly higher for small amplitudes (±10%) with SMC (25 Hz) than PI+FF (17.5 Hz) or PI (11.5 Hz).

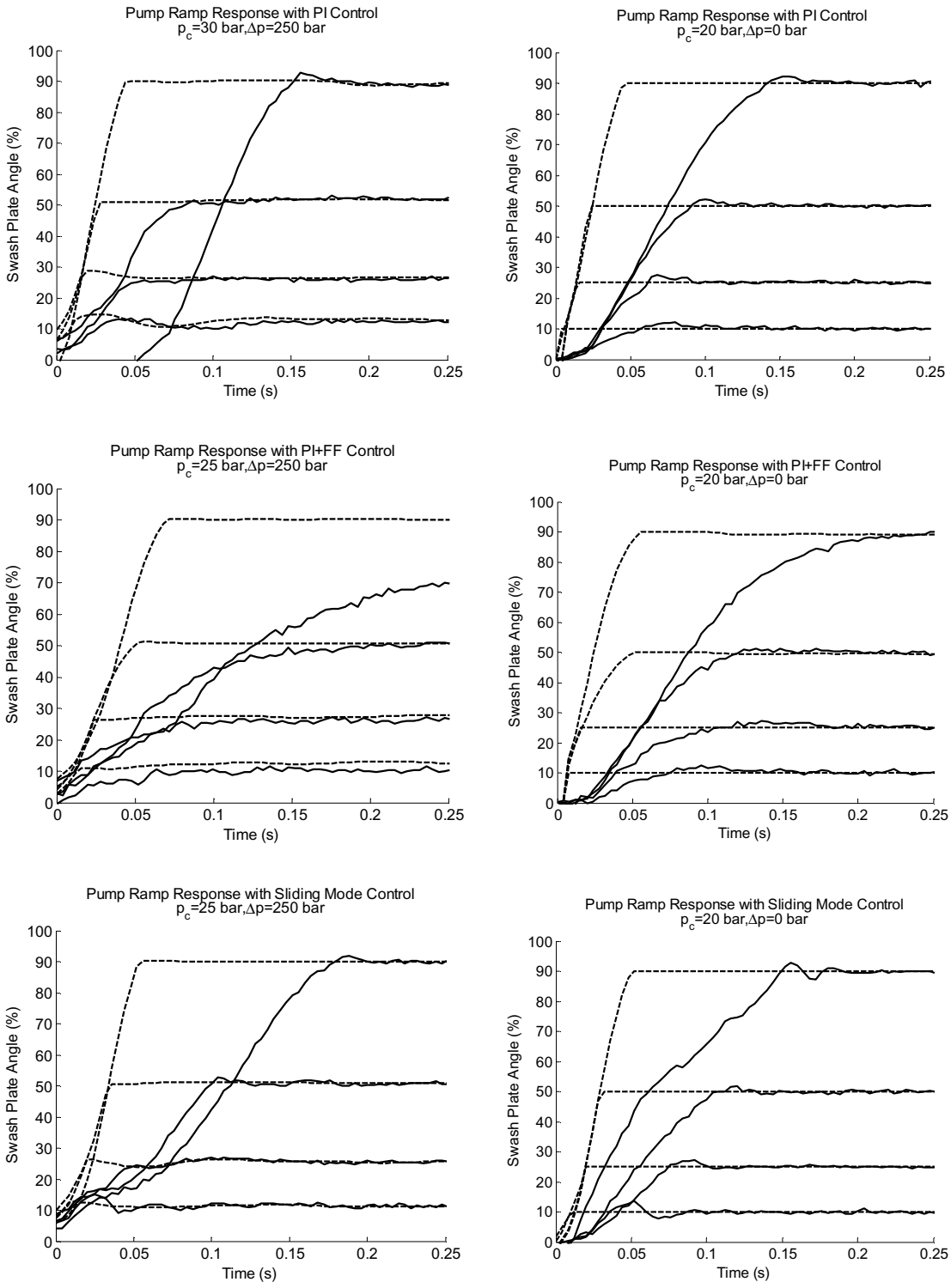

Figure 6.7 Pump ramp response measured on DC excavator

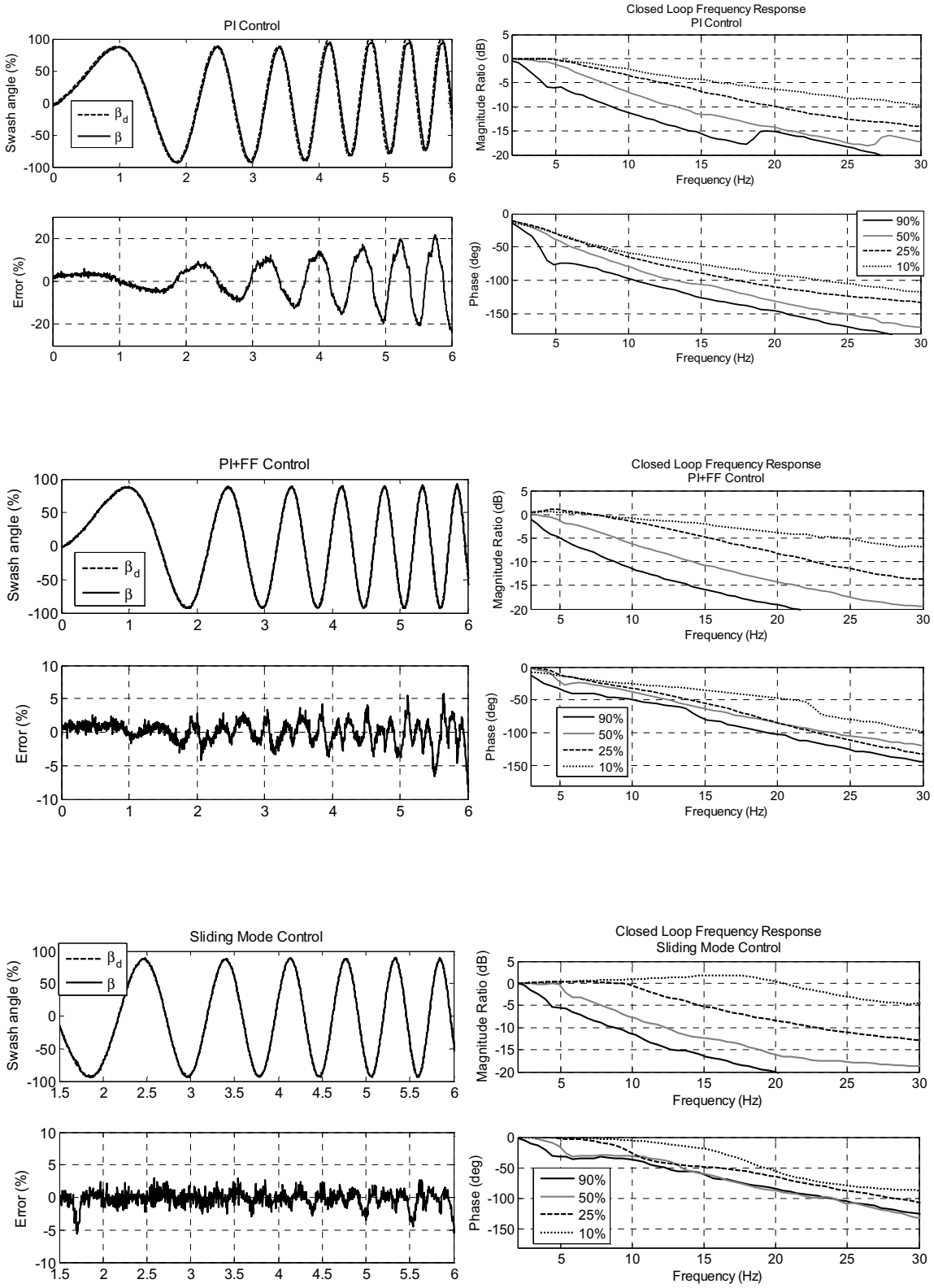

Figure 6.8 Pump frequency response measured on DC excavator

6.4. Measurement of DC Actuator Control

As discussed in section 5.2, DC actuators operate in two modes. Transitions between modes can result in growing velocity oscillations, an instability which is due to the circuit's nonlinear switching characteristic. Figure 6.9 shows measurements from the DC excavator boom cylinder with no load in the bucket and the stick and bucket cylinders fully extended. Unstable mode switching is observed while rapidly lowering the boom in the interval t = 11 to 12.5 s. Figure 6.10 depicts the same motions with pressure control. With transient pressure regulation, the circuit lowers in pumping mode rather than switching repeatedly between modes. The interval from t = 0 to 4 seconds is included to show the influence of the load force, which prevents the circuit from reaching the switching condition $p_1 = p_2$ at lower velocities and accelerations.

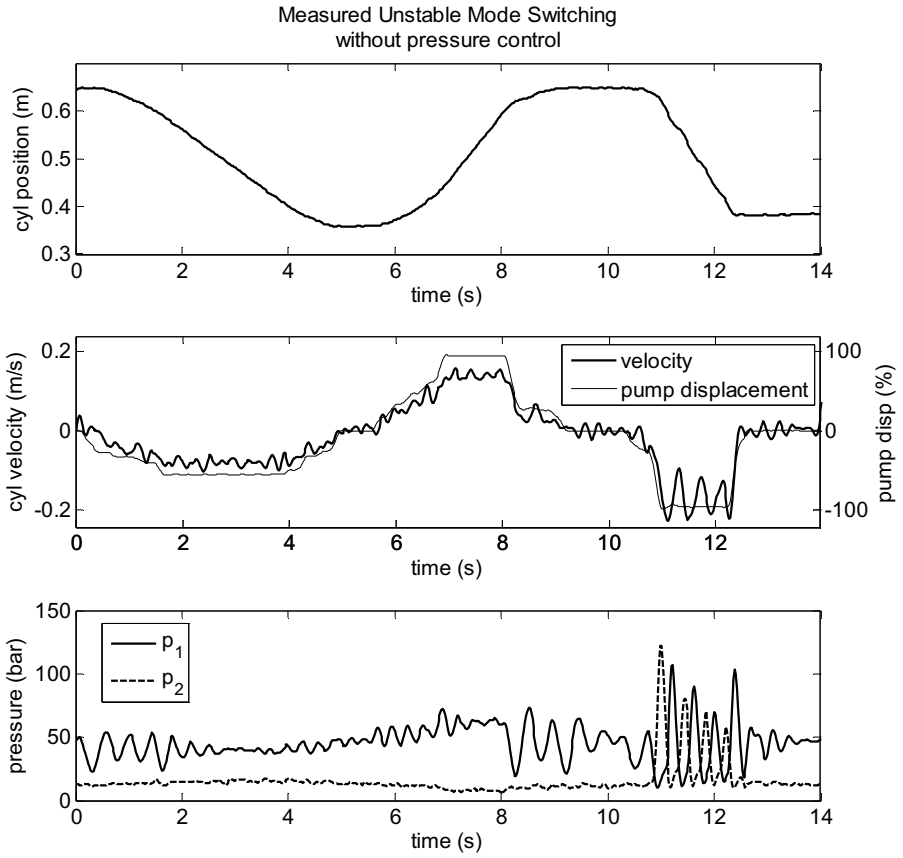

Figure 6.9 Unstable pump mode switching

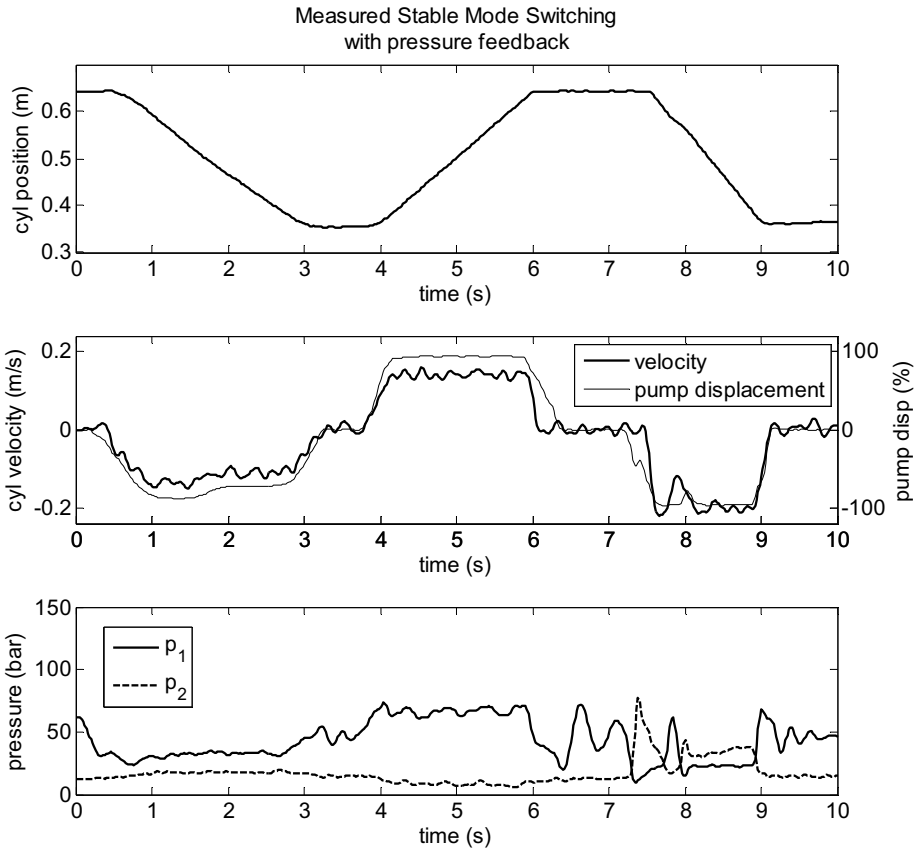

Figure 6.10 Pump mode oscillation eliminated by transient pressure feedback

In section 5.2, simulations of unstable mode switching were plotted parametrically on a pressure – velocity plane to illustrate the transitions between different operating modes. The same measurements from Figure 6.9 and Figure 6.10 are plotted this way in Figure 6.11. For clarity, only the interval when the cylinder is retracting quickly is included. The effectiveness of the stabilizing control is evident.

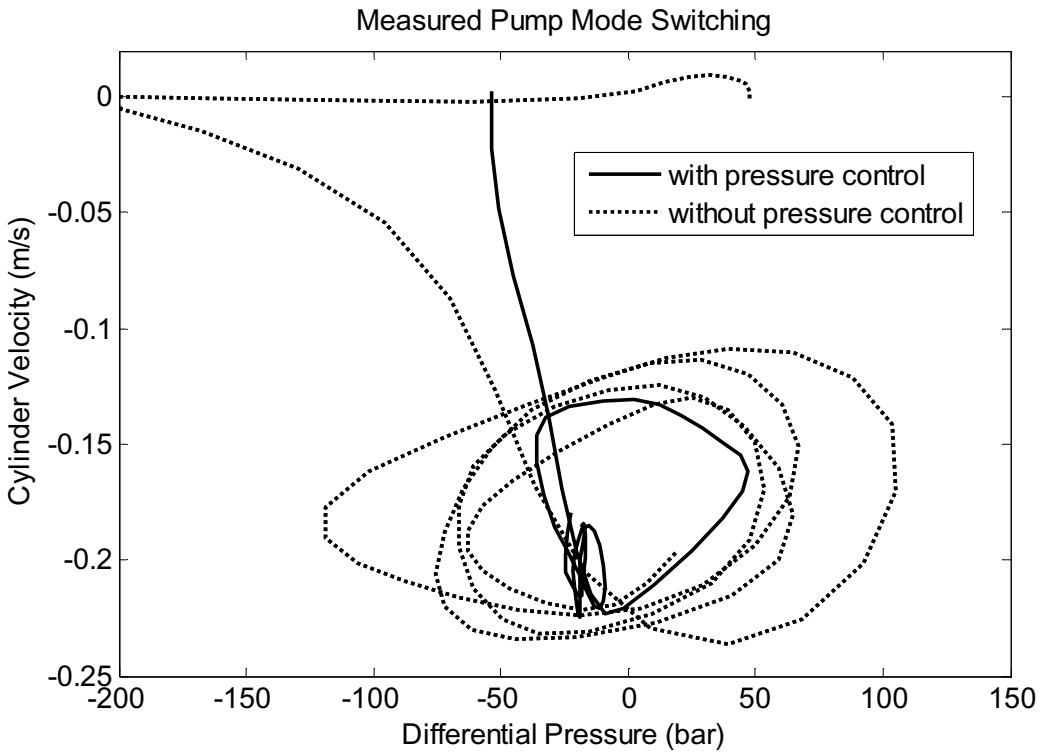

Figure 6.11 Parametric plot of pump mode oscillation

6.5. DC Excavator Productivity Test

A performance test was conducted in cooperation with Caterpillar, Inc. to evaluate the DC excavator with respect to productivity and efficiency. Two mini excavators were tested: the prototype DC excavator and a standard excavator of the same model. The test site is shown in Figure 6.12. Measured quantities included the mass of soil loaded, fuel mass consumed, and cycle times. The excavator loaded soil into a 6-ton dump truck, after which the truck was weighed to determine the soil mass. Fuel measurements were obtained by weighing an external fuel tank with a precision scale (5 g resolution). Data was acquired on the DC excavator from all onboard sensors. The standard excavator was not instrumented. All testing was conducted at the same location with the same professional operator on the same day. Identical fuel was used for all tests.

Figure 6.12 Productivity test site

Table 4. Excavator productivity test results

Machine	Soil loaded (metric ton)	Fuel consumed (kg)	Cycle time (s)
Standard LS	6.85 ±0.43	0.529 ±0.046	11.86 ±0.67
Prototype DC	6.97 ±0.47	0.319 ±0.037	10.32 ±1.09
Difference	+1.73%	-39.7%	-12.9%

Table 5. Excavator performance comparison

Machine	Fuel consumption rate (kg/h)	Productivity (ton/h)	Fuel Efficiency (ton/kg)
Standard LS	8.04	104.3	13.0
Prototype DC	5.57	121.7	21.9
Difference	-30.8%	+16.6%	+68.7%

Each trial consisted of loading a set number of buckets of loose soil into the truck bed, after which the truck and fuel tank were weighed and the dirt was returned to the hole. The standard excavator was operated first, followed by the DC

excavator. The test results are summarized in Table 4, with the mean measured values and 95% confidence intervals based on a t-distribution. On average, the DC excavator moved the same quantity of soil in 13% less time and with 40% less fuel than the standard excavator. There is not a statistically significant difference between the amount of soil loaded by the two excavators, as expected. The cycle time improvement is not significant at a 95% confidence level, but is significant with 90% confidence.

Table 5 lists performance metrics calculated from the results in Table 4. These figures correspond to a 69% improvement in fuel efficiency (soil per fuel) and a 17% improvement in productivity (soil per time). Figure 6.13 shows how energy from the engine is distributed through the hydraulic system. The total energy was calculated from steady-state pump loss models using measured speed, pressures and displacements and integrating pump power with respect to time. The average cycle energy efficiency is 45%, which represents the fraction of useful work that is obtained from the engine power delivered to the hydraulic system. Actuator work was calculated from measured positions and pressures. Because actuator forces are not directly measured, energy losses due to seal friction are counted as actuator work.

Servo pump losses and fan/charge pump losses were calculated from steady-state models. Line losses were calculated from the pressure difference between the pump and actuator ports and flow rates estimated from the actuator velocities. Other losses included actuator seal leakage and relief valve losses, and any discrepancy between the total energy input and the sum of energy outputs.

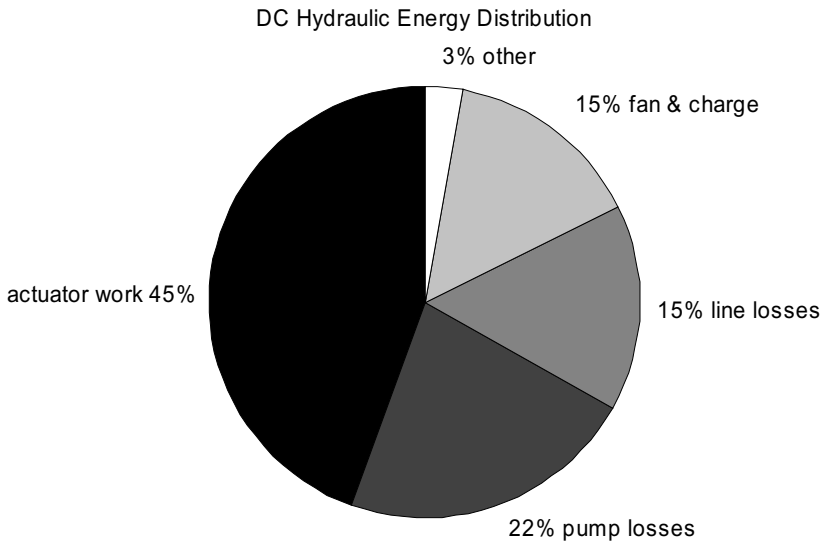

	Work	Pump Loss	Line Loss	Fan/ charge	Other	Total
Energy (MJ)	1.37	0.69	0.48	0.46	0.09	3.09

Figure 6.13 DC excavator energy utilization, average of all trials

Fuel savings with the DC excavator are primarily due to the elimination of valve metering losses. The DC hydraulic system also recovers power while lowering the boom and slowing the cabin swing rotation. The average recovered energy per trial was 0.16 MJ, which is 5.2% of the total. Energy recovery was responsible for about 5 of the 40% fuel savings.

Cycle times were 14% shorter with the DC excavator. Most of the time reduction (1.32 seconds, or 78%) was during the digging phase of the cycle. Higher energy efficiency means more power is available to the actuators, allowing the operator to dig faster. The swing and return to dig times improved slightly due to higher available flow rates during simultaneous motions.

6.6. Chapter Summary

- A prototype DC mini excavator has been constructed as a representative example of mobile multi-actuator machines. The DC excavator is equipped with four servo pumps connected to the machine's primary actuators. Two-way valves allow the pumps to alternately power secondary functions.
- Fuel tests were also conducted to evaluate the proposed optimal power management algorithm. A suspended load transfer cycle was selected for its low speed and power requirements. Compared to unoptimized operation, power management resulted in fuel savings of 56%.
- Unstable switching between operating modes is observed on the boom and stick cylinders of the DC excavator. Measurements demonstrate the effectiveness of pressure feedback for eliminating oscillations due to mode switching.
- Pump swash plate control laws were implemented and tested on the DC excavator. A nonlinear sliding mode control law improved tracking error by as much as a factor of 4 and bandwidth by a factor of 2 compared to conventional PI control.
- A standardized evaluation of the DC excavator's productivity and fuel efficiency was conducted and compared to an excavator of the same type with a conventional hydraulic system. For the truck loading cycle tested, the DC excavator's productivity (soil mass per time) was 17% higher and its fuel efficiency (soil mass per unit of fuel) was 69% greater than the standard machine.

CHAPTER 7 CONCLUSION

The primary topic of the thesis is the development of a method for optimizing the operation of mobile machines with multiple displacement controlled (DC) hydraulic actuators. This topic is studied here for the first time. Previous research on power management has mainly been limited to rule-based strategies such as defining high-power and low-power working modes. Where a formal optimization approach has been pursued, the constraints imposed by conventional valve-controlled hydraulic systems limit the range in which engine speed and pump displacement can be varied. In contrast, DC decouples the actuator pressures and flow rates, thereby relaxing the constraints on speed and displacement and allowing more opportunity for optimizing the system operation

The proposed power management method is a static optimization algorithm that minimizes the instantaneous rate of fuel consumption by adjusting the operating points of the hydraulic pumps and diesel engine. Detailed efficiency maps for the engine and pumps are considered. The optimization problem is reduced to a bounded minimization in one dimension. Engine speed is chosen as the design variable. A golden section (Fibonacci) search routine is used to minimize the objective function.

One challenge for optimizing the operation of multi-actuator machines is the relatively large solution space. The number of inputs, outputs and design variables increases linearly with the number of actuators. This discourages an off-line solution because of the difficulty of implementing a lookup table or similar map. Instead, the optimization runs online with the system in real time. A large number of states also impedes dynamic optimization techniques, since the

computational burden of dynamic programming increases exponentially with the number of actuators. A static optimization approach is better suited to the requirements of a mobile machine. However, multi-actuator machines frequently change velocity and load, making it impractical to optimize the system operation only at steady-state. Moreover, the dynamic response of linear actuators is typically much faster than that of the diesel engine. In previous research, the system dynamics have simply been neglected. To avoid actuator transients from dictating frequent changes in engine speed, a new method is proposed for constraining the engine speed based on the average or maximum actuator velocities required by the operator.

In support of the power management development, nonlinear models are presented for variable displacement pumps and DC linear and rotary actuators. A sliding mode control law is presented for robustly controlling pump displacement in spite of uncertain control pressure and swash plate moment. DC actuators operate in two modes, depending on the direction of the load. An analysis of the actuator dynamics explains how the nonlinear mode switching characteristic can cause a limit cycle behavior with repeated switching between modes. Stable mode switching can be assured by design (increasing damping or increasing static load) or by a control law that increases the damping of the closed-loop system, such as pressure or acceleration feedback. The feasibility of the proposed control is demonstrated by simulation and experiment.

A prototype multi-actuator machine was developed as part of the research. The prototype is a 5-ton compact excavator that was retrofitted with a DC hydraulic system for all 8 actuators. The DC excavator is fully instrumented for measuring energy efficiency and fuel consumption. Fuel measurements for a truck loading cycle with a professional operator yielded a 69% improvement in fuel efficiency compared to a conventional excavator. The proposed power management algorithm also contributes to total fuel savings. For a low power load-positioning

duty cycle, optimal power management reduced fuel consumption by 56% compared to the same system at constant engine speed.

Of course, there is always opportunity for future research. One of the limitations of the present DC hydraulic system is the lack of energy storage. Recovered power that cannot be used instantaneously by other actuators or auxiliary consumers is lost. In the future, a hydraulic hybrid system architecture will be designed that will have hydraulic energy storage capability. Since the power management method proposed here does not consider the system's energy state, a new approach will be necessary for managing energy storage in an optimal way.

The future development of more sophisticated hydraulic systems will likely include systems with switched dynamics. The DC actuator mode switching stability problem that was considered in this thesis is part of the larger problem of dynamic systems with discrete and continuous states. Future research will be required to ensure the stability and performance of such multi-modal systems.

BIBLIOGRAPHY

.

BIBLIOGRAPHY

Achten, P. A. J. 1997. Transforming Future Hydraulics--A new design of a hydraulic transformer. 8th Scandinavian International Conference on Fluid Power. Linkoping, Sweden.

Ahn, K. K. and D. Q. Truong. 2009. Development of energy saving hybrid excavator using hybrid actuator. Seventh International Conference on Fluid Power Transmission and Control. Hangzhou, China.

Andruch, J. and J. Lumkes. 2009. Regenerative Hydraulic Topographies using High Speed Valves. SAE Commercial Vehicle Engineering Congress (COMVEC), Chicago, Illinois, USA.

Berbuer, J. 1988. Neuartige Servoantriebe mit primärer Verdrängersteuerung. Ph.D. Thesis. RWTH Aachen. Aachen, Germany.

Berg, H. 1999. Regelung verstellbarer Hydromotoren am Konstantdrucknetz. Ph.D. Thesis. Dept. of Aircraft Systems, Technical University of Hamburg-Harburg. Düsseldorf, Germany.

Bildstein, M. 1998. Application of electro-hydrostatic actuators (EHA) for future aircraft primary flight controls. 1. Internationales Fluidtechnisches Kolloquium in Aachen (1IFK). Aachen, Germany.

Bishop, E. D. 2009. Digital Hydraulic Transformer--Approaching Theoretical Perfection in Hydraulic Drive Efficiency. 11th Scandinavian International Conference on Fluid Power SICFP09. Linkoping, Sweden.

Blackburn, J.F.; Reethof, G. and Shearer, J.L. 1960. Fluid Power Control. Technology Press of MIT, pp. 548-550.

Bonivento, C., M. Ruggeri, et al. 1997. Fuzzy logic control of a variable displacement hydraulic pump, London, UK, Imperial College Press.

Borghi, M., M. Milani, et al. 2005. Studying the Efficiency of a Compact Excavator Primary Workgroup Hydraulic Control System. 2005 SAE Commercial Vehicle Engineering Conference (COMVEC 2005), Rosemont, Illinois, USA, SAE.

Bu, F. 2001. Nonlinear model based coordinated adaptive robust control of electro-hydraulic systems. Ph.D. Thesis. School of Mechanical Engineering, Purdue University. West Lafayette, Indiana, USA.

Chun, S. Y. and B. H. Seo. 1993. Design of an artificial intelligence controller for effective control of engine speed and pump flow according to working condition of an excavator. International Conference on Computers, Communications and Automation TENCON '93. Beijing, China. 361-365.

Cook, J. A., J. Sun, J. H. Buckland, L. V. Kolmanovsky, H. Peng and J. W. Grizzle. 2006. Automotive powertrain control -A survey. Asian Journal of Control. 8(3):237-260.

Crolla, D. A., Q. Ren, S. Eldemerdash and F. Yu. 2008. Controller design for hybrid vehicles - state of the art review. 2008 IEEE Vehicle Power and Propulsion Conference (VPPC). Piscataway, NJ, USA. 6.

Dean, P. and R. Fales. 2007. Modern Control Design for a Variable Displacement Hydraulic Pump. Proc. Of the American Control Conference, New York City, USA.

Du, H. 2002. Pressure control with power limitation for hydraulic variable displacement piston pumps. Proc. of the American Control Conference, Anchorage, AK, USA.

EPA 1999. EPA Nonregulatory Nonroad Duty Cycles. United States Environmental Protection Agency, Office of Mobile Sources. www.epa.gov/otaq/regs/nonroad/equip-hd/cycles/nrcycles.htm

Filipi, Z., L. Louca, B. Daran, C.-C. Lin, U. Yildir, B. Wu, M. Kokkolaras, D. Assanis, H. Peng, P. Papalambros, J. Stein, D. Szkubiel and R. Chapp. 2004. Combined Optimisation of Design and Power Management of the Hydraulic Hybrid System for the 6×6 Medium Truck. International Journal of Heavy Vehicle Systems. 11(3):372-402.

Grabbel, J. 2004. Robust control Strategies for displacement controlled Rotary Actuators using Vane Type Motors. Ph.D. Thesis. Dept. of Aircraft Systems, Technical University of Hamburg-Harburg. Hamburg, Germany.

Grabbel, J. and M. Ivantysynova. 2005. An Investigation of Swash Plate Control Concepts for Displacement Controlled Actuators. International Journal of Fluid Power. 6(2):19-36.

Gupta, P. and A. Alleyne. 2005. Centralized and Decentralized Powertrain Controllers for an Earthmoving Vehicle. 2005 American Control Conference. Portland, Oregon, USA.

Habibi, S. R. and G. Singh. 2000. Derivation of Design Requirements for Optimisation of a high Performance Hydrostatic Actuation System. International Journal of Fluid Power. 1(2):11-28.

Hahmann, W. 1973. Das dynamische Verhalten hydrostatischer Antriebe mit Servopumpe und ihr Einsatz im Regelkreis. Ph.D. Thesis. RWTH. Aachen, Germany.

Hewett, A. J. 1994. Hydraulic Circuit Flow Control. U.S. Patent No. 5,329,767.

Heybroek, K. 2008. Saving Energy in Construction Machinery using Displacement Control Hydraulics. Ph.D. Thesis. Div. of Fluid and Mechanical Engineering Systems, Dept. of Management and Engineering, Linkopings Universitet. Linkoping, Sweden.

Heybroek, K., J. Larsson and J. O. Palmberg. 2006. Open Circuit Solution for Pump Controlled Actuators. 4th FPNI PhD Symposium. Sarasota, Florida, USA. 27-40.

Heybroek, K., J. Larsson and J. O. Palmberg. 2009. The Potential of Energy Recuperation in Valve Controlled Mobile Hydraulic Systems. 11th Scandinavian International Conference on Fluid Power (SICFP09). Linkoping, Sweden.

Ivantysyn, J. and M. Ivantysynova. 2001. Hydrostatic Pumps and Motors. New Delhi, India: Akademia Books International.

Ivantysynova, M. 2000. Displacement Controlled Linear and Rotary Drives for Mobile Machines with Automatic Motion Control. SAE Int. OFF-Highway & Powerplant Congress. Milwaukee, Wisconsin, USA.

Ivantysynova, M., J. Grabbel and J.C. Ossyra. 2002. Prediction of swash plate moment using the simulation tool CASPAR. ASME International Mechanical Engineering Congress, New Orleans, USA, IMECE 2002-39322.

Ivantysynova, M., O. Kunze and H. Berg. 1995. Energy saving hydraulic systems in aircraft—a way to save fuel. 4th Scandinavian International Conference on Fluid Power. Tampere, Finland.

Ivantysynova, M., R. Rahmfeld and J. Weber. 2008. Method for Controlling a Hydraulic System of a Mobile Working Machine. United States patent no. 7,386,978.

Jang, D.S., H.S. Ahn, Y.L. Cho, K.Y. Kim and J.H. Jang. 2009. Development of the intelligent robotic excavator for the autonomous excavating system. 11th Scandinavian International Conference on Fluid Power SICFP 09, Linkoping, Sweden.

Jansson, A. and J.O. Palmberg. 1990. Meter-in and meter-out orifices in mobile hydraulic systems. Proceedings of The International Off-highway and Power Plant Congress and Exposition. Milwaukee, WI, USA.

Jelali, M. and A. Kroll. 2003. Hydraulic Servo-systems: Modelling, Identification and Control. Springer-Verlag.

Kagoshima, M., M. Komiyama, T. Nanjo and A. Tsutsui. 2007. Development of New Hybrid Excavator. Kobelco Technology Review. 27: 39-42.

Kakuzen, M., N. Hayashi and J. Fujioka. 1988. Automatic control for hydraulic excavators. R&D: Research and Development Kobe Steel Engineering Reports. 38(3):14-17.

Karhu, O., J. Moya, J. Uusisalo, and K. Huhtala. 2007. Enabling Autonomous Functions on Hydraulic Excavator Attachment. 10th Scandinavian International Conference on Fluid Power (SICFP07). Tampere, Finland.

Keyworth, A. 1969. Electrohydraulic displacement control with mechanical feedback. US Patent No. 3,429,225.

Khalil, H. 2007. *Nonlinear Systems*, 3 ed., Pearson Education.

Kontz, M. E. and W. Book. 2007. Flow Control for Coordinated Motion and Haptic Feedback. International Journal of Fluid Power. 8(3):11.

Kramer, K. and E. Fletcher. 1984. Electrohydraulic Valve System. United States Patent No. 4,437,385.

Kreth, N. 1979. Untersuchungen zum dynamischen Verhalten eines geschlossenen hydrostatischen Kreislaufs mit Verstelleinheiten. Ph.D. Thesis. Universitat Dortmund. Dortmund, Germany.

Lawrence, P. D., S. E. Salcudean, N. Sepehri, D. Chan, S. Bachmann, N. Parker, M. Zhu and R. Frenette. 1995. Coordinated and Force-Feedback Control of Hydraulic Excavators. 4th International Symposium on Experimental Robotics, ISER'95. Stanford, California, USA.

Lee, J.M., Park, S.H. and Kim, J.S. 2009. Robust control of the pressure in a control-cylinder with direct drive valve for the variable displacement axial piston pump. IMechE Journal of Systems and Control Engineering, Vol. 223, No. 14.

Lewis, E. and H. Stern. 1962. Design of Hydraulic Control Systems. McGraw-Hill, pp. 260-266.

Lin, T. and Q. Wang. 2010. Research on Hybrid Powered Hydraulic Excavators. 7th International Fluid Power Conference (7IFK), Aachen, Germany.

Linjama, M., A. Laamanen and M. Vilenius. 2003. Is it Time for Digital Hydraulics? 8th Scandinavian International Conference on Fluid Power (SICFP03). Tampere, Finland.

Linjama, M., H.-P. Vihtanen, A. Sipola and M. Vilenius. 2009. Secondary Controlled Multi-Chamber Hydraulic Cylinder. 11th Scandinavian International Conference on Fluid Power, SICFP09. Linkoping, Sweden.

Lodewyks, J. 1994. Der Differentialzylinder im geschlossenen hydrostatischen Kreislauf. Ph.D. Thesis. RWTH. Aachen, Germany.

Long, G. and J. Lumkes. 2010. Comparative Study of Position Control with 2-way and 3-way On/Off Electrohydraulic Valves. International Journal of Fluid Power, Vol. 11, No. 1.

Love, L. 2009. Fluid Power Research: A Fundamental Concern for U.S. Energy Policy. NFPA Industry and Economic Outlook Conference. Presentation. Chicago, Illinois.

Merritt, H. 1967. Hydraulic Control Systems. Wiley, pp. 237-241.

Mikeska, D., 2002. A Precise Steady-State Model of Displacement Machines for the Application in Virtual Prototyping of Power-Split Drives. 2nd FPNI PhD Symposium. Modena, Italy.

Ming-Hui, C., K. Yuan, et al. (2003). Model-following controller based on neural network for variable displacement pump. JSME International Journal, Series C (Mechanical Systems, Machine Elements and Manufacturing) 46(1): 176-87.

Montgomery, A. and A. Alleyne. 2006. Optimizing the Efficiency of Electro-Hydraulic Powertrains. 2006 ASME International Mechanical Engineering Congress and Exposition, IMECE 2006. Chicago, Illinois, USA. 1-9.

Nanjo, T., E. Imanishi, K. Ootani and A. Tsutsui. 2007. Simulation and Evaluation Technique for Power System and Related Energy Saving on Hydraulic Excavator. Kobelco Technology Review. 27: 28-34.

Ossyra, J.C. 2004. Control Concepts for Vehicle Drive Line to Reduce Fuel Consumption. Ph.D. Thesis. Technical University of Hamburg-Harburg. Hamburg, Germany.

Ossyra, J. C. and M. Ivantysynova. 2004. Optimization of power losses in off-road vehicles using drive line control. 3rd FPNI PhD Symposium on Fluid Power. Terrassa, Spain.

Pedersen, H. 2007. Automated Hydraulic System Design and Power Management in Mobile Applications. Ph.D. Thesis. Institute of Energy Technology, Aalborg University. Aalborg, Denmark.

Pedersen, H., T. Andersen and M. Hansen. 2006. Power Management in Open Circuit Hydraulic Systems. 4th FPNI PhD Symposium. Sarasota, USA.

Pedersen, H., T. Andersen and M. Hansen. 2007. Power Management in Hydraulically Actuated Mobile Equipment. 2007 ASME International Mechanical Engineering Congress and Expo. IMECE2007. Seattle, USA.

Pelosi, M. 2007. Energy Consumption of an LS-based Excavator Hydraulic System. M.S. Thesis. Faculty of Engineering, Universita Degli Studi di Parma. Parma, Italy.

Pfiffner, R., L. Guzzella and C. H. Onder. 2003. Fuel-optimal control of CVT powertrains. Control Engineering Practice. 11(3):329-336.

Press, W.H., S.A. Teukolsky, W.T. Vetterling and B.P. Flannery. 2007. Numerical Recipes: The Art of Scientific Computing. Cambridge University Press, pp. 496-499.

Rahmfeld, R. and M. Ivantysynova. 1998. Energy saving hydraulic actuators for mobile machines. Proc. of 1st Bratislavian Fluid Power Symposium, Casta-Pila, Slovakia.

Rahmfeld, R. 2002. Development and Control of Energy Saving Hydraulic Servo Drives for Mobile Systems. Ph.D. Thesis. Dept. of Aircraft Systems, Technical University of Hamburg-Harburg. Hamburg, Germany.

Rahmfeld, R. and M. Ivantysynova. 2001. Displacement Controlled Linear Actuator with Differential Cylinder—A Way to Save Primary Energy in Mobile Machines. 5th International Conference on Fluid Power Transmission and Control, ICFP 2001. Hangzhou, China. 296-301.

Rahmfeld, R., M. Ivantysynova and J. Weber. 2004. Displacement Controlled Wheel Loader – a simple and clever Solution. Fourth International Fluid Power Conference, 4.IFK. Dresden, Germany.

Roosen, K. 1997. Energieeinsparung durch ein neues Schaltungskonzept fur ventilgesteuerte hydraulische Linearantriebe. Olhydraulik und Pneumatik 41(4):262-274.

Roth, J. 1983. Regelungskonzepte fur lagegeregelte elektrohydraulische Servoantriebe. Ph.D. Thesis. RWTH. Aachen, Germany.

Rühlike, I. 1997. Elektrohydraulische Antriebssysteme mit drehzahlveranderbarer Pumpe. Ph.D. Thesis. Technical University of Dresden. Dresden, Germany.

Scheidl, R., M. Garstenauer and B. Manhartsgruber. 2000. Switching Type Control of Hydraulic Drives – A Promising Perspective for Advanced Actuation in Agricultural Machinery. International Off-Highway and Powerplant Congress and Exposition. Milwaukee, WI, USA.

Shenouda, A. 2006. Quasi-Static Hydraulic Control Systems and Energy Savings Potential Using Independent meternig Four-Valve Assembly Configuration. Ph.D. Thesis. Woodruff School of Mechanical Engineering, Georgia Institute of Technology. Atlanta, Georgia, USA.

Shenouda, A. and W.J. Book. 2008. Optimal mode switching for a hydraulic actuator controlled with four-valve independent metering configuration. International Journal of Fluid Power. 9(1):9.

Singh, S. 1997. The State of the Art in Automation of Earthmoving. ASCE Journal of Aerospace Engineering. 10(4).

Singh, S. 2002. The State of the Art in Automation of Earthmoving, 2002. Workshop on Advanced Geomechatronics.

Sprockhoff, V. 1979. Untersuchungen von Regelungen am hydrostatischen Zylinderantrieb mit Servopumpe. Ph.D. Thesis. RWTH. Aachen, Germany.

Thuring, P. 2008. Model Predictive Control Based Energy Management Algorithm for a Hybrid Excavator. MS Thesis. Dept of Automatic Control, Lund University. Lund, Sweden.

Uusisalo, J., K. Huhtala and M. Vilenius. 2009. Effects of remote control on usability of hydraulic excavator. Proceedings of the ASME Dynamic Systems and Control Conference (DSCC2009).

Wendel, G. 2000. Regenerative Hydraulic Systems for Increased Efficiency. 2000 International Exposition for Power Transmission and Technical Conference.

Wendel, G. 2002. Hydraulic System Configurations for Improved Efficiency. International Exposition for Power Transmission and Technical Conference and SAE International Off-Highway Congress. Las Vegas, Nevada, USA.

Wieczorek, U. and M. Ivantysynova 2000. CASPAR—a computer-aided design tool for axial piston machines. Bath Workshop on Power Transmission and Motion Control. pp. 113-126. Bath, UK.

Williams, K. 2008. Towards an optimal energy management strategy for hybrid hydraulic powertrains based on dual stage power split principle. 5th FPNI Ph.D. Symposium. Krakow, Poland.

Williamson, C. 2007. Active Vibration Damping for a Skid-Steer Loader Using Displacement-Controlled Actuators. MS Thesis. School of Mechanical Engineering, Purdue University, West Lafayette, Indiana, USA.

Williamson, C. and M. Ivantysynova. 2007. The Effect of Pump Efficiency on Displacement-Controlled Actuator Systems. Tenth Scandinavian International Conference on Fluid Power SICFP'07. Tampere, Finland. 301-326.

Williamson, C., J. Zimmerman and M. Ivantysynova. 2008. Efficiency Study of an Excavator Hydraulic System Based on Displacement-Controlled Actuators. ASME/Bath Workshop on Fluid Power and Motion Control (FPMC08). Bath, UK.

Williamson, C. and M. Ivantysynova. 2008. Pump Mode Prediction for Four-Quadrant Velocity Control of Valveless Hydraulic Actuators. 7th JFPS International Symposium on Fluid Power, Toyama, Japan. Vol. 2, pp.323-328.

Williamson, C. and M. Ivantysynova. 2009. Active Vibration Damping for an Off-Road Vehicle with Displacement Controlled Actuators. International Journal of Fluid Power (10)3:5-16.

Williamson, C. and M. Ivantysynova. 2010, 1. Power Optimization for Multi-Actuator Pump-Controlled Systems. 7th International Fluid Power Conference (7IFK), Aachen, Germany.

Williamson, C. and M. Ivantysynova. 2010, 2. Stability and Motion Control of Inertial Loads with Displacement Controlled Hydraulic Actuators. 6th FPNI PhD Symposium, West Lafayette, Indiana, USA.

Wu, B., C. C. Lin, Z. Filipi, H. Peng and D. Assanis. 2004. Optimal power management for a hydraulic hybrid delivery truck. Vehicle System Dynamics. 42(1-2):23-40.

Xiao, Q., Q. Wang and Y. Zhang. 2008. Control strategies of power system in hybrid hydraulic excavator. Automation in Construction. 17(4):361-367.

Yao, B., F. Bu, J. Reedy and G. T. C. Chiu. 2000. Adaptive robust motion control of single-rod hydraulic actuators: Theory and experiments. IEEE/ASME Transactions on Mechatronics. 5(1):79-91.

Yao, B. and S. Liu. 2002. Energy-saving control of hydraulic systems with novel programmable valves. World Congress on Intelligent Control and Automation. Shanghai, China. 3219-3223.

Zhang, R., A. Alleyne and E. Prasetiawan. 2002. Modeling and H2/H-infinity MIMO Control of an Earthmoving Vehicle Powertrain. Journal of Dynamic Systems, Measurement, and Control. 124:625-628.

Ziegler, R. 1990. Auslegung und Optimierung schneller Servopumpen. Ph.D. Thesis. Universitat Karlsruhe. Karlsruhe, Germany.

Zimmerman, J., M. Pelosi, C. Williamson and M. Ivantysynova. 2007. Energy Consumption of an LS Excavator Hydraulic System. 2007 ASME International Mechanical Engineering Congress and Exposition IMECE2007. Seattle, Washington, USA.

Zimmerman, J. 2008. Design and Simulation of an Energy Saving Displacement-Controlled Actuation System for a Hydraulic Excavator. M.S. Thesis. School of Mechanical Engineering, Purdue University, West Lafayette, IN, USA.

Zimmerman, J. and M. Ivantysynova. 2009. Effect of installed hydraulic corner power on the energy consumption and performance of multi-actuator displacement controlled mobile machines. 2009 ASME Dynamic Systems and Control Conference & Bath/ASME Symposium on Fluid Power and Motion Control, Hollywood, CA, USA.

APPENDICES

Appendix A. Excavator Specifications

Table A-1. Mini Excavator

Parameter	Value	Unit
Make & Model	Bobcat 435H	
Year of Manufacture	2007	
Mass (approximate)	5000	kg
Width	1.93	m
Height	2.54	m
Max dig depth	3.42	m
Max dump height	3.66	m
Max reach	5.61	m
Travel speed (low)	1.25	m/s
Travel speed (high)	2.41	m/s

Table A-2. Engine

Parameter	Value	Unit
Make & Model	Kubota V2003-M-DI-TE2B-BC1	
Fuel type	Diesel	
Air intake	Turbocharged	
Cylinders	4	
Displacement	2.0	l
Speed range	1245-2770	rev/min
Max rated power	36.5	kW

Table A-3. Engine Speed Control

Parameter	Value	Unit
Governor type	Mechanical	
Actuator type	Electric motor and ball screw	
Actuator make & model	Thomson Electrak 1SP12-09A4	
Actuator stroke length	5.1	cm
Max speed at no load	7.6	cm/s
Position sensor (integrated with actuator)	Potentiometer	
Motor drive	Apex SA60 H-bridge	
Engine speed sensor type	Variable reluctance	

Table A-4. Hydraulic Components

Component	Mfgr.	Model	Type	Size
Variable displacement pump	Parker	PCA018	axial piston swash plate	18 cc/rev
Charge pump	Rexroth	PF1-014	external gear	14.1 cc/rev
Swing motor			radial piston	820 cc/rev
Fan motor	Sauer Danfoss	SNM2	external gear	8 cc/rev
Travel motor	Sauer Danfoss			28 cc/rev
Control valve	Moog	D636	single stage linear motor servovalve	20 l/min @ 70 bar

Sensor Specifications

Table A-5. Pressure Sensors

Mfgr.	Model	Type	Range (bar)	Output (V)	90% step response time (ms)	Accuracy (bar)
Parker	IQAN-SP500	Diaphragm strain gauge	0-500	0.5-4.5	5.0	5
Parker	IQAN-SP35	Diaphragm strain gauge	0-35	0.5-4.5	5.0	0.35
WIKA	S-10	Diaphragm strain gauge	0-250	0-10.0	<1	0.63

Table A-6. Position Sensors

Mfgr.	Model	Type	Range	Output	Resolution
Rota	LA	Magnetostrictive	2.0 m	0.5-4.5 V	0.3 mm
Parker	RS60	Hall Effect	47	0.5-4.5 V	1.4°
Contelec	Vert-X 22E	Hall Effect	∞	0.5-4.5 V	2.2°

Appendix B. Control Programs

Matlab Control Code for Optimal Power Management

```
function [swash,n_ed,J,iter,fuelrate,Q_des] =
opt_pwr(joy,maxjoy,p,p_fan,englever)
%#eml
persistent last_n
if isempty(last_n)
    last_n = 1300;
end

dp = [p(1)-p(2),p(3)-p(4),p(5)-p(6),p(7)-p(8)];
n_min = 1300;
n_max = 2700;

n_ed_max = n_min + 0.01*englever*(n_max-n_min);
Qmax = 67;  % max pump flow (l/min)

Qdmax = 0.01*maxjoy*Qmax;
n_ed_min = 1000*Qdmax/(1.377*18);

 [n_ed,J,iter,arg] = golden(n_ed_min,n_ed_max,[last_n,joy',dp,p_fan]);
M_best = arg(1);
fuelrate = arg(2);
swash = [(100/18.3)*arg(3:6)];
Q_des = arg(7:10);

last_n = n_ed;
end % opt_pwr function

%-------------------------------------------------------------------------
---
function [xopt,fx,iter,argout] =  golden(xlow,xhigh,argin)
% GOLDEN SECTION (FIBONACCI) SEARCH
% [J,argout] =  golden(x,argin)
% where argin = [last_n,dp,p_fan]
% and   argout = [Te_sat,fc,V,Q];
% Based on a simple algorithm from Numerical Methods for Engineers, 4
ed by Chapra and Canale

% constants:
R = (5^0.5-1)/2;
maxiter = 500;
tolx = 1;

xl = xlow; xu = xhigh;
iter = 1;
err = 2*tolx;
d = R*(xu-xl);
```

```
x1 = xl+d;
x2 = xu-d;
[f1,argout] = cost_fun(x1,argin);
[f2,argout] = cost_fun(x2,argin);
if f1<f2
    xopt = x1;
    fx = f1;
else
    xopt = x2;
    fx = f2;
end

while (err>tolx)&&(iter<maxiter)
    d = R*d;
    if f1<f2
        xl = x2;
        x2 = x1;
        x1 = xl+d;
        f2 = f1;
        [f1,argout] = cost_fun(x1,argin);
    else
        xu = x1;
        x1 = x2;
        x2 = xu-d;
        f1 = f2;
        [f2,argout] = cost_fun(x2,argin);
    end
    iter = iter+1;
    if f1<f2
        xopt = x1;
        fx = f1;
    else
        xopt = x2;
        fx = f2;
    end
    if xopt~=0
        err = (1-R)*abs((xu-xl)/xopt)*100;
    end
end % while loop
end % golden()

%-------------------------------------------------------------------------
----
function [J,argout] =  cost_fun(n,argin)
% Cost function for excavator operating point optimization %
% J =  cost_fun(n,argin)
% Inputs:
%   n   engine speed in rpm
%   argin = [last_n,dp,p_fan], where
%       last_n  optimal engine speed from last time step (rpm)
%       joy = [w1 v2 v3 v4] desired actuator velocities in %
%       dp = [dp1 dp2 dp3 dp4]  pump differential pressures in bar
%       p_fan  fan/charge pump pressure in bar
%
% Outputs:
```

```
%   J       operating cost
% argout = [Te_sat,fc,V,Q]

% This function calculates the cost of operating the machine at the
% given point in terms of a fuel consumption rate.  Constraints are
% enforced implicitly by adding a large cost if the given operating
% point is out of the possible range.
% Chris Williamson
% July 31, 2010

last_n = argin(1);
joy = argin(2:5);
dp = argin(6:9);
p_fan = argin(10);

Ts = 0.02;
dw = (pi/30)*(n-last_n)/Ts;  % approx acceleration in rad/s^2
J = 0;
bigJ = 50;  % relatively large penalty for violating physical
constraints
T_pump = zeros(4,1);
V = zeros(1,4);
Q = zeros(1,4);
ratio = 1.377;  % pump speed / engine speed
eta_belt = 0.97;  % belt torque efficiency

% engine parameters
I = 0.79;  % kg*m^2  effective mass moment of inertia of engine
b = 1.28;  % N*m*s   coeff of viscous friction

%==============================%
%%%%HYDRAULIC CYLINDERS DATA%%%%
%==============================%
%BOOM%
D_ABm=95.25e-3; %[m] Bore Diameter
D_RBm=50.8e-3; % [m] Rod Diameter
A_ABm=pi/4*(D_ABm)^2; % [m2] Bore Area
A_RBm=pi/4*(D_RBm)^2; %[m2] Rod Area
alpha_Bm=((A_ABm-A_RBm)/A_ABm);% (ratio of rod to piston area)
%ARM%
D_AA=82.6e-3; %[m] Bore Diameter
D_RA=50.8e-3; % [m] Rod Diameter
A_AA=pi/4*(D_AA)^2; % [m2] Bore Area
A_RA=pi/4*(D_RA)^2; %[m2] Rod Area
alpha_A=((A_AA-A_RA)/A_AA); % (ratio of rod to piston area)
%BUCKET%
D_ABk=76.2e-3; %[m] Bore Diameter
D_RBk=44.5e-3; % [m] Rod Diameter
A_ABk=pi/4*(D_ABk)^2; % [m2] Bore Area
A_RBk=pi/4*(D_RBk)^2; %[m2] Rod Area
alpha_Bk=((A_ABk-A_RBk)/A_ABk); % (ratio of rod to piston area)
%SLEW ROTARY MOTOR%
Vd_S=820e-3;  % [l/rev] Motor Displacement
tau_S=91/17; % Gear ratio radial motor/slew
```

```
A = [A_ABm A_AA A_ABk];
alpha = [alpha_Bm alpha_A alpha_Bk];

% calculate pump flow rates from joystick signals
Qmax = 18.3*2.600*[1 1.377 1.377 1.377];  % max pump flow in l/min
Q = Qmax.*joy/100;  % pump flow rates in l/min

% calculate engine shaft torque
[T_pump(1),V(1)] = parker_inv_model3(n,dp(1),Q(1));
for i = 2:4
    [T_pump(i),V(i)] = parker_inv_model3(ratio*n,dp(i),Q(i));
    T_pump(i) = T_pump(i)*ratio/eta_belt;
end
T_fan = fan_pump(n,p_fan);
T_e = sum(T_pump)+T_fan+I*dw;  % engine torque

% saturate negative engine torque
if T_e < -b*n*pi/30
    T_e = -b*n*pi/30;
end

% engine data
n_eng =
[1300,1300,1300,1300,1300,1300;1400,1400,1400,1400,1400,1400;1500,1500,
1500,1500,1500,1500;1600,1600,1600,1600,1600,1600;1700,1700,1700,1700,1
700,1700;1800,1800,1800,1800,1800,1800;1900,1900,1900,1900,1900,1900;20
00,2000,2000,2000,2000,2000;2100,2100,2100,2100,2100,2100;2200,2200,220
0,2200,2200,2200;2300,2300,2300,2300,2300,2300;2400,2400,2400,2400,2400
,2400;2500,2500,2500,2500,2500,2500;2600,2600,2600,2600,2600,2600;2700,
2700,2700,2700,2700,2700;];
m_eng = [0   19.0000   36.8000   55.5000   75.5000   97.9709;...
         0   23.1000   47.5000   70.6000   88.5000  114.8401;...
         0   28.5000   56.8000   86.6000  108.1000  140.2736;...
         0   29.8000   59.7000   89.4000  118.8000  154.1582;...
         0   31.2000   62.4000   94.8000  126.3000  163.8904;...
         0   31.1000   62.3000   94.9000  126.4000  164.0202;...
         0   31.1000   62.4000   94.9000  124.1000  161.0357;...
         0   32.6000   65.1000   99.0000  130.7000  169.6000;...
         0   32.6000   65.1000   97.6000  129.7000  168.3024;...
         0   29.8000   61.0000   90.8000  122.7000  159.2190;...
         0   29.8000   61.0000   90.9000  122.5000  158.9594;...
         0   29.6000   59.5000   90.7000  121.6000  157.7916;...
         0   29.8000   59.6000   90.8000  120.1000  155.8451;...
         0   19.3250   38.6500   57.9750   77.3000  100.3067;...
         0    8.6250   17.2500   25.8750   34.5000   44.7682];

% check torque constraint
Te_max = interp1(n_eng(:,5),m_eng(:,5),n,'linear','extrap');  % max
engine torque at given speed
Te_sat = T_e;
if T_e > Te_max
    J = bigJ+0.01*T_e;
    Te_sat = Te_max;
```

```
end
% saturate negative torque for calculating fuel rate
if T_e < 0
    Te_sat = 0;
end

% ***************************** CALCULATE COST **********************
% calculate fuel consumption rate
fc = engine_poly_model(n,Te_sat);  % kg/hr

% calculate cost function value
J = J + fc;
argout = [Te_sat,fc,V,Q];
end % function

%-------------------------------------------------------------------------
----
function [Me,Vi]=parker_inv_model3(speed,pressure,flow)
% Four quadrant inverse loss model for Parker PCA018 18 cc/rev axial
piston swash
% plate pump.  Third order polynomial from polyfitn, including
artificial
% points at 0% swash plate angle.
%
% Inputs:
%   shaft speed (1000..4500 rpm)
%   differential pressure p_out - p_in (-350..350 bar)
%   outlet flow (-n*Vmax..n*Vmax l/min)
%
% Outputs:
%   Me: shaft torque in N*m
%   Vi: derived displacement volume in cc/rev
%   err: out of range error code (0=ok,1=speed,2=pressure,3=flow rate)
%
% Chris Williamson
% Sept 9, 2009
X1 = speed;
X2 = abs(pressure);

% saturate speed and pressure
if speed < 1000
    speed = 1000;
else if speed > 4500
        speed = 4500;
    end
end
if abs(pressure) > 350
    pressure = 350*sign(pressure);
end

if (abs(flow)/(0.001*speed)) > 18.3  % if given flow is too high for
given speed
    flow = sign(flow)*0.001*speed*17;  % set flow rate to max possible
end
```

```
if pressure*flow >= 0  % pumping mode
    X3 = abs(flow);
    % Shaft Torque
    Me =    -1.9563e-009*X1^3 + 2.0572e-008*X1^2*X2 + 2.7677e-
007*X1^2*X3 + 1.2367e-005*X1^2 - 1.962e-008*X1*X2^2 - 2.7812e-
006*X1*X2*X3 - 0.00011321*X1*X2 - 3.6321e-006*X1*X3^2 - 0.0015766*X1*X3
- 0.01826*X1 + 1.3713e-007*X2^3 + 1.5358e-006*X2^2*X3 + 1.8239e-
005*X2^2 + 1.7415e-005*X2*X3^2 + 0.013877*X2*X3 + 0.15031*X2 + 4.4313e-
005*X3^3 + 0.0085965*X3^2 + 2.0566*X3 + 1.9416;
    % Derived Displacement
    Vi =    -4.3361e-010*X1^3 + 4.8726e-011*X1^2*X2 + 5.7604e-
008*X1^2*X3 + 3.7648e-006*X1^2 - 1.7424e-010*X1*X2^2 - 7.5693e-
009*X1*X2*X3 - 4.0223e-007*X1*X2 - 7.1182e-008*X1*X3^2 -
0.0004944*X1*X3 - 0.0099649*X1 + 4.6825e-010*X2^3 + 1.3188e-008*X2^2*X3
+ 1.4183e-006*X2^2 + 2.7413e-007*X2*X3^2 + 1.5309e-005*X2*X3 +
0.0030095*X2 + 1.0388e-006*X3^3 + 0.00016662*X3^2 + 1.2963*X3 + 7.7859;
    if Me < 0
        Me = 0;
    end
else % motoring mode
    X3 = -1*abs(flow);
    Me = 8.0264e-010*X1^3 - 1.16e-008*X1^2*X2 + 9.8192e-008*X1^2*X3 -
5.0576e-006*X1^2 - 1.5603e-008*X1*X2^2 - 1.4239e-006*X1*X2*X3 +
7.9359e-005*X1*X2 - 2.6801e-006*X1*X3^2 - 0.00077373*X1*X3 +
0.0061884*X1 + 5.2217e-008*X2^3 - 1.1684e-006*X2^2*X3 - 3.5234e-
005*X2^2 + 1.4154e-005*X2*X3^2 + 0.010767*X2*X3 - 0.10708*X2 - 3.7539e-
005*X3^3 + 0.0058076*X3^2 + 1.277*X3 + 3.3395;
    Vi =    -4.3361e-010*X1^3 + 4.8726e-011*X1^2*X2 - 5.7604e-
008*X1^2*X3 + 3.7648e-006*X1^2 - 1.7424e-010*X1*X2^2 + 7.5693e-
009*X1*X2*X3 - 4.0223e-007*X1*X2 - 7.1182e-008*X1*X3^2 +
0.0004944*X1*X3 - 0.0099649*X1 + 4.6825e-010*X2^3 - 1.3188e-008*X2^2*X3
+ 1.4183e-006*X2^2 + 2.7413e-007*X2*X3^2 - 1.5309e-005*X2*X3 +
0.0030095*X2 - 1.0388e-006*X3^3 + 0.00016662*X3^2 - 1.2963*X3 + 7.7859;
  if Me > 0
        Me = 0;
    end
end

% change sign of Vi if flow direction is negative
if flow<0
   Vi = -1*Vi;
end

% saturate displacement
if abs(Vi)>18.3
    Vi = 18.3*sign(Vi);
end

end % function

%-------------------------------------------------------------------------
function M_fan = fan_pump(n,p_fan)
```

```
%calculate excavator fan/charge pump shaft torque based on catalogue
data
% and 2nd order polynomial of speed and pressure

% Saturate input conditions
if p_fan > 70
    p_fan = 70;
end
if n < 1200
    n = 1200;
else if n > 2700
        n = 2700;
    end
end

M_fan = .38122e-6*n^2  +.13118e-5*n*p_fan  -.12008e-2*n  -.34227e-
3*p_fan^2+.29671*p_fan-.72214;

end % function

%-------------------------------------------------------------------------
----
function fuel=engine_poly_model(n,M)
% 2nd order polynomial model for Kubota 2.0 liter Diesel engine
% updated with artificial points at scaled max torque
% Inputs:
%   shaft speed (1300 - 2700 rpm)
%   shaft torque (0 - 170 Nm)

% Outputs:
%   fuel rate in kg/h
%
X1 = n;
X2 = M;
fuel = 1.5832e-006*X1^2 + 1.6088e-005*X1*X2 - 0.0056207*X1 - 3.1954e-
005*X2^2 + 0.024848*X2 + 5.6585;
end
```

Matlab Control Code for Pump Displacement Control

```
function u = SMC(B,Bd,Bd_dot,p_cntrl,n,dp)
%#eml

% inputs:
%  B = measured swash plate angle (norm)
%  Bd = desired swash plate position (norm)
%  Bd_dot = desired swash plate velocity (1/s)
%  p_cntrl = pump control pressure (bar)
%  n = pump shaft speed (rpm)
%  dp = pump port differential pressure (bar)

% output: valve control signal (norm)

% pump parameters
k = 8810;   % [N/m]     centering spring constant
r = 0.051;        % (m) distance from center of pump to center of
% control piston
Brad = B*(17.5/100)*(pi/180);  % convert beta to radian
x = r*tan(Brad);
d = 0.022;        % setting piston diameter (m)
A = 0.25*pi*d^2; % setting piston area (m^2)
% Cv = (24/6e4)/sqrt(70e5);  % [m^3/s / Pa^0.5]
Cv_norm = 1/sqrt(15e5);

%---------------feedforward--------------------------------------------
-
Mx = parker_mx(n,dp,100*B);
delta_p = 1e-5*(2*k*x - Mx/r)/A; %(bar) back pressure due to
% disturbances
u_ff = 0.04*Bd_dot*(1/Cv_norm)*(0.5e5*(p_cntrl -
delta_p*sign(Bd_dot)))^-0.5; % with compensation for springs and Mx
% u_ff = 0.04*Bd_dot*(1/Cv_norm)*(0.5e5*p_cntrl)^-0.5; % without
% compensation for centering springs and control moment
%---------------feedback-----------------------------------------------
H = 0.4;  % switching signal magnitude
bl = 0.05; % error boundary layer
e = B - Bd;

if abs(e)>bl
    u_fb = -H*sign(e);
else
    u_fb = -H*(abs(e)/bl)*sign(e);
end

%--control signal
u = -(u_ff + u_fb);
end % SMC()


%---------------------------------------------------------------------
----
```

```
function mean =parker_mx(speed,pressure,disp)
% Polynomial model of swash plate moment Mx for Parker PCA018 axial
piston pump
% [mean,amplitude]=PARKER_MX(speed,pressure,swash)
%
% Inputs:
%   shaft speed (1000..4500 rpm)
%   differential pressure p_1 - p_2 (-350..350 bar)
%   swash plate angle (-100..100%)
%
% Outputs:
%   Mx_mean: mean swash plate moment [N*m]
%
%  Notes:
%  The polynomial returns bad results if pressure = 0 exactly.
%  The CASPAR simulations and polynomials are for a 2-quadrant
pump/motor.
%  Mx is assumed to be the same for overcenter swash plate angles.
%  Chris Williamson
%  4/1/2010
%
X1 = speed;
X2 = abs(pressure);
X3 = abs(disp);

if sign(pressure)>0    % pumping mode
    mean = 5.2059e-007*X1^2 - 2.7246e-005*X1*X2 + 1.0981e-005*X1*X3 -
0.0018279*X1 - 6.9607e-005*X2^2 - 4.1046e-005*X2*X3 + 0.094256*X2 +
6.0701e-005*X3^2 - 0.011317*X3 + 1.4451;
else % motoring mode
    mean =  3.4412e-008*X1^2 - 2.6941e-005*X1*X2 - 2.0407e-005*X1*X3 +
0.00082761*X1 - 8.7251e-005*X2^2 + 9.576e-005*X2*X3 + 0.098716*X2 -
6.8676e-005*X3^2 + 0.031709*X3 - 1.5724;
end

% check input parameters
if X2 > 350
    mean = nan; %amplitude = nan;
end

if speed < 1000
    mean = nan; %amplitude = nan;
else if speed > 4500
        mean = nan; %amplitude = nan;
    end
end

if X3 > 100
    mean = nan; %amplitude = nan;
end

end % function
```

VITA

VITA

Education

B.S. Mechanical Engineering, Mathematics Minor, April 2005

Brigham Young University (Provo, Utah, USA)

M.S. Mechanical Engineering, August 2007

Purdue University (West Lafayette, Indiana, USA)

Thesis: Active vibration damping for a skid-steer loader using displacement-controlled actuators

Major Professor: Monika Ivantysynova

Ph.D., December 2010

Dept. of Agricultural & Biological Engineering, Fluid Power Specialization.

Purdue University (West Lafayette, Indiana, USA)

Thesis: Power management and trajectory optimization for multi-actuator mobile machines with displacement controlled actuators

Major Professor: Monika Ivantysynova

Current Employment

Senior Staff Engineer, Bucyrus International (South Milwaukee, WI, USA)

Special Projects Department, Simulation & Controls Group

Publications

Williamson, C. and Ivantysynova, M. 2010. Stability and Motion Control of Inertial Loads with Displacement Controlled Hydraulic Actuators. 6th FPNI PhD Symposium. West Lafayette, Indiana, USA. Recognized Paper.

Williamson, C. and Ivantysynova, M. 2010. Power Optimization for Multi-Actuator Pump-Controlled Systems. 7th International Fluid Power Conf. Aachen. Aachen, Germany.

Williamson, C., Lee, S. and Ivantysynova, M. 2009. Active Vibration Damping for an Off-Road Vehicle with Displacement Controlled Actuators. International Journal of Fluid Power (10)3:5-16.

Williamson, C. and Ivantysynova, M. 2008. Pump Mode Prediction for Four-Quadrant Velocity Control of Valveless Hydraulic Actuators. 7th JFPS International Symposium on Fluid Power, Toyama, Japan. Vol. 2, pp.323-328.

Williamson, Christopher, and Coblitz, Kristine (ed.). CCEFP Research Focus, Project 1A.2: Optimal Power Management for Mobile Fluid Power Machines Using Displacement-Controlled Actuators, Fluid Power Journal, September/October 2008.

Williamson, C., Zimmerman, J. and Ivantysynova, M. 2008. Efficiency Study of an Excavator Hydraulic System Based on Displacement-Controlled Actuators. ASME/Bath Workshop on Fluid Power and Motion Control (FPMC08). Bath, UK.

Zimmerman, J., Pelosi, M., Williamson, C. and Ivantysynova, M. 2007. Energy Consumption of an LS Excavator Hydraulic System. 2007 ASME International Mechanical Engineering Congress and Exposition IMECE2007. Seattle, Washington, USA.

Williamson, C. 2007. Active Vibration Damping for a Skid-Steer Loader Using Displacement-Controlled Actuators. MS Thesis. School of Mechanical Engineering, Purdue University.

Williamson, C. and Ivantysynova, M. 2007. The Effect of Pump Efficiency on Displacement-Controlled Actuator Systems. 10th Scandinavian International Conference on Fluid Power SICFP'07. Tampere, Finland. 301-326.

Patent Applications

Displacement-Controlled Hydraulic System for Multi-Function Machines. International Application No. PCT/US2009/063492. Filing date 11/06/2009.

System and Method for Blade Level Control of Earthmoving Machines. International Application No. PCT/US2009/063495. Filing date 11/06/2009.

System and Method for Enabling Floating of Earthmoving Implements. International Application No. PCT/US2009/063496. Filing date 11/06/2009.

System and Method for Pump-Controlled Cylinder Cushioning. International Application No. PCT/US2009/063498. Filing date 11/06/2009.

Awards

Ross Fellowship, 2007

Purdue SURF Graduate Mentor of the Summer 2008

Recognized Paper, 6th FPNI PhD Symposium 2010